EXPLORING THE FEASIBILITY OF A PASSIVELY ACTUATED BINARY-PITCH PROPELLER FOR GROUP 2 UAVS

By

CALEB T. RHYNE

Bachelor of Science in Mechanical and Aerospace Engineering

Oklahoma State University

Stillwater, Oklahoma

2014

Submitted to the Faculty of the
Graduate College of the
Oklahoma State University
in partial fulfillment of
the requirements for
the Degree of
MASTER OF SCIENCE
July, 2018

EXPLORING THE FEASIBILITY OF A PASSIVELY ACTUATED BINARY-PITCH PROPELLER FOR GROUP 2 UAVS

Thesis Approved:

Dr. Andrew S. Arena

Thesis Adviser

Dr. Richard J. Gaeta

Dr. Joseph Conner

Name: CALEB T. RHYNE

Date of Degree: JULY, 2018

Title of Study: EXPLORING THE FEASIBLITY OF A PASSIVELY ACTUATED BINARY-PITCH PROPELLER FOR GROUP 2 UAVS

Major Field: MECHANICAL AND AEROSPACE ENGINEERING

Abstract: In the early years of aviation, the type of propulsion system implemented limited aircraft performance. Up until the introduction of the jet engine in 1939, and still today, aircraft used a fixed-pitch propeller based propulsion system. Fixed-pitch propellers have low manufacturing costs and have a weight advantage over other propulsion types. However, when choosing the proper propeller for an aircraft, the designer must compromise between areas of performance, i.e. a propeller designed to optimize take-off performance may have poor performance in cruise, and vice versa. In recent years, unmanned aerial vehicles, or UAVs, have become increasingly popular, both in the amateur hobbyist world as well as in commercial and military applications. As with large-scale aircraft, UAVs suffer in performance largely due to the use of fixed pitch propellers. Large aircraft make use of constant speed propellers driven by oil – based hydraulic systems from the vehicles engine, which are not available for small UAVs. A system is designed, constructed and tested for Group 2 UAVs using the two primary performance points, take-off and cruise, as the basis for analysis. The system is governed by propeller RPM and allows for operator control based on throttle input.

TABLE OF CONTENTS

Chapter Page

LIST OF TABLES

Table Page

LIST OF FIGURES

Figure Page

Figure Page

Figure Page

CHAPTER I

INTRODUCTION

In the early years of aviation, the type of propulsion system implemented limited aircraft performance. Up until the introduction of the jet engine in 1939, and still today, aircraft used a fixed-pitch propeller based propulsion system. Fixed-pitch propellers have low manufacturing costs and have a weight advantage over other propulsion types. However, when choosing the proper propeller for an aircraft, the designer must compromise between areas of performance, i.e. a propeller designed to optimize take-off performance may have poor performance in cruise, and vice versa. This coupled with the limited power of engines put a ceiling on overall aircraft performance. The use of variable-pitch propellers are necessary for aircraft to maintain optimal efficiency while having the necessary performance output for the required mission.

In recent years, unmanned aerial vehicles, or UAVs, have become increasingly popular, both in the amateur hobbyist world as well as in commercial and military applications. As with large-scale aircraft, UAVs suffer in performance largely due to the use of fixed pitch propellers. Large aircraft make use of constant speed propellers driven by oil –based hydraulic systems from the vehicles engine. These can be passive or active. However, the mechanisms that drive these are not widely available for small scale UAVs. With the increasing use of UAVs, there needs to be an improvement in the power plant used in order to improve performance.

With the use of propellers, this suggests the need to implement a system to allow for the varying of the propellers pitch.

There are different ways this may be accomplished, using a physical device to actuate the change, or possibly using the aerodynamics of the propeller itself to alter a blades orientation. Examples of each are explored in the Literature Review in Chapter 2. This paper explores one way to passively alter a propellers pitch in two-positions via a mechanical device based on the RPM provided by the engine. The following outlines the goals and objectives of the research.

GOAL: Determine the viability of employing a passive binary variable-pitch mechanism for the use in Group 2 UAVs.

OBJECTIVES:

1. Conduct literary search on current variable pitch models and how they relate to UAS.
2. Conduct thorough search on possible designs and methods that utilize rotational frequency to change a given mechanical output suitable for UAS.
3. Develop VBA and basic CAD models to determine necessary structural sizes for mechanism to achieve required pitch change at appropriate engine RPM and feasibility of design for a prototype.
4. Create detailed solid works model of passive mechanism based on VBA model results designed for use with the DA-100 or other comparable engines.
5. Conduct basic FEA for the strength and operation of the device through SolidWorks to demonstrate functionality.
6. Build mechanism based on detailed Solid Works model and perform a proof of strength test.
7. Test the mechanism on an electric motor while being recorded with a high-speed camera to monitor the devices actuation.

CHAPTER II

HISTORY AND REVIEW OF LITERATURE

2.1 HISTORY AND BACKGROUND

2.1.1 WHAT IS PROPELLER PITCH?

The blade of a propeller is a 3D airfoil, or essentially a miniature wing that has more extreme twist. Since each section of a blade travels at different tangential velocities for similar rotational velocities, the twist allows each section of the blade to achieve the same effective angle of attack with respect to the flow, thus keep the thrust produced equal along the length of the blade. This can be seen in the figure below.

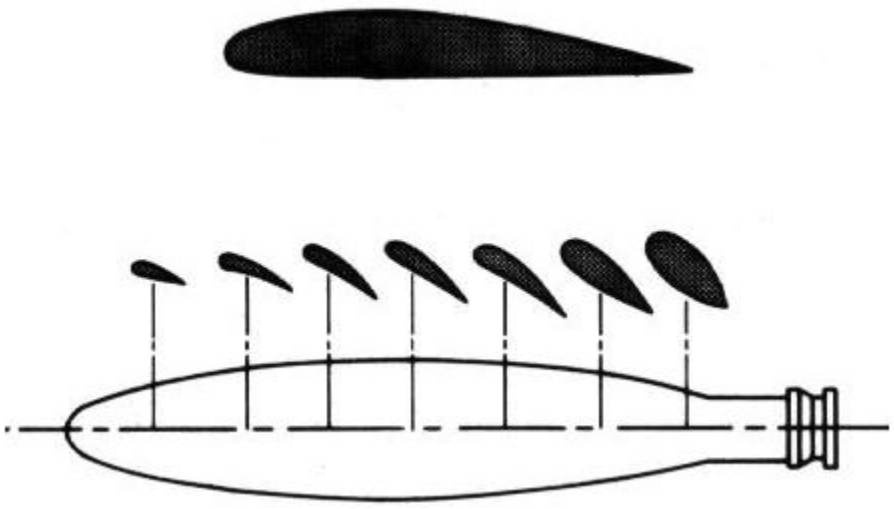

Figure 1 Representation of blade angle [3]

The relative wind velocity seen by a propeller blade is the product of the rotational velocity of the propeller itself and the forward velocity of the aircraft. A side view of a propeller in line with the

plane of rotation can be seen in the next figure. The term blade angle is sometimes used instead of pitch. However, they are not the same, though pitch is directly proportional to the blade angle. Pitch is the distance the propeller would travel with one full revolution. With this there are the geometric pitch, which is the theoretical distance a propeller should travel in one advance [3], and the effective pitch, or the distance the propeller actually travels [3]. There are losses associated with friction between the propeller and air as well as how much the blade "slips" in the air, resulting in an average of about 80% efficiency. This accounts for the difference between the geometric pitch and the effective pitch.

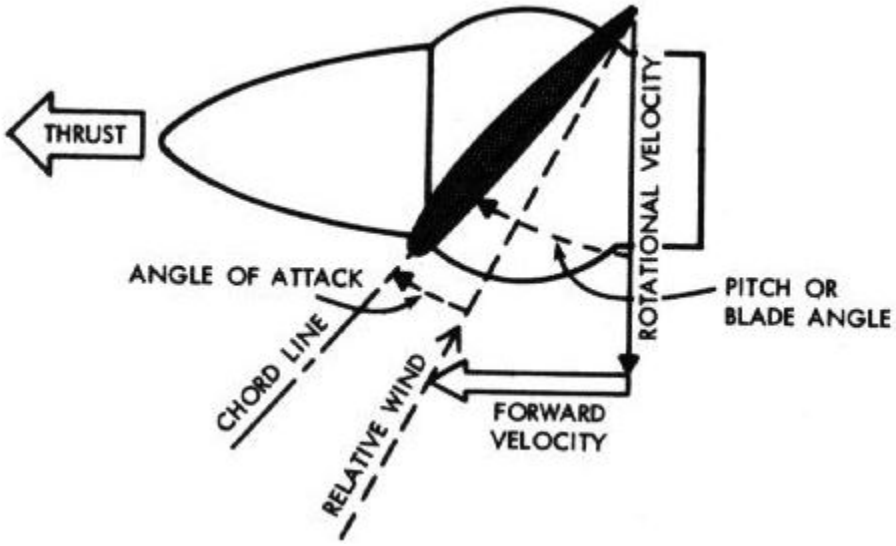

Figure 2 Blade angle relative to plane of rotation [3]

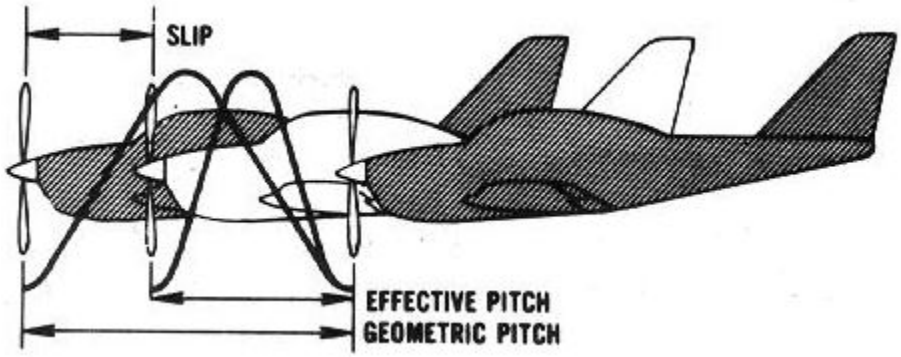

Figure 3 Example of Geometric Pitch [3]

A simple calculation can be made to find the pitch of a propeller along its span, shown below;

$$P = 2\pi R tan(\beta), \tag{2.1}$$

where P is the geometric pitch, R is the radius from the center of the disk of rotation, and β is the blade angle. In order to find the blade angle at each section to maintain a constant pitch, one needs only to solve for β.

2.1.2 The Importance of Using a Variable Pitch Propeller

A variable pitch propeller allows an aircraft to optimize propeller efficiency over a range of advance ratios. The advance ratio is a dimensionless variable that describes the forward distance traveled by a propeller in one revolution. It is the ratio of the incoming free stream velocity and the product of the propellers angular velocity and diameter and is represented by the letter J. The efficiency, η, is shown by the product of the advance ratio and the ratio of the thrust and power coefficients. Both can be seen in equations [2.2] and [2.3].

$$J = \frac{V_\infty}{nD} \tag{2.2}$$

$$\eta = J\frac{C_t}{C_p} \tag{2.3}$$

Typically, propeller efficiencies are compared at similar advance ratios. A propeller designed for a certain flight condition or RPM can underperform or over perform at other flight conditions. For example, a propeller designed for take-off will cause the engine to turn at an RPM that is too high for the engine at a cruise condition and must be throttled down, reducing the performance. On the other hand, one that has a pitch designed for cruise will not have the amount of power required for take-off for the opposite reason, as the engine will not reach the necessary RPM [4].

There are two methods of addressing this problem, as discussed by the Italian researcher Enrico Pistolesi in 1923, one being a mechanical actuation such as an aircraft version of a “gear

shift" [4]. With the technology at the time, there was no mechanical way to "shift gears" while airborne. The complexity of such a device left it largely unexplored. Aside from that, "there was no mechanical method of producing a gradual change in speed without a loss of power" [4], the key word here being gradual. The second way to produce a gradual change in in speed would be to alter the shape of the propeller blades in some way. By merely altering its shape, uniform acceleration is achieved along the length of the blade. This also allows for near perfect adaptation for all flight regimes, where a "gear shift" style would still limit the performance to be optimized for particular regimes. Ways to alter the shape or geometry of a blade is to vary its diameter, chord length, or pitch. Varying a blades chord length mid-flight is the most difficult if not impossible to accomplish. There were early attempts to achieve this by stacking two blades on top of each other, and fanning one out when desired [4]. This proved to be too complex and unreliable, so this method isn't much researched. Theoretically, a perfect solution would be to simultaneously alter the diameter and the pitch [4], but again this proves to be too difficult and complex. Instead, the most practical and viable option is by varying solely the pitch of the blade.

Changing the pitch of a constant diameter blade requires changing the blade angle. Using equation [2.4], the new pitch equation can be shown as

$$P' = 2\pi R tan(\beta + \delta), \tag{2.4}$$

where δ is the angle changed. It should be noted that once a change in β occurs, the geometric pitch is not equal throughout the blade. However, "it can be shown that the total pitch for a blade after rotation may be assumed to be approximately the pitch of the section at [.75] the radius" [4].

In the article "Variable Pitch Propeller" by Pistolesi [4], he aims to show the benefits gained from using such a propeller by comparing the theoretical performances of a normal and supercharged engine at various altitudes and with fixed pitch propellers to the performances of

each engine at similar altitudes but with propellers of varying geometry. The airfoil selected was a well-researched airfoil, number 96 of the National Advisory Committee for Aeronautics, or N.A.C.A. The aircraft being modeled was assumed to have a weight of 2500 kg (5511.6-lbs) and a wing area of 53 square meters (570.5 square feet). Engine performance was measured as a function of torque. The normal engine followed a "law of decrease" [4] for increasing altitude and followed the basic functions

$$Q = Q_0 \mu, \tag{2.5}$$

$$\mu = \delta^{1.235}, \tag{2.6}$$

Where Q is the engine torque, Q_0 is the torque at sea level, μ is a decreasing function of the relative density δ. The supercharged engine was assumed to only decrease by half at the maximum altitude analyzed rather than the nearly one fifth suffered by normal engine. For both engines, the RPM was held constant at 1700. The following figures show the engine performances at various altitudes according to these functions.

Altitude	ft	0	13123	26247	39370
	m	0	4000	8000	12000
δ		1	0.669	0.429	0.253
μ		1	0.609	0.352	0.192

Figure 4 Torque (μ) relation to density- Normal Engine [4]

Altitude	ft	0	13123	26247	39370
	m	0	4000	8000	12000
δ		1	0.669	0.429	0.253
μ		1	0.900	0.750	0.500

Figure 5 Torque (μ) relation to density- Supercharged Engine [4]

For both engines, the RPM was held constant at 1700. Figure (6) shows the relation between RPM and Velocity for each engine at various altitudes for a fixed pitch propeller when RPM is not regulated. Figure (5) shows how increasing altitude effects both engines. Looking at the supercharged engine, even starting as low as 4000 m the RPM of the engine exceeds 1700, and only increases to achieve the same speeds at higher altitudes. In order to maintain constant RPM, the pilot would need to throttle down, which, as mentioned earlier, would result in a loss of power. Figure (7) shows the thrust, τ, and torque, k, coefficients as they relate to the advance ratio for various pitch degrees. The thrust and torque coefficients are given as

$$\tau = \frac{T}{\rho R^2 \Omega^2}, \tag{2.7}$$

$$k = \frac{Q}{\rho R^5 \Omega^2}, \tag{2.8}$$

where T is the thrust, ρ is air-density, and Ω the angular velocity.

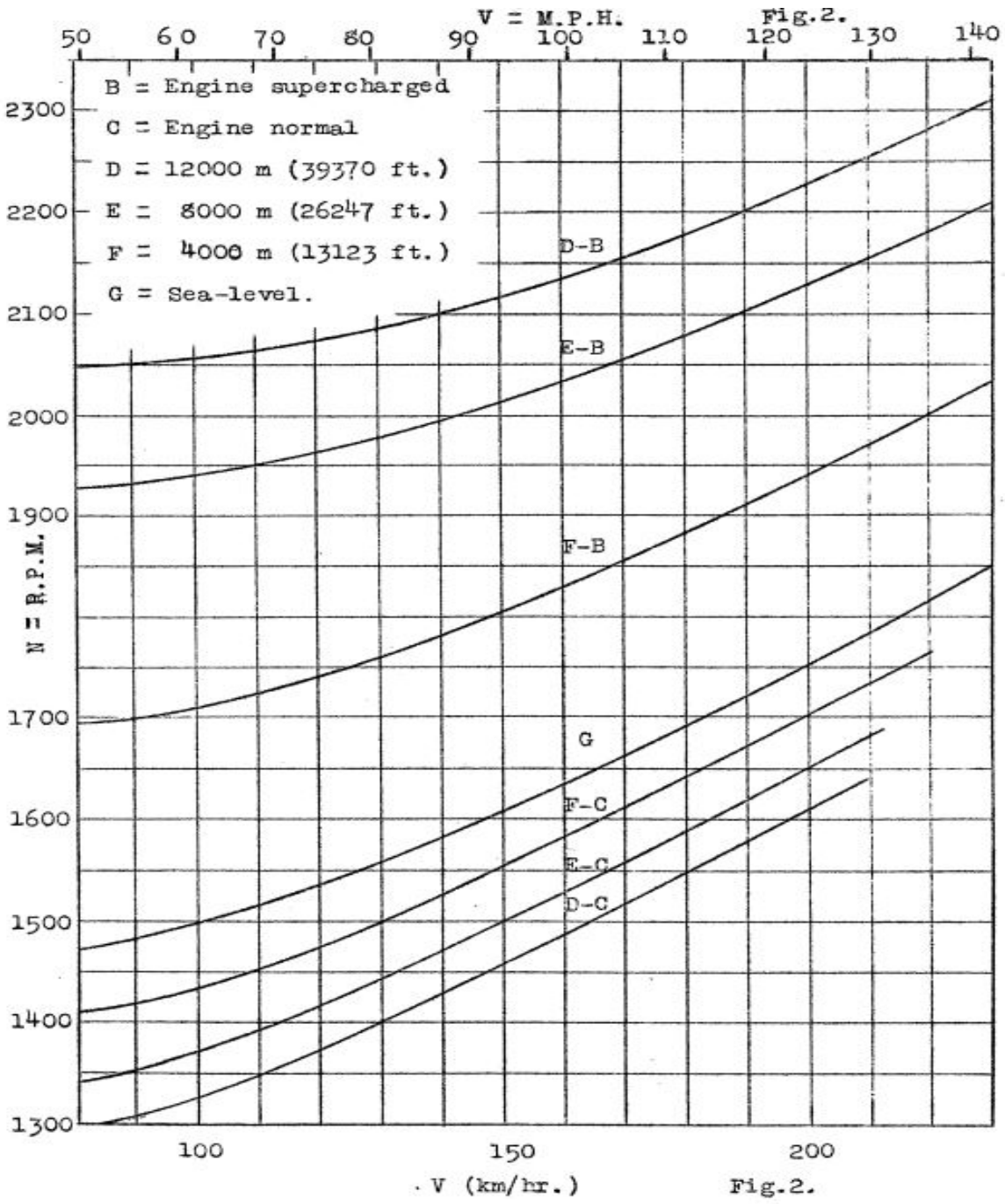

Figure 6 RPM at various velocities for both engines [4]

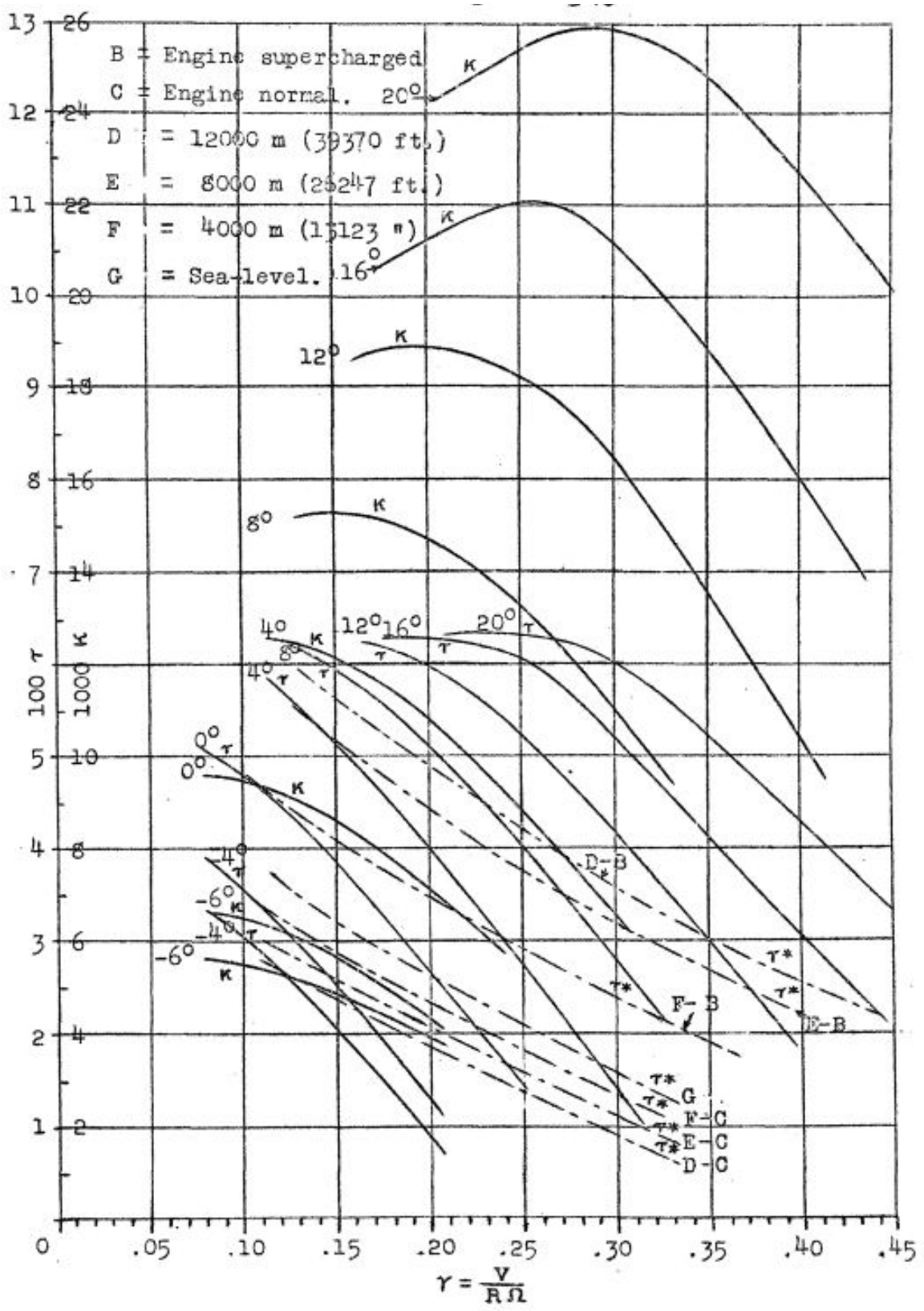

Figure 7 Thrust and Torque coefficients at various altitudes [4]

The polar plots for the modeled aircraft and engine performance for both the fixed pitch and variable pitch options on both engine cases as well as the plot showing the differences in speed and climbing performances at each altitude for both propeller variants can be found in the appendices. The following figures show the improved performances for both engines.

To	1000 m / 3281 ft	From	5' 3"	to	4' 32"	Gain	0' 31"
"	2000 m / 6562 ft	"	11' 33"	"	10' 24"	"	1' 9"
"	3000 m / 9842 ft	"	20' 54"	"	18' 36"	"	2' 18"
"	4000 m / 13123 ft	"	36' 54"	"	31' 24"	"	5' 30"
"	4500 m / 14764 ft	"	51' 24"	"	41' 36"	"	9' 48

Figure 8 Performance increase for Normal Engine [4]

To	1000 m / 3281 ft	From	4' 38"	to	4' 11"	Gain	0' 27"
"	2000 m / 6563 ft	"	9' 20"	"	8' 41"	"	0' 39"
"	3000 m / 9842 ft	"	14' 36"	"	13' 36"	"	1' 0"
"	4000 m / 13123 ft	"	20' 30"	"	19' 0"	"	1' 30"
"	5000 m / 16404 ft	"	29' 0"	"	25' 6"	"	3' 54"
"	6000 m / 19685 ft	"	44' 6"	"	32' 18"	"	11' 48"
"	7000 m / 22966 ft	"			40' 36"		

Figure 9 Performance increase for Supercharged Engine [4]

It can be seen from the figures above and the improved speeds and power outputs that having a variable pitch option can vastly improve the performance of an aircraft. This revelation occurred early on in aviation, and this simple analysis shows the necessity of having and employing a variable pitch propeller.

2.2 HISTORY OF THE MODERN VARIABLE PITCH PROPELLER

To further add on to the points made in the previous section, William F. Durand, who served as the chairman for N.A.C.A., stated in 1918 that “the invention of such a device is of the highest order of importance” [10]. It was found in the early years of research that propeller blades could use the Aerodynamic forces felt to physically twist the blade, but there was no way of controlling the pitch change. Coupled with the advancements in engine technology, propellers were seeing higher aerodynamic loads from spinning at higher RPM. These factors required there to be a thinner airfoil selection. The common material for prop production at the time was wood due to its cheap and easy to manufacture nature, but also had good strength at low speeds due to the propellers thickness but did not have the strength needed for high speeds. The higher RPMs seen with the newer engines required something closer to the strength of metal. Production of metal propellers was a strong topic of research at the time.

Frank Caldwell was the leading researcher on propellers in America if not the world. After graduating from MIT in 1912, Caldwell went on to work briefly at Curtiss Aeroplane and Motor Company before establishing himself at the McCook Field development facility in Dayton, Ohio. He is credited with several improvements in research methods and tests such as the “whirl test”, which is a destructive propeller test inside a wind tunnel, run at high speeds over long periods of time [10]. Some of his biggest accomplishments related to propellers themselves is the multi-piece propeller hub, which was instrumental in the development of the modern day variable-pitch system. The multi-piece hub allowed for individual blades to be produced and rotated as needed. This led to the development of what is called the “ground adjustable variable pitch propeller” [10].

Caldwell began developing variable-pitch propeller systems as early as 1919. There were several ideas and inventions across the world seemingly simultaneously presenting new variations

of devices capable of the feat. One of the most promising to Caldwell was by Seth Hart and Robert I. Eustis in 1917, which consisted of a cable controlled by the pilot connected to the propeller hub. This, however, quickly suffered from mechanical wear and "there was considerable difficulty with adequate retention of its wooded blades" [10] which ultimately led to the projects abandonment in the early 1920s. Wallace Rupert Turnbull of Canada is credited by some as demonstrating the first use of inflight variation, which is outstanding considering most of the research was done in his backyard shed. Caldwell received a patent on his own mechanism in 1922. His mechanism was two-position mechanically actuated that had "better cable retention" than those developed by others.

In 1929, Caldwell patented another mechanism, this one being a two-position hydraulically actuated. Once his design was revealed, it was largely rejected by the aircraft community, especially by Boeing engineers. The common thought, for good reason, was that hydraulic systems were large and heavy.

Caldwell was able to demonstrate his two-position system on the Boeing 247 Monomail. Initially the first "modern" [10] aircraft was using the ground adjustable system. It was discovered that having the pitch set to cruise would not allow the aircraft to even get off the ground, requiring the pilots to compromise with a propeller setting that suffered in performance in both flight regimes. This compromise kept the plane from reaching the required 6000 ft. altitude to make the flight over the Rocky Mountains. After Caldwell was sent to investigate the issue, the hydraulic system was added to the Monomail and its performance was drastically improved, reducing the takeoff distance by 20%, increasing rate of climb by 22% and increasing overall cruise speed by 5.5%, allowing the aircraft to reach the intended altitude [10]. This in turn showed the aviation community the importance of his system, and that the benefits outweighed the added complexity and weight. The final iteration of his design incorporated a governor that controlled the pitch based on RPM, and was the original constant speed propeller used today,

called the Hydromatic propeller. This system uses the engines oil pressure in a hydraulic system to change the pitch according the engine speeds being produced. Figure (10) shows a basic example of how the system operates.

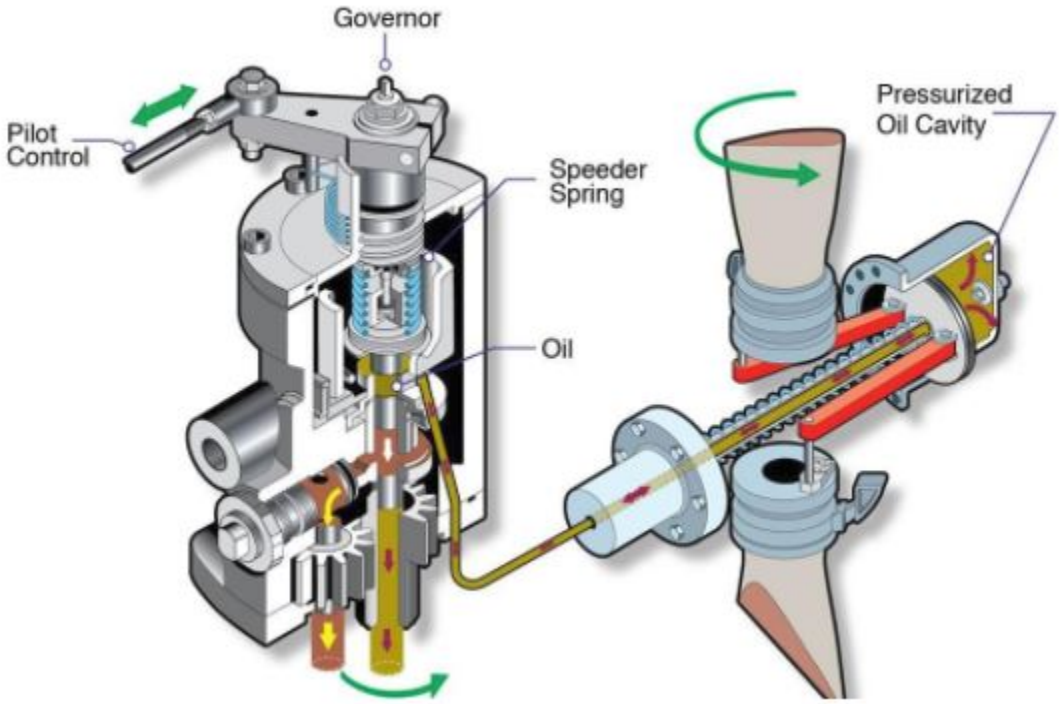

Figure 10 Example of the modern Constant Pitch system [12]

The governor in the figure is set to be steady at a particular RPM set by the pilot. At steady state, the flyweights expand f the engine over speeds, shown in figure (11) or contract if the engine under speeds, shown in figure (12), according to the centrifugal force experienced. This allows the oil pressure go to or from the propeller to change the pitch accordingly.

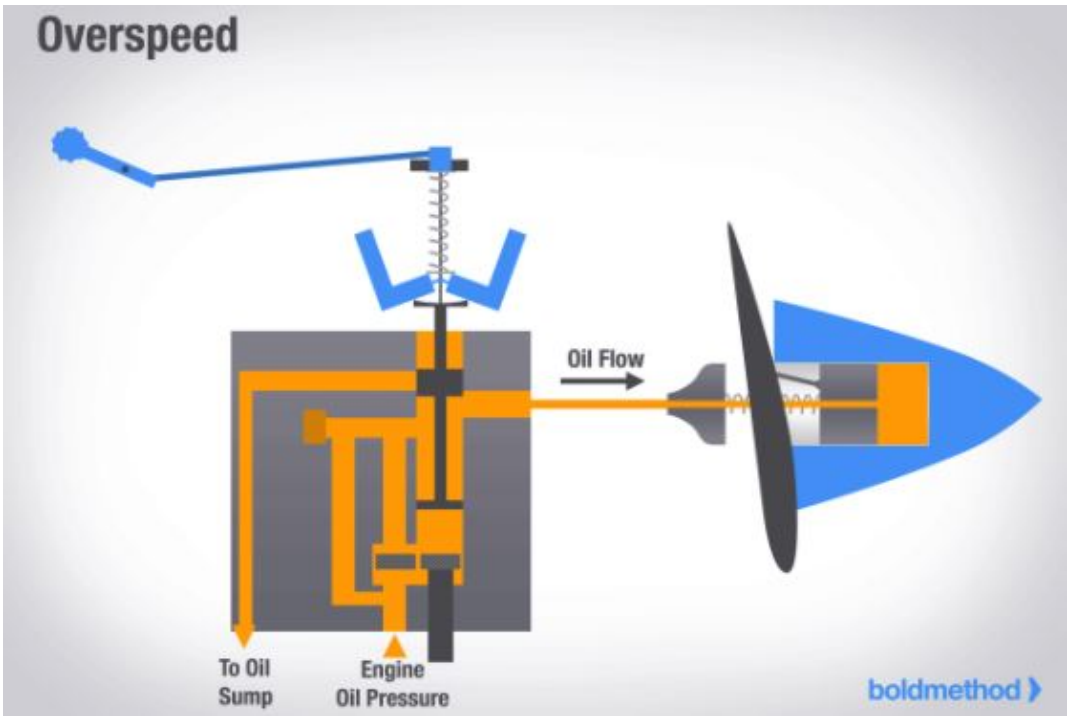

Figure 11 Over sped governor pitch change [14]

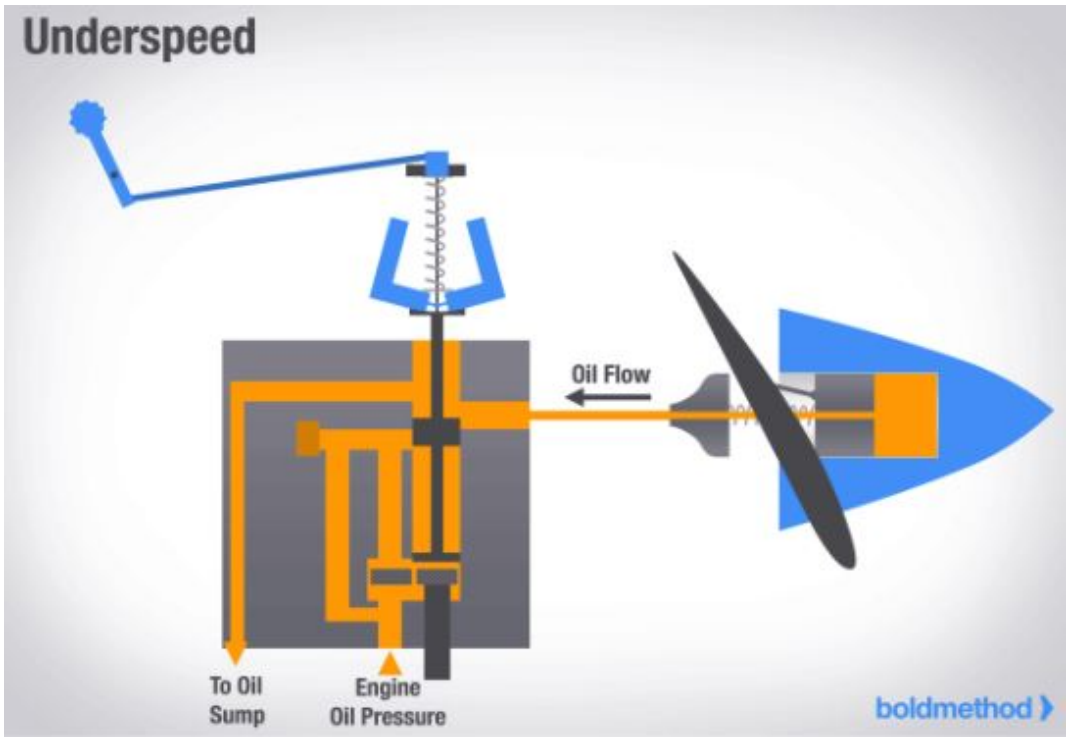

Figure 12 Under sped governor pitch change [14]

2.3 LITERATURE REVIEW

Modern systems for varying the pitch of a propeller just aren't viable for use in most unmanned systems. Most of small scale UAVs rely on electric propulsion, and even those that rely on an internal combustion engine lack the hydraulic systems needed by modern systems, i.e. the fuel is usually an oil gas mixture. Several articles were reviewed over systems that could allow for a passive pitch change without the complexities of their larger counterpart.

2.3.1 CONSTANT TORQUE PROPELLER

In an article by Burger and Hartfield from Auburn University [23], a mechanical device to passively change the pitch based on the torque output is examined. This study was centered around maintaining constant torque for an engine-propeller combination by sizing a constant torque spring and using this to change the pitch of the propeller based on the torque seen by the propeller. The engine used was a Hacker A30-10XL. There were several propellers examined before the authors settled on the CAM 13x7. The mechanism itself can be seen in figures (13) and (14). The propeller blades are attached to a central hub with beveled gears translated to the central motor shaft. The torque spring is attached to the motor shaft base. As the motor spins, the torque seen by the propeller is provided by the torque spring. If the torque on the propeller is higher or lower than what the torque spring provides, then the pitch is inherently changed until the two torques equal each other.

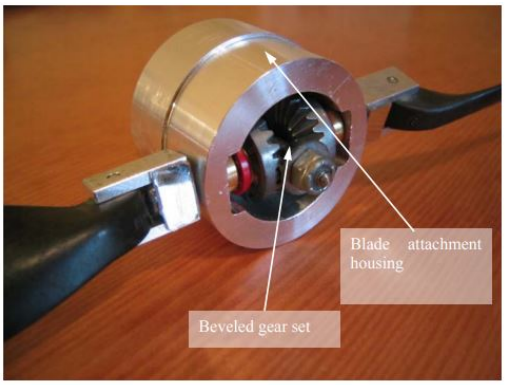

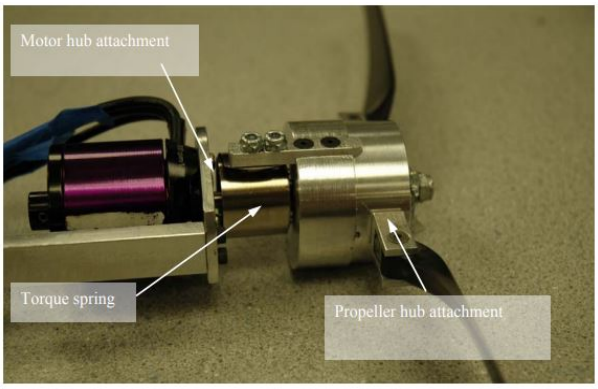

Figure 13 Gear system for pitch change [23]

Figure 14 Torque spring and system assembly [23]

The experiment began with both a static test and a wind tunnel test at 60-ft/sec of the engine-propeller combination to find the highest thrust to torque output. A max static thrust of approximately 1.2-lbf was found at a torque of 1-in-lbf while the forward flight test found a max thrust at a torque of about 1.25 -in-lbf. [23]. It should be noted that the simulated forward flight speed resulted in a relatively constant thrust output from the point of max static thrust. This lead to the assumption that the system would be optimized for static conditions, with the thrust being near the maximum for forward flight conditions [23].

Two tests were then run to compare fixed pitch to both a variable pitch propeller as well as the passive mechanism. The first test between a fixed pitch variant and the variable pitch counterpart was performed to show the benefits of having a variable pitch propeller. The pitch was changed manually for a static test as well as at 60-ft/s free stream speed [23]. The second test implemented the designed mechanism and compared it to the fixed pitch variant at similar free stream speeds as the first test. The power provided by the motor was set to a constant .076 horsepower for each test. The results of this test can be seen in figure (15). It's obvious that the mechanism provides improved performance over the fixed pitch variant for all free stream speeds starting from static position.

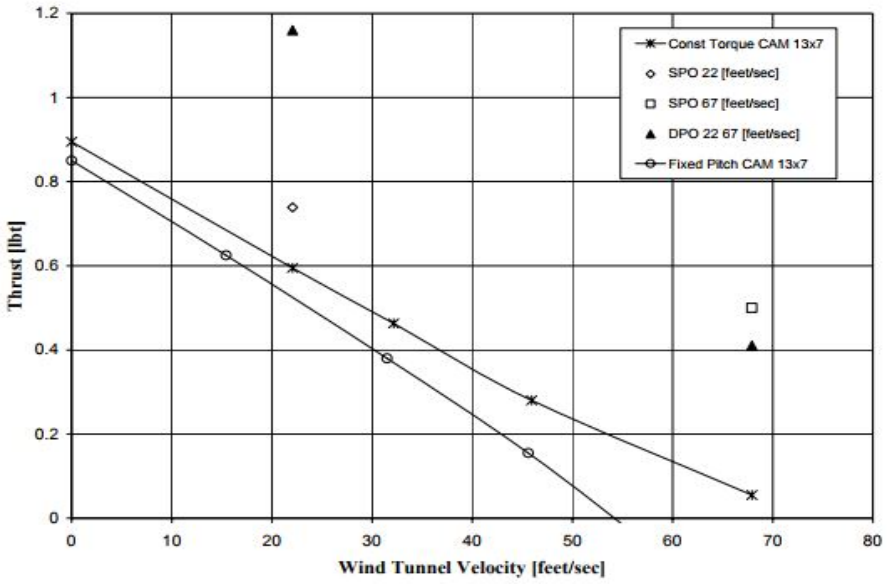

Figure 15 Constant torque performance results [23]

2.3.2 PASSIVELY VARYING A PROPELLERS PITCH FOR SMALL UAS

In another study at North Carolina State University [13], Heinzen, Hall and Gopalarathnam developed a model for a propeller design that utilizes the characteristic pitching moments of an airfoil to initiate a change in pitch across a range of advance ratios based on the propeller aerodynamics. This design is inherently passive as the driving force is related to the flow. This is achieved by tailoring the governing moment equations for the airfoil to have a "pitching –moment equilibrium point at a positive-lift point", and the blade pitch angle, upon being disturbed must tend back to its equilibrium point" [13]. Further deriving the equations, it is found that the pivot point (point at which the blade itself rotates about) must be behind the aerodynamic center.

A computational analysis was then conducted using available propeller codes. Initially two codes were under consideration for use, one being QPROP from MIT, and the other being a code developed at the Air Force Research Labs [13]. QPROP uses blade element theory as well as vortex calculations to give performance results [13]. The code from AFLR uses a similar blade

element method but is coupled with basic momentum calculations [13]. QPROP was ultimately chosen for its inclusion of vortex calculations. By adjusting the moment equations in QPROP, the researchers were able to produce the theoretical performance values of a Graupner 10 x 8 Cam Slim propeller at various pitch angles versus the performance of a variable pitch version of that same propeller to show the potential envelope expansion, which can be seen in figure (16).

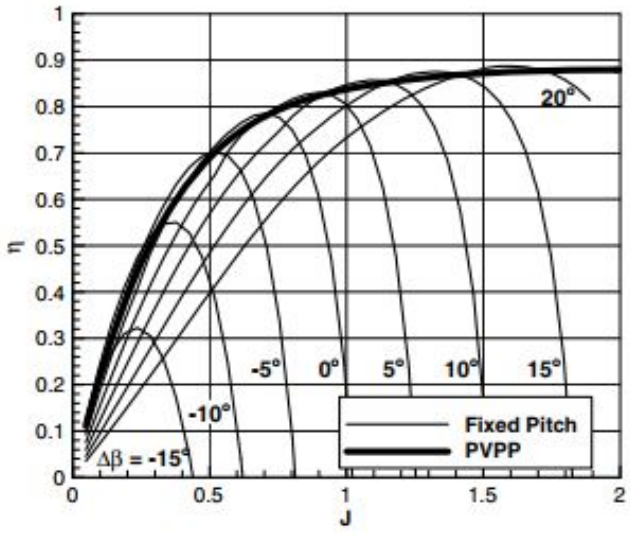

Figure 16 Designed efficiency parameters [13]

Once the code was developed, a physical model of a propeller was then designed and constructed. The airfoil chosen for the design was the Eppler 325 reflexed airfoil [13]. A reflexed airfoil is one that has positive a positive pitching moment. The remaining geometry of the propeller blade was then found, mainly the amount of twist and the sweep of the blade planform. Figure (17) shows different sweeps associated with the planform being held straight at 20%, 50% and 80% of the chord line respectively, with the 80% chord line being the chosen planform. The propeller diameter was initially designed at 20 in but was reduced to 18 in to keep the tip from being too flat [15] [13]. A mold was then created with the given propeller geometry, and propeller blades constructed using fiberglass and unidirectional carbon tow [13]. The mechanism if left alone would feel the effects of a mass imbalance about the pivot axis, which would have a

negative impact on how the propeller rotates. To counter this, a series of weights were added to the base of each blade to act as a C.G. and inertia balance.

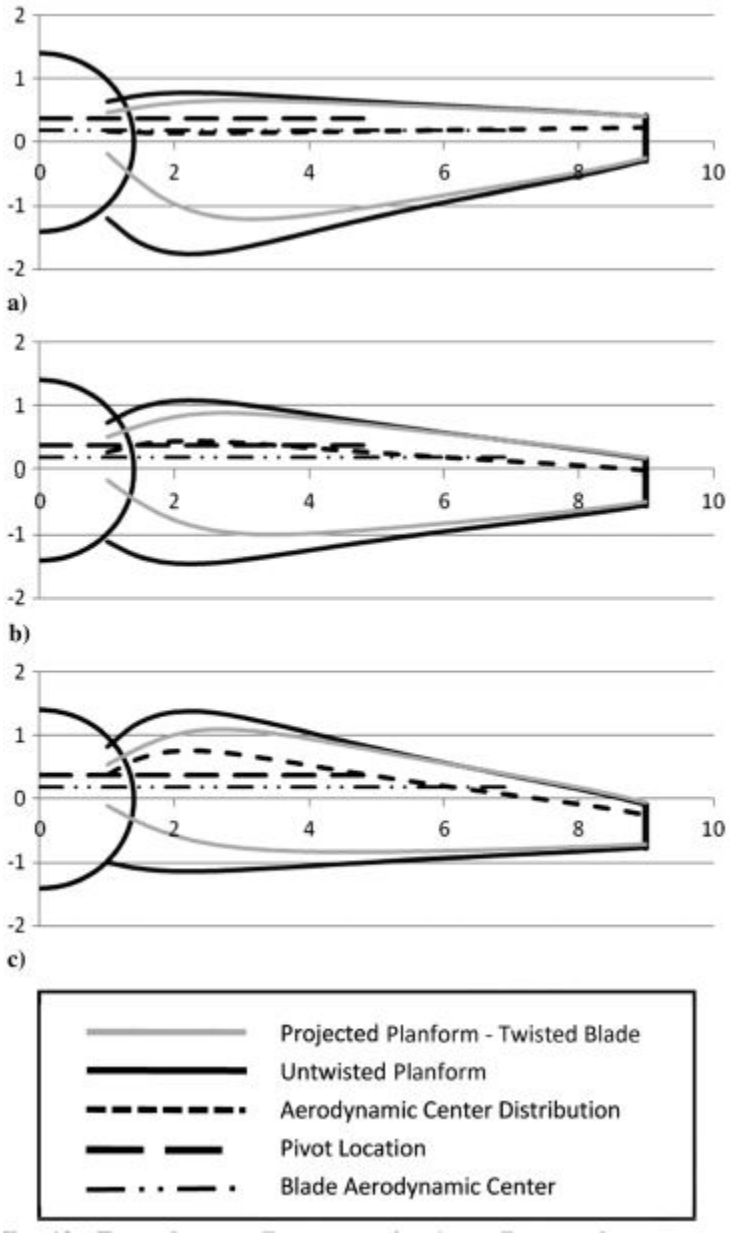

Figure 17 Planform for proposed propeller [13]

The motor used for testing was a custom made electric engine that provided up to 25-lbf of thrust and 1 ft. lb. of torque [13]. The propeller was intended to be tested in a wind tunnel at 3,000, 4,000 and 5,000 RPM with a free stream speed of 50 feet per second. The first two test

parameters were performed without issues, but the third test at 5,000 RPM had difficulties. The vibration on the mechanism was too much and the synchronization gears would slip, resulting in this parameter being discarded [13]. Figures (18) shows the results of these tests. Both figures show the performance of the designed propeller against its theoretical performance as well as the performance of the blades at given pitch angles. It can be seen that the designed propeller outperforms its fixed pitch counterpart over a range of advance ratios.

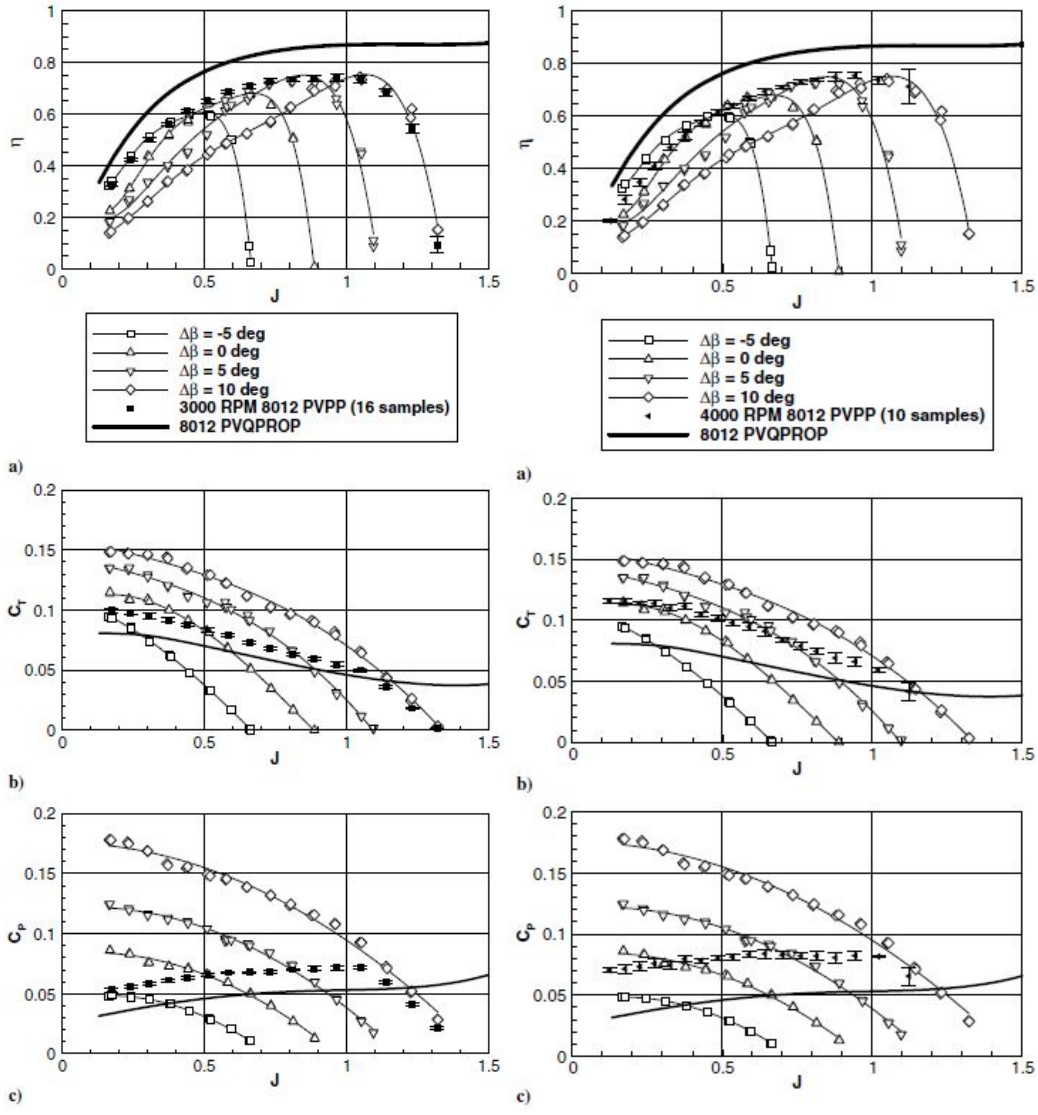

Figure 18 PVPP performance vs fixed pitch and predicted values [13]

One of the key features of these designs focuses around “small” UAVs. As with the constant torque design, the max thrust seen for the initial design only reached a max static thrust of 1.25-lbf. Both designs rely on having a constant variable; Burger and Hartfield held the engine at a constant torque while Heinzen, Hall and Gopalarathnam held the propeller aerodynamics at a constant moment. One area lacking adequate inquiry is a mechanical system capable of passively varying pitch. For typical aircraft, there are two main areas of performance during a flight: take-off and cruise. We find that at low to static forward velocity optimum efficiency occurs at lower advance ratios, requiring a high angular velocity. A finer pitch propeller or one with a smaller angle of attack achieves this, as it reduces the load on the engine. For cruise, however, a more coarse pitch is required as optimum efficiency occurs at higher advance ratios. A mechanical system can be designed to have binary actuation according to the RPM requirements of each mission leg, thereby improving the efficiency during these two stages.

CHAPTER III

DESIGN AND METHODOLGY

3.1 METHODOLOGY

Defined by the Department of Defense, unmanned systems are divided into five groups Figures (19) and (20) show how unmanned systems are classified and examples of each. The variable pitch design proposed encompasses group 2 UAVs, having a max gross takeoff weight less than 55 pounds with a velocity less than 250 knots at an altitude under 3500 feet above ground level. Examples of group 2 craft include the Scan Eagle. For reference, group 3, 4 and 5 systems are equivalent to the Tiger Shark, Predator, and RQ-4 Global Hawk respectively.

UAS Category	Max Gross Takeoff Weight	Normal Operating Altitude (Ft)	Airspeed	Current Army UAS in Operation
Group 1	< 20 pounds	< 1200 above ground level (AGL)	<100 Knots	RQ-11B Raven
Group 2	21-55 pounds	< 3500 AGL	<250 Knots	No current system
Group 3	< 1320 pounds	<18,000 mean sea level (MSL)		RQ-7B Shadow
Group 4	> 1320 pounds		Any Airspeed	MQ-5B, MQ-1C
Group 5		> 18,000 MSL		No current system

Figure 19 UAS Group categories [16]

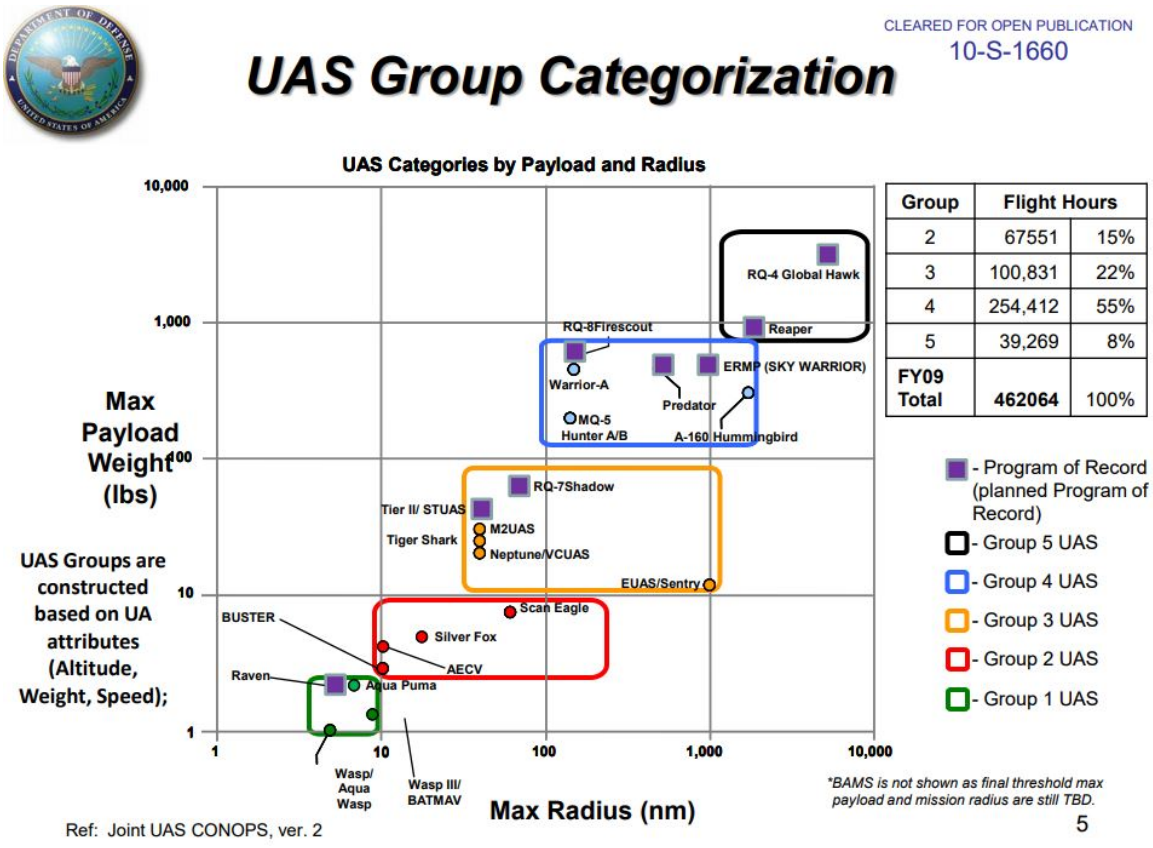

Figure 20 Example aircraft for UAS groups [16]

Systems exist already for manual pitch change. Most unmanned systems at the group 2 level and below use a ground based actuation system, meaning the pitch is changed between flights. This does not provide the benefits of in-flight variation and the ultimate purpose of having variable pitch capable propellers. Since small-scale systems do not have some of the same capabilities as larger aircraft engines such as monitored oil and manifold pressure, as well as a hydraulic system, options of determining when pitch variation should occur are limited. One option is to monitor the RPM of the propeller. Both passive designs and manual actuation by way of remote servos can use this method. Several options were explored before determining the best design option to pursue.

3.1.2 DESIGN OPTIONS

First, it was determined that a passive route was best to alleviate operator workload. It was also determined that for simplicity, the optimal RPM for cruise and takeoff should be the only two design points on the basis that these two points are where engine performance is most critical. One of the first options explored involved using an optical sensor to determine RPM of either the propeller blades or the motor shaft. A microcomputer system, such as the Raspberry Pi, would then use this data to actuate the pitch change once the relevant RPM is reached. Some issues with this type of system are its complexity as well as its reliability. Using a computer system that relies on a given code to operate introduces error and the infamous "ghost in the machine" which refers to digital machines acting on their own due to accumulated error. Robustness is also called into question. If any of the sensors involved were moved in any way or disconnected from the rest of the system, the system would fail. Another design option is a mechanical system utilizing the RPM by centrifugal force to actuate pitch change. Designs following this model are also complex with the increase of moving parts, but tend to be more robust and reliable.

One problem faced by all options is the method of actuation. One type of aircraft that makes use of variable pitch propellers even at a small-scale hobbyist level are rotorcraft. Helicopters utilize swash plates on both the main rotor and tail rotors. A swash plate gives the ability to change the pitch of a propeller blade depending on its location during rotation. Initially, a swash plate approach was taken but required modified spacers attached the propeller mount to allow room for the extra hardware needed. This would require changes made to existing airframes built to accommodate certain engines sizes. The added hardware would add weight to both the digital and mechanical design options and deemed excessive and complex. A swash plate design was discarded in favor of a design that could be integrated into the propeller hub, therefore removing any added hardware and changes to airframe. What ultimately separates digital and

mechanical actuation is the ability to be included in the propeller hub. For this reason, a mechanical approach was determined as the best design option to pursue.

3.1.3 DESIGN CONCEPTS

Several designs have already been discussed. Digital and mechanical systems outside of the propeller hub were discarded because of reliability and complexity. Centrifugal force is provided by the RPM is needed in order for a mechanical device to be implemented within the hub. Several designs were explored using this concept.

The initial design utilized springs attached to a central mount built into the propeller base plate. Weights connected to linear bearings were then attached to the springs. As the angular velocity increased, the weights would pull away from the central mount along the linear bearings. The pitch would be changed based on the distance the weight traveled. A basic illustration of this concept can be seen in figure (21). There were several issues with this design however, the main being reliable and consistent synchronized pitch change across each blade. In order for balance to be maintained, two or more spring-mass combinations needed to be implemented. The addition of each spring-mass combination added a new independent variable that needed to operate harmoniously with each of the other variables. In the event one combination performed outside of its design parameters, the aerodynamic forces of the propeller blades would change with respect to other blades as well as the balance within the hub. In an attempt to mitigate this, a gear system was implemented in order to synchronize the blade rotation. Ultimately the entire system had too high of complexity to be implemented effectively and consistently.

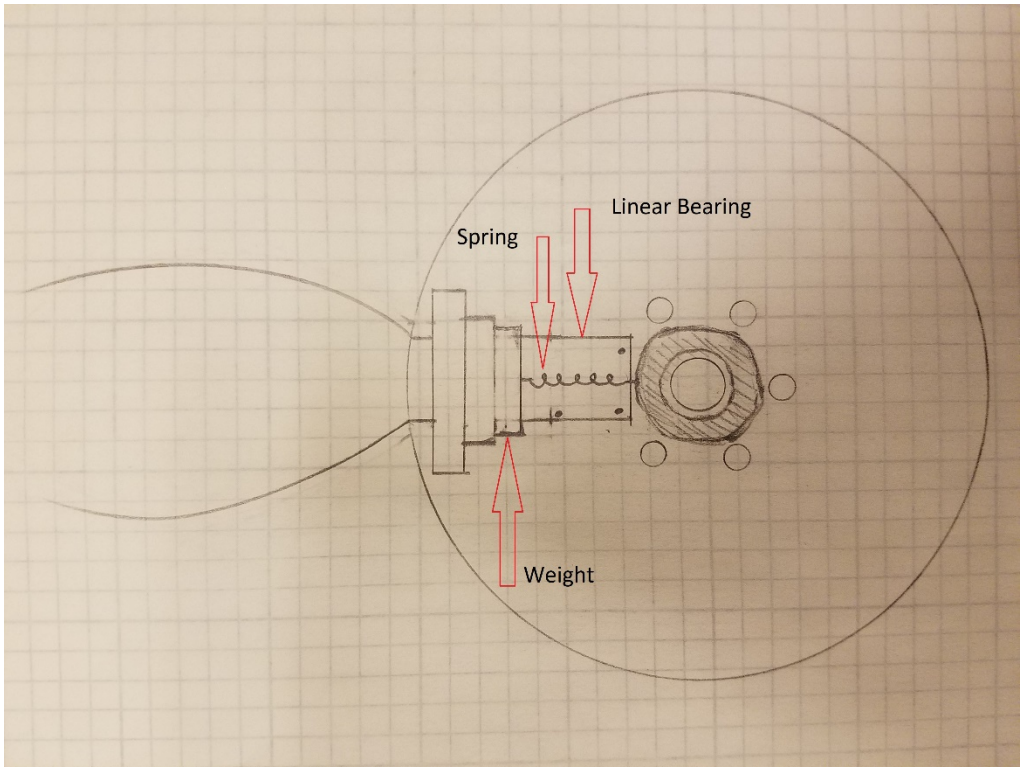

Figure 21 First design attempt

The centrifugal governor has been widely used since the late 1700s. Circa 1787, Thomas Mead received a patent for his centrifugal governor to control the rotation of a windmill [17]. James Watt later used this design with the addition of a throttle control valve with the intent of controlling the amount of steam entering the pistons of the steam engine. This invention later became known as the Watt governor. Several other governors have since been invented and continue to be used today. Modern turboprop aircraft use a Hartnell governor in order to maintain optimum angular velocity by adjusting propeller pitch. Centrifugal governors have a mechanical advantage of having centralized actuation allowing for synchronized movements. As the weights change from their initial, a sleeve is then lifted which can be designed to have links to various moving parts and have synchronous movement among each part, limiting the number of independently moving parts. This design option was chosen because of this unique trait coupled with placement within the propeller hub.

3.1.4 TYPES OF CENTRIFUGAL GOVERNORS

3.1.4.1 PENDULUM OR GRAVITY ASSISTED

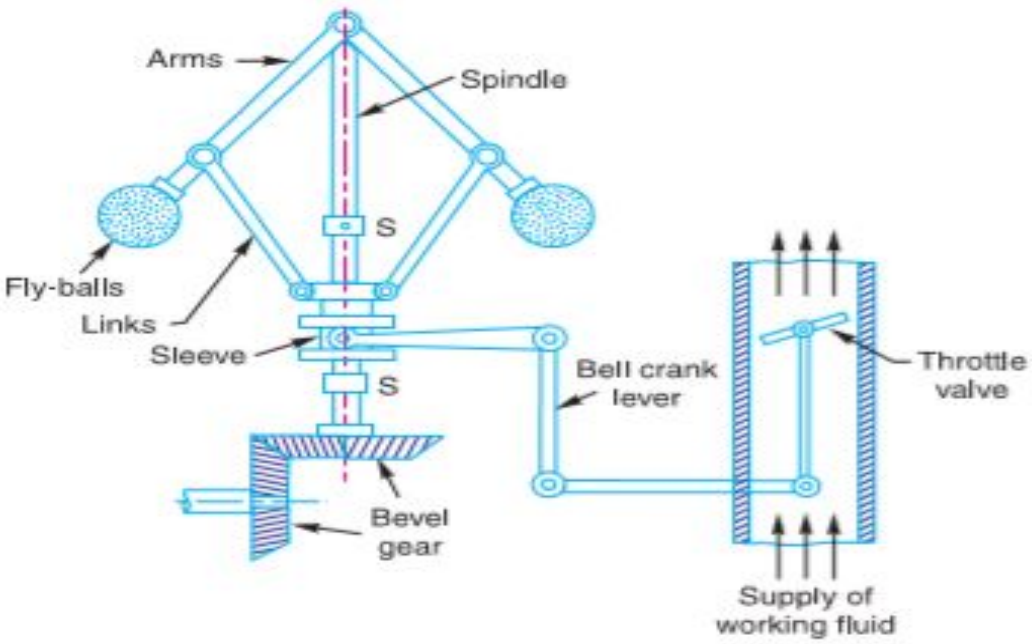

Figure 22 Watt Governor [18]

The best-recognized gravity assisted governor is the Watt governor, shown in figure (22). The term gravity assisted derives from the mechanisms dependence on gravity to return the arms to their lower starting positions. The first use of the Watt governor functioned as a throttle valve control for the steam engine. As the angular velocity increases, the flyweights depicted rise, lifting a sled causing a change in the throttle valve position. When performing an analysis on a Watt governor, the sleeve, or sled, along with the linking arms connecting the sleeve to the flyweights are assumed to have negligible mass. Applying a moment balance about the uppermost connecting point, point O, the governing equation is a function of the centrifugal force F_c, h, the height from the center of mass of the flyweights to point O, the weight of the flyweights and the radial distance of the weights center of mass from the axis of rotation and is listed as

$$F_c \times h = m \times g \times r. \tag{3.1}$$

The centrifugal force F_c is a function of the flyweight mass, radial distance and the angular velocity ω.

$$F_c = m \times r \times \omega^2. \tag{3.2}$$

The distance the sleeve travels is important to the proposed design, as it will be responsible for change in pitch acquired. An interesting characteristic of the Watt governor is its independence of the flyweight mass. Solving for the height at a particular time of operation, h becomes a function of gravity and the angular velocity,

$$h = \frac{g}{\omega^2}. \tag{3.3}$$

3.1.4.2 LOADED GOVERNORS

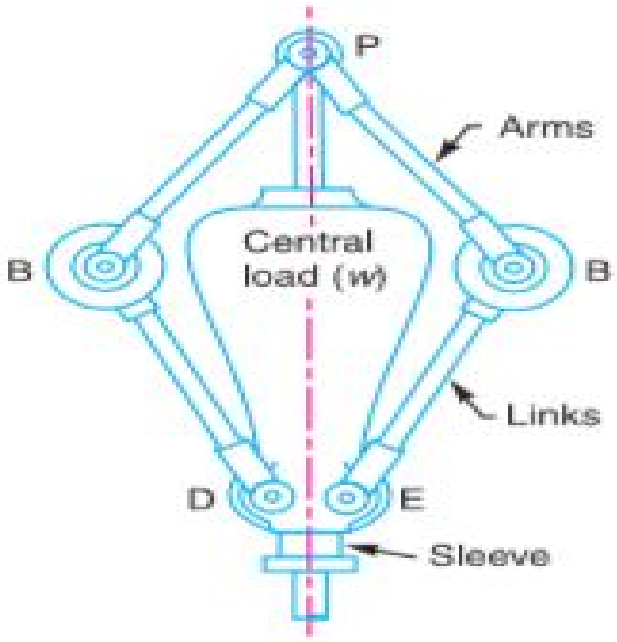

Figure 23 Porter Governor [18]

A variation of gravity-assisted systems is the loaded governor. This type is divided into three subsystems that are identified as dead weight and spring loaded. The Porter and Proell are examples of deadweight while the Hartnell is a spring loaded. Examples of each can be seen in

figures (23). The Porter governor has a central load around the central axis adding resistance to the sleeve. Assuming the lengths of all arms are equal and reanalyzing with the mass of the weights m and the central load M, the height equation becomes

$$h = \frac{m+M}{m}\frac{g}{\omega^2}. \tag{3.4}$$

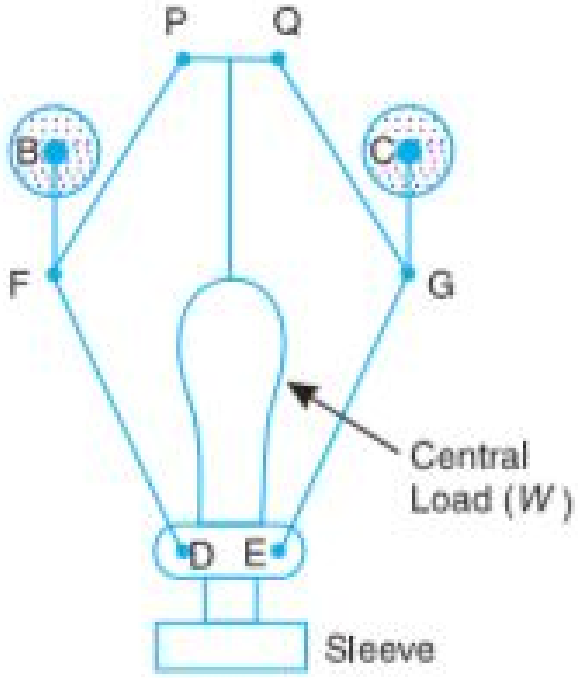

Figure 24 Proell Governor [18]

The Proell is a variant of the porter governor where the flyweights attach to a vertical extension above the connection point, adding a level of sensitivity not seen by the Porter. Assuming the primary arms are equal, the height equation becomes a function of flyweight and central load mass, gravity, and angular velocity with the addition of the ratio of the vertical length from the center of the flyweight mass to the base and the vertical length of connection point F to the base,

$$h = \frac{FM}{BM}\left(\frac{m+M}{m}\right)\frac{g}{\omega^2}. \tag{3.5}$$

The biggest detriment to the governors discussed is the one factor they rely on to function; gravity. Because of this requirement, these systems need to be upright throughout operation. When lean is applied, friction losses begin to overtake the governor's ability to lift the weights or sleeves. Since aircraft operate at various angles of attack, these options are not suitable for use, especially since the proposed design will attach directly to the engine or motor shaft typically at a horizontal orientation. The Hartnell governor relies on spring loading in the place of gravity, offering a more practical application. Mentioned earlier, modern propeller aircraft utilize this type of design.

3.2 HARTNELL DESIGN

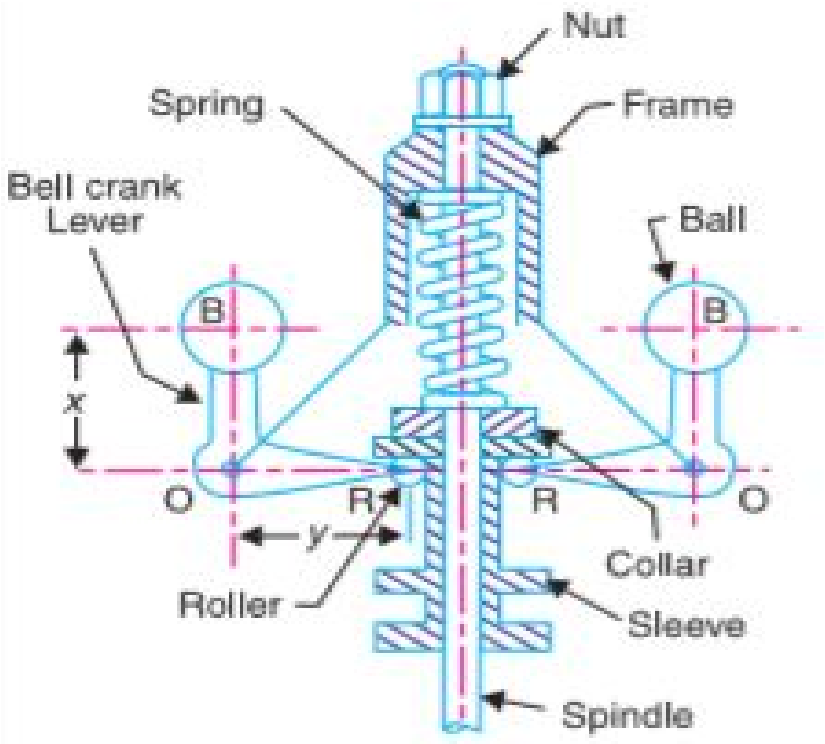

Figure 25 Hartnell Governor [18]

The conventional Hartnell design uses two or more arms called "Bell Crank Levers" that rotate individually about separate points according to the systems angular velocity to lift a collar against a spring. Typically the levers are attached to the frame about their points of rotation. The governor can be adjusted by adjusting the nut on top of the device, which is connected to the

spring, changing its spring constant. This alters the angular velocity required to activate. This allows an engine to maintain constant RPM throughout use. For instance, if the RPM set by the pilot is 4000, but the current RPM reads 5000, then the levers rotate compressing the spring and lifting the sled or collar. This opens a channel, and using the pressure differential from the engine, allows oil to flow either to or from the device that actuates pitch change. In this case, the pitch would become coarser adding a higher load to the engine and reducing the RPM. Likewise if the RPM drops below the given setting, the reverse happens and the levers rotate inwards, allowing for oil to flow in the opposite direction as before and rotating the propeller blades to a finer pitch.

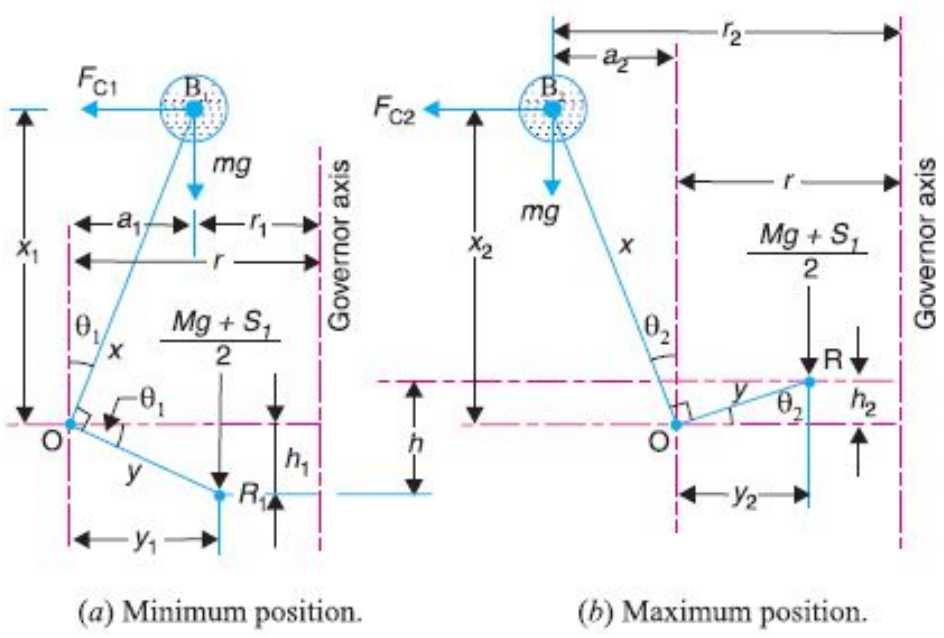

Figure 26 A). Min position of Hartnell arms, B). Max position of Hartnell arms [18]

The geometry and statics of the Hartnell governor are very basic. To maintain conventional nomenclature, the variables x and y in all figures referencing the Hartnell governor are switched in the defining equations. It's important to note that the height of the lever arm is from the point of rotation to the center of mass of the flyweight and that the horizontal arm does not extend to the center of the hub. The minimum and maximum positions are defined by the moments about point O in the following equations:

$$\frac{M\times g+S_1}{2}\times x_1 = Fc_1 \times y_1 - m \times g \times a_1, \tag{3.6}$$

$$\frac{M\times g+S_2}{2}\times x_2 = Fc_2 \times y_2 + m \times g \times a_2. \tag{3.7}$$

Where M is the mass of the collar or sled, m is the mass of the weights, S is the spring force experienced and Fc is the centrifugal force all at the respective geometric positions for either the minimum (represented by the subscript 1) or the maximum (represented by the subscript 2). The obliquity of the arms refers to the angle between the weights and the point of rotation. Based on the small angle theory, obliquity effects and the moment caused by the weights can be neglected, reducing equations [3.6-3.7] to the two equations:

$$\frac{M\times g+S_1}{2}\times x_1 = Fc_1 \times y_1, \tag{3.8}$$

$$\frac{M\times g+S_2}{2}\times x_2 = Fc_2 \times y_2. \tag{3.9}$$

Solving for and then subtracting the two spring forces gives [3.10]

$$S_2 - S_1 = 2(Fc_2 - Fc_1)(\frac{y}{x}). \tag{3.10}$$

The height, h, of the collar refers to the distance the collar is lifted and is defined geometrically as

$$h = (r_2 - r_1)\frac{x}{y}. \tag{3.11}$$

The spring stiffness is a function of the two spring forces and the height of the sled. Combining equations [3.8-3.11] gives the spring stiffness s, more commonly referred to as the spring constant, in equation [3.12]

$$s = \frac{S_2-S_1}{h}. \tag{3.12}$$

Understanding how much of an effect each component has on the systems operation is important in determining the values and proportions the components have and are easily found

via a simple sensitivity study. Using the governing equations in Excel's Visual Basic determined the impact of the three main aspects of the design on angular velocity; the height of the lever, represented by the variable y, the horizontal length of the lever arm represented by the variable x, and the mass of each flyweight. Each study increased the value of the variable incrementally while holding the spring stiffness and the two variables not being considered constant. The results are shown in tables (1-3).

Table 1 Y-axis sensitivity

y	ω(y)	% diff	r(y)
0.5	1.452173	0	2.37101
0.75	1.426676	1.787165	2.456515
1	1.402476	3.543489	2.54202
1.25	1.379468	5.270514	2.627525
1.5	1.357556	6.96966	2.71303
1.75	1.336656	8.642235	2.798535
2	1.316692	10.28945	2.88404
2.25	1.297598	11.91242	2.969545
2.5	1.27931	13.51219	3.05505

Table 2 X-axis sensitivity

x	ω(x)	% diff	r(x)
1.5	1.291696	0	2.99674
1.75	1.29151	0.014464	2.997607
2	1.291389	0.023838	2.998169
2.25	1.291306	0.030257	2.998554
2.5	1.291247	0.034846	2.998829
2.75	1.291203	0.03824	2.999032
3	1.291169	0.040819	2.999187
3.25	1.291144	0.042827	2.999307
3.5	1.291123	0.044419	2.999403

Table 3 Mass sensitivity

m	ω(m)	% diff	r(m)
0.5	1.026841	0	2.37101
0.75	0.726086	41.42136	2.37101
1	0.592847	73.20508	2.37101
1.25	0.513421	100	2.37101
1.5	0.459217	123.6068	2.37101
1.75	0.419206	144.949	2.37101
2	0.38811	164.5751	2.37101
2.25	0.363043	182.8427	2.37101
2.5	0.34228	200	2.37101

The first column of each table represents the length in inches of each variable. The second column denoted by the ω shows the angular velocity while the third column shows the percent difference each increments has compared to the initial result. The final column shows the maximum radius achieved by each. The horizontal portion of the lever has little to no effect on

angular velocity, where the mass of the flyweights have a severe impact. It is also clear that the vertical lever arm has a greater effect on the maximum radius.

Knowing the mass has the greatest impact on angular velocity allows the remaining components to be chosen without much concern for any adverse effects on the desired result. Table (4) shows the geometric optimization between the lever arm lengths and their resulting maximum radii when holding the flyweight mass and spring stiffness constant. Referencing figure (26), the intermediate radius, or the distance between point O and the center of rotation was chosen to be 2.3-inches for adequate room. The travel of the collar is also a design choice. Once a height is decide on it can be used in conjunction with the intermediate radius to determine the remaining geometry by defining the angle, theta. For definitive movement, a travel distance of .6-inches was chosen.

Table 4 Geometry Optimization

		X											
	0.8	0.8	1	1.2	1.4	1.6	1.8	2	2.2	2.4	2.6	2.8	3
Y	0.5	2.6	2.55	2.514286	2.4875	2.466667	2.45	2.436364	2.425	2.415385	2.407143	2.4	2.3
	0.75	2.75	2.675	2.621429	2.58125	2.55	2.525	2.504545	2.4875	2.473077	2.460714	2.45	2.35
	1	2.9	2.8	2.728571	2.675	2.633333	2.6	2.572727	2.55	2.530769	2.514286	2.5	2.4
	1.25	3.05	2.925	2.835714	2.76875	2.716667	2.675	2.640909	2.6125	2.588462	2.567857	2.55	2.45
	1.5	3.2	3.05	2.942857	2.8625	2.8	2.75	2.709091	2.675	2.646154	2.621429	2.6	2.5
	1.75	3.35	3.175	3.05	2.95625	2.883333	2.825	2.777273	2.7375	2.703846	2.675	2.65	2.55
	2	3.5	3.3	3.157143	3.05	2.966667	2.9	2.845455	2.8	2.761538	2.728571	2.7	2.6
	2.25	3.65	3.425	3.264286	3.14375	3.05	2.975	2.913636	2.8625	2.819231	2.782143	2.75	2.65
	2.5	3.8	3.55	3.371429	3.2375	3.133333	3.05	2.981818	2.925	2.876923	2.835714	2.8	2.7
	2.75	3.95	3.675	3.478571	3.33125	3.216667	3.125	3.05	2.9875	2.934615	2.889286	2.85	2.75
	3	4.1	3.8	3.585714	3.425	3.3	3.2	3.118182	3.05	2.992308	2.942857	2.9	2.8

The maximum radius is used to determine the overall size of the system with the smallest design being most optimal. However, for initial prototyping, a larger diameter system may be used with larger components being easier to work with for a proof of concept. The table above illustrates various geometric options. A maximum radius of three inches allows for larger components while not being overly large for the motor. This does require a larger overall hub radius, being 3.5

inches to completely contain the system. The dimensions were chosen remembering that the vertical arm extends to the center of mass of the weight while the horizontal arm does not extend to the center of the hub. The angle, θ, between the horizontal arm and horizontal plane after rotation is found by taking the sin of the height divided by the horizontal arm length. This angle is used to determine the horizontal distance the flyweight center of mass travels after rotation. Adding this distance to the chosen radius of 2.3-inches gives the maximum radius. The table above highlights four potential options. Ultimately, having a vertical arm length of 2-inches with a horizontal arm length of 1.5-inches was determined to be optimal as it allowed for smaller angles of rotation and .8-inches between the end of the horizontal arm and hub center giving adequate room without requiring an oversized collar or sled.

Equations [3.8], [3.9] and [3.12], are used to define a spring constant for given geometry and RPM requirements. The given geometry gives a value for theta of 23.57 degrees. Dividing this value in half gives 11.78 degrees on either side of the upright position allowing for clearly defined minimum and maximum positions. Two RPM design points were examined, 1000 for preliminary study and 5000 to closely match Group 2 unmanned systems operating points, where cruise is at some point below the activation point of 5000 RPM. Both points have 500 RPM added on to define the maximum position of the lever to allow for rapid actuation. Converting these values to angular velocities gives 104.7 radians-per-second and 157.0 radians-per-second for the preliminary study, and 523.5 radians-per-second and 575.9 radians-per-second for normal operations. The angular velocities are used to determine the centrifugal forces for the flyweights of various masses. Again using Excel's VBA, the equations are used in a loop for weights of varying mass starting from 1-gram to 550-grams. A spring constant is then determined for each mass used. This code was verified by comparing solutions to example problems in *Theory of Machines* [18]. Figure (27) shows an example of the inputs and outputs of the model.

	1	2	3	4	5	6	7	8	9	10	11
3		Metric (cm)	English (in)								
4	x0=	3.81	1.5		input a number greater than h				Input		
5	y0=	5.08	2						Output		
6											
7	Θ=	23.57817848	0.411516846								
8	Θ1=	11.78908924	0.205758423		Degrees below horizontal						
9	Θ2=	11.78908924	0.205758423		Degrees above horizontal						
10	r=	5.842	2.3		Intermediate radius						
11	r1=	4.80410701			Min radius					CommandButton	
12	r2=	6.87989299			Max radius						
13	h=	1.524	0.6								
14					Min distance traveled by spring						
15	RPM1=	5000			Max distance traveled by spring						
16	RPM2=	5500									
17											
18	ω1=	523.5987756			Frequency per second						
19	ω2=	575.9586532			Frequency per second						

Figure 27 Example spreadsheet input

Figure (28) shows the results of the settings shown in the previous figure and gets a general sense of the end design. The mass and its respective diameter are used to determine a good relative size for a flyweight that would be large enough to work with. Ultimately a mass of .125-kg was chosen for simplicity. This mass was used to dial in specific a spring constant to use as a search criteria. At a minimum and maximum speed of 5000 and 5500 RPM, the spring constant is 206654.2 N/m or 206.6-N/mm for general commercial springs. Based on SolidWorks design, the spring required needed to have a minimum inside diameter larger than .625-in to allow for central structure with an outside diameter designed to fit a 1.25-in hole. A viable spring close to the requirements was not available for these higher speeds. The design RPM was reduced to 4000-4500 RPM. Keeping the mass the same gives a new spring constant of 146.6-N/mm. If the mass is kept the same, the only component that needs to be changed between different RPM ranges is the spring constant. The spring constant for a mass of .125-kg at 1000-1500 RPM is 25.06-N/mm. Comparable springs matching the required dimensions were found for the design RPM range of 131.2-N/mm and 27.49-N/mm for the preliminary study.

Spheres are an excellent choice for flyweights as the center of mass is known with a volume of:

$$V = \frac{4}{3}\pi r^3. \tag{3.13}$$

This equation can be rearranged to solve for the diameter with a density for steel of 7700 kg-per-meter-cubed and the given masses. A column was added to the spreadsheet to also show the diameters of the flyweights. The mass and its respective diameter are used to determine a good relative size for a flyweight that would be large enough to work with. Several options were cross referenced with material manufacturers to find a valid sphere that could be used, eventually finding a 1.25-inch diameter sphere with a mass of .129-kg.

	1	2	3	4	5	6	7
21	Point	M (kg)	Ball Diam (in)	Fc1 (N)	Fc2 (N)	k (N/m)	k (N/mm)
130	109	0.109	1.181622268	1435.61	2487.659	180202.5	180.2025
131	110	0.11	1.185224797	1448.781	2510.481	181855.7	181.8557
132	111	0.111	1.188805559	1461.951	2533.304	183509	183.509
133	112	0.112	1.192364878	1475.122	2556.126	185162.2	185.1622
134	113	0.113	1.195903074	1488.293	2578.949	186815.4	186.8154
135	114	0.114	1.199420456	1501.463	2601.771	188468.7	188.4687
136	115	0.115	1.202917328	1514.634	2624.594	190121.9	190.1219
137	116	0.116	1.206393987	1527.805	2647.417	191775.1	191.7751
138	117	0.117	1.209850722	1540.976	2670.239	193428.4	193.4284
139	118	0.118	1.213287817	1554.146	2693.062	195081.6	195.0816
140	119	0.119	1.216705547	1567.317	2715.884	196734.8	196.7348
141	120	0.12	1.220104183	1580.488	2738.707	198388.1	198.3881
142	121	0.121	1.223483991	1593.659	2761.529	200041.3	200.0413
143	122	0.122	1.226845227	1606.829	2784.352	201694.5	201.6945
144	123	0.123	1.230188146	1620	2807.174	203347.8	203.3478
145	124	0.124	1.233512995	1633.171	2829.997	205001	205.001
146	125	0.125	1.236820017	1646.342	2852.82	206654.2	206.6542
147	126	0.126	1.240109447	1659.512	2875.642	208307.5	208.3075
148	127	0.127	1.243381519	1672.683	2898.465	209960.7	209.9607
149	128	0.128	1.246636459	1685.854	2921.287	211613.9	211.6139
150	129	0.129	1.24987449	1699.024	2944.11	213267.2	213.2672
151	130	0.13	1.253095831	1712.195	2966.932	214920.4	214.9204
152	131	0.131	1.256300693	1725.366	2989.755	216573.7	216.5737
153	132	0.132	1.259489287	1738.537	3012.578	218226.9	218.2269
154	133	0.133	1.262661818	1751.707	3035.4	219880.1	219.8801
155	134	0.134	1.265818486	1764.878	3058.223	221533.4	221.5334
156	135	0.135	1.268959487	1778.049	3081.045	223186.6	223.1866
157	136	0.136	1.272085016	1791.22	3103.868	224839.8	224.8398
158	137	0.137	1.275195261	1804.39	3126.69	226493.1	226.4931
159	138	0.138	1.278290407	1817.561	3149.513	228146.3	228.1463
160	139	0.139	1.281370637	1830.732	3172.335	229799.5	229.7995
161	140	0.14	1.284436128	1843.902	3195.158	231452.8	231.4528

Figure 28 Example spreadsheet output

The equations provided use the desired RPM and given mass and geometry to determine the spring constant required. Since the constant is a function of the centrifugal forces at the minimum and maximum positions, which are themselves functions of angular velocity, the RPM

range is difficult to find if it is unknown and the spring constant is. If equation [3.12] is solved for ω_2, the resulting equation is:

$$\omega_2 = \sqrt{\frac{r_1\omega_1^2}{r_2} + \frac{shx}{2mr_2y}}. \tag{3.14}$$

where the only unknown variable is ω_1. Figures (29) and (30) show the resulting plots for both springs.

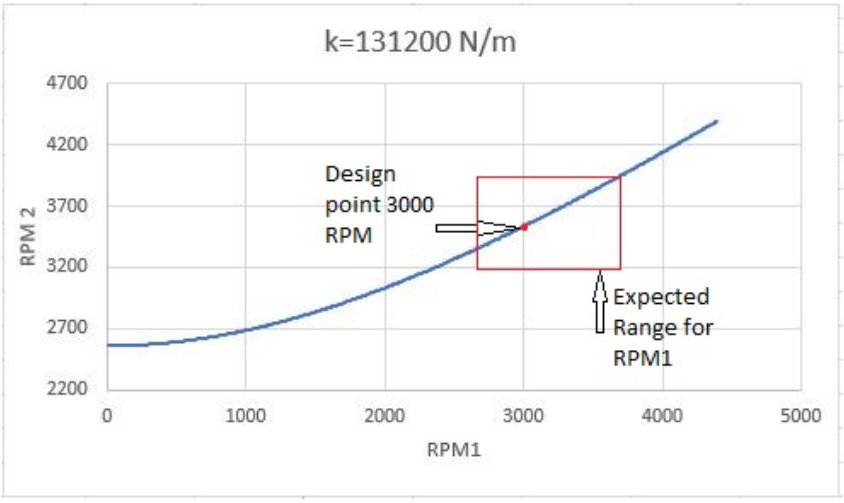

Figure 29 Potential RPM region

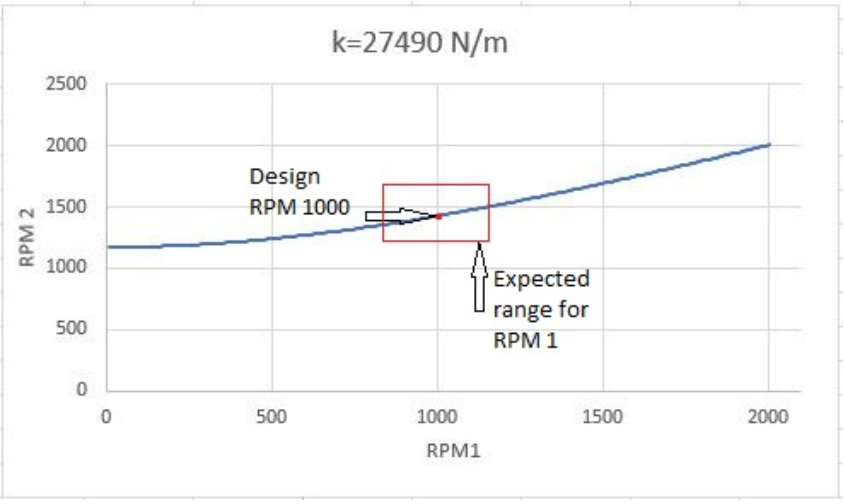

Figure 30 Potential RPM region

These plots show the RPM combinations that provide a solution for a given spring constant. If the reverse is Pin pointing the exact range from these values is very difficult. However, based on the original design point and taking into account the effect increasing mass has as well as the intuitive effect of increasing the spring stiffness, a general region containing the expected range can be determined. Exact values for the range can be backed out by using the spring constant and the movement height to determine the centrifugal force expected at the max position, Fc_2. This provides the angular velocity, ω_2. Substituting these values into equation [3.12] results in the angular velocity for the minimum position, ω_1. The following figures show the comparison between finding the angular velocities versus defining them.

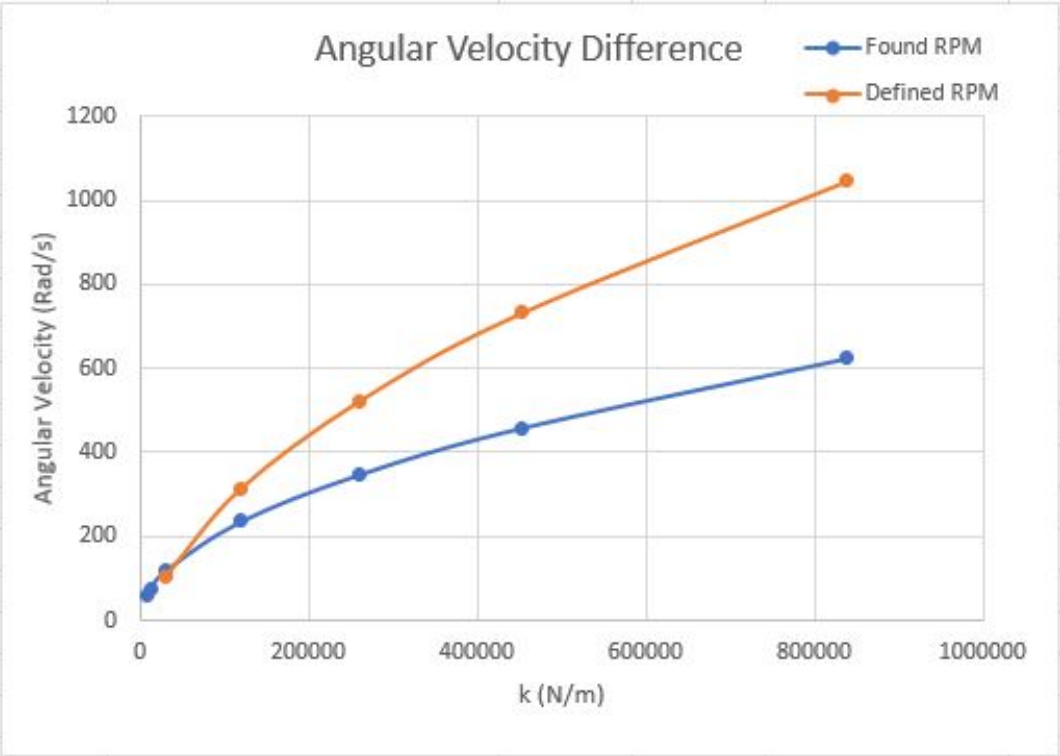

Figure 31 Difference in angular velocity between found and defined RPM

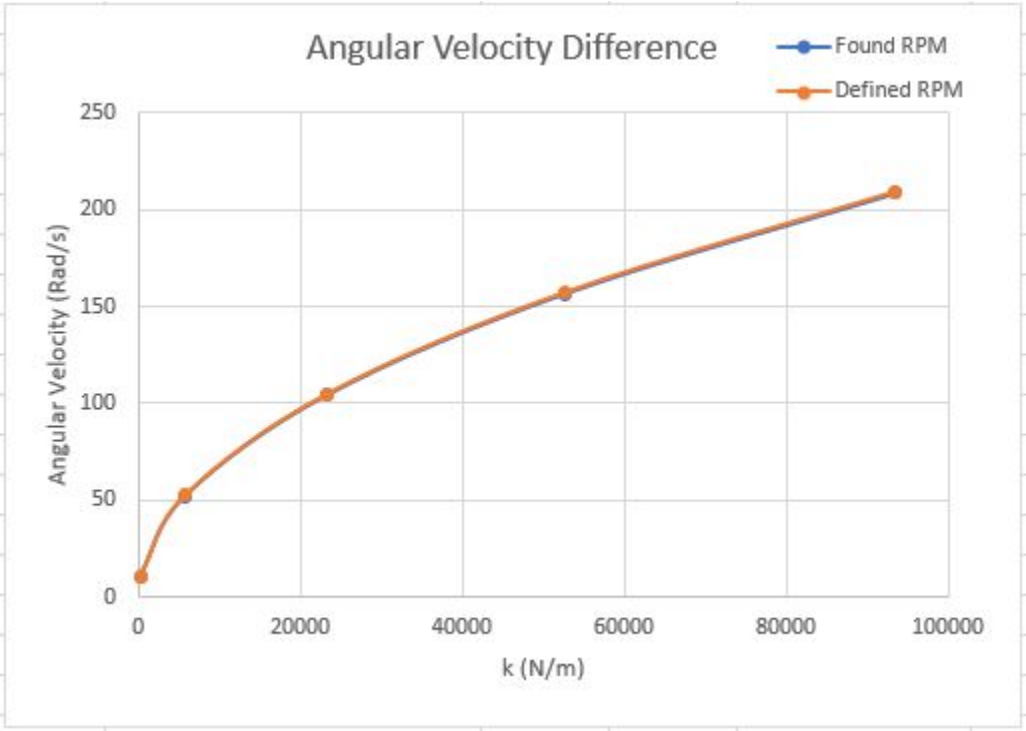

Figure 32 Difference between angular velocity when RPM ratio is used

Figure (31) shows a large discrepancy between the two methods that continues to diverge with increasing RPM. This method has an RPM difference of 500 between the max and min positions. Interestingly, a sweet spot scales with the RPM with each mass and geometries used. For a mass of .129-kg, increasing the second RPM by only 1.44 times the first RPM results in agreement between the two methods, shown in figure (32). Taking the spring constants of the two springs found, the resulting activation RPMs are 1814 for the large spring and 830 for the smaller spring. The drop in the required RPM is a result decreasing both the spring stiffness as well as increasing the mass of the flyweight for this larger spring. The increase in mass outweighs the increase in spring stiffness for the smaller spring.

3.3 SOLIDWORKS DESIGN

3.3.1 ITERATION 1: CONCEPTUAL DESIGN

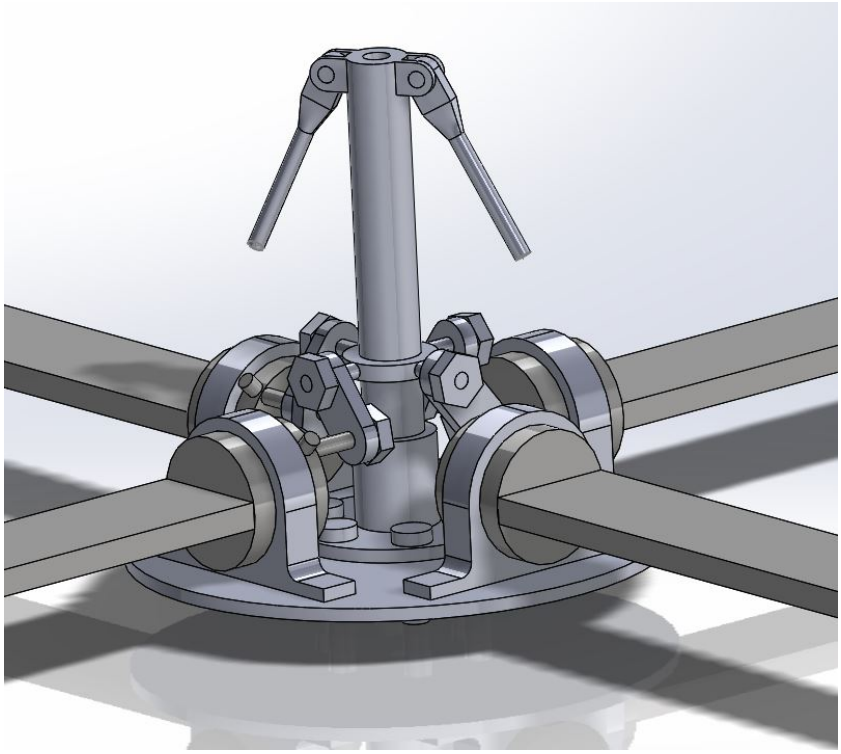

Figure 33 First CAD design- Watt

The initial conceptual design started with a simple watt governor style mechanism. Shown in figure (33). The design remains unfinished once the Hartnell design was found to be more favorable. Instead, it remains to show the evolution of the actuation mechanism. The central shaft contains what would have been the governor. The arms containing the fly-weights are attached at the top of the shaft and are in turn attached to the circular “shed” shown. The custom propellers are secured in rotary ball bearings which are themselves secured in bearing housing attached to the base plate. Each propeller has a plate which attaches at its base on the interior side of the bearing and has a pin which protrudes inward. These pins attach to the circular “sled” via linkages which are free to rotate about both connection points, allowing for linear to rotational motion. The linkage model ultimately contains too many points of failure, each of which could

yield a catastrophic result, such as loss of a blade and severe unbalanced aerodynamics. This system was discarded for a more favorable system which is less cluttered and reduces the number of potential failure points by half.

3.3.2 ITERATION 2

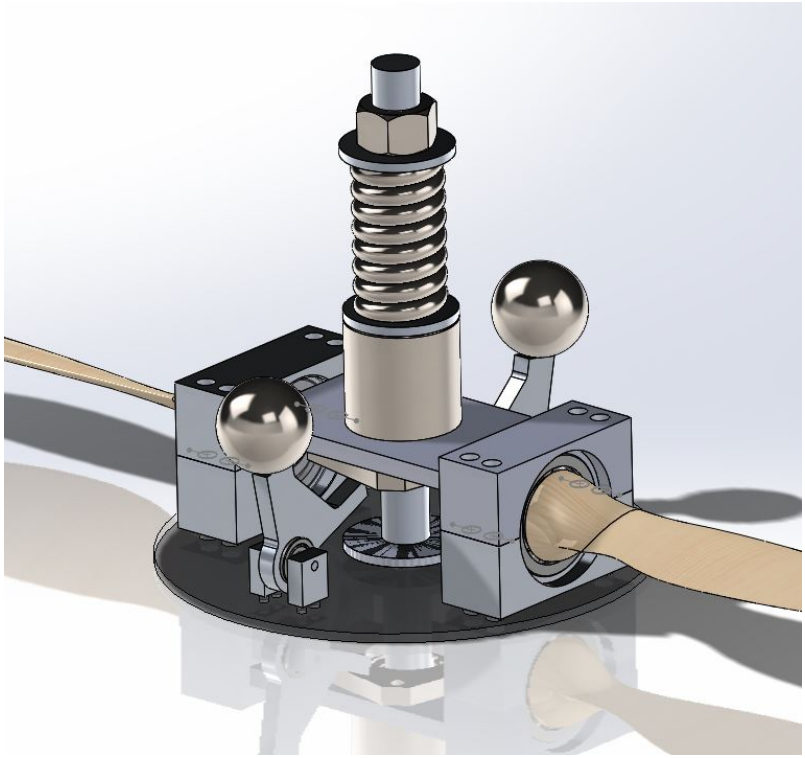

Figure 34 Second CAD design- Hartnell

Iteration 2 incorporated two major changes to the original design: the switch from a Watt design to a Hartnell and the method of translating linear motion to rotational. Figure (34) shows an example of the second iteration. This iteration was based on the geometries found using the excel model previously discussed. The overall diameter sits at 6.5 inches and is 6.75 inches tall. The central shaft has a diameter of .625-inches and is threaded to fit a .625-11 thread count nut. Attached to the nut is a flat washer or flat plate. This combination acts as the upper limit for the linear movement of the spring sled system. The spring is designed to have an inside diameter capable of loosely fitting the central shaft inside of it and rests on the top of the “sled”, which in

this case is the housing for a linear bearing. The entire central system is attached directly to the base plate and motor via the required bolt patterns for the motor mount. The flyweights shown were initially designed for .125-kg steel spheres. These weights are then attached to the custom designed arms which are secured to the base plate and are free to rotate about two adjacent bearings. As the RPM increases, the fly weights pull outwards, rotating about their respective bearings and in turn raising the sled and compressing the spring. Once the RPM begins to decrease the spring then pushes the system back to its resting positions.

The propellers are fit into a pair of bearings designed to hold .75-inch diameter shafts. Two adjacent bearings were chosen for stability purposes as most bearings are too thin with too much slop for cantilever applications. The added thickness also allowed for more surface traction, better securing the propeller from centrifugal forces. The bearings are secured within two custom housing pieces, a top and bottom, both identical. A groove the thickness and diameter of the two bearings is made where the outer wheel of the bearings are secured, allowing for free movement of the internal ring. These collars are secured to the base plate with bolts that pass through both the top and bottom pieces. As with the previous design, there is a small plate or disk that attaches on the interior side of the bearing and contains a similar pin. Instead of fitting into a linkage system, these pins fit into a custom made block that is attached to the linear bearing housing and is a part of the sled, creating a simple pin and slot system which acts to keep all angles the same and changes them simultaneously.

All components made from raw materials were to be made of aluminum. However, manufacturing costs and difficulties dictated that another material route be explored.

3.3.3 ITERATION 3

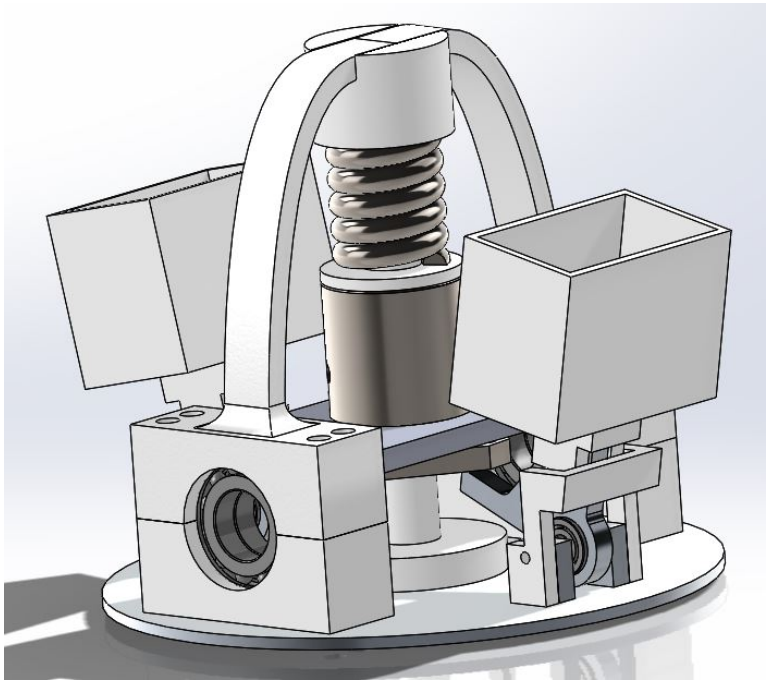

Figure 35 3rd CAD design- Hartnell

Rather than using aluminum, 3D printing the complex parts using acrylonitrile butadiene styrene, or ABS, filament proved to be a valid alternative to the aluminum. 3D printing also has the added benefit of rapid prototyping allowing more freedom for error correction and component production. The components changed to ABS include the top and bottom propeller bearing collars, the central shaft, and the attachment points for the flyweight arms as well as the flyweights themselves. In order to use ABS, there needed to be some design changes to the structure of the system. This iteration is shown in figure (35). Due to ABS strength being much lower than aluminum, the load bearing components needed to be altered. The central shaft was turned into a non-load bearing part and instead acts as a guide for the sled and spring. An arch extends to the top of the central shaft from the bearing collars with a circular cup to house the upper portion of the spring, to prevent unwanted lateral movement, and translates the load experienced throughout the system. Pieces were added to the arm attachment points that limit the

amount of rotation once the desired point is reached. Attaching the .125 kg steel balls to the arms was one of the manufacturing difficulties encountered. To mitigate this two weight cups were designed to hold epoxy up to the weight equal to the steel balls.

3.4 FEA ON LOAD BEARING COMPONENTS

With ABS having a lower strength than aluminum, basic finite element analysis needed to be performed using SolidWorks Simulation to ensure adequate component strength. The article "Material Characterization of Fused Deposition Modeling (FDM) ABS by Designed Experiments" [19] characterizes various print methods to determine the relative strength of each compared to typical injection molding. Injection molding is the process of creating an enclosed mold and injecting super-heated material under high pressure to fill in the vacant cavities, creating one solid piece. The typical strength of injection molded ABS parts are between 44 and 48 MPa but can be as low as 22 MPa. 3D printed parts were found to have between 65%-72% of the tensile strength of their injection molded counter parts, depending on layer orientation: fibers that traveled along the direction of the force applied were stronger than fibers that had crisscrossed layers. The SolidWorks material selection has an ABS tensile strength of 30 MPa. There is an option to create a custom material with custom properties; however, with large variations in the material strength, this value was left alone. Each analysis assumed a maximum 70% of the given ultimate tensile strength for 3D printed parts being equal to 21 MPa.

3.4.1 FEA SETUP AND PARAMETERS

Figure (36) and (37) show the two components designed in SolidWorks. Both parts were designed to fit the same base dimensions. Figure (36) shows linear supports while figure (37) has a curved arch. Both components are 4.66-in tall and have a flat middle section to accommodate the circular spring "cup". The cup was designed as a separate part to simplify printing. Cross-sectional dimensions for both components were also kept constant at .25-in x .625-in.

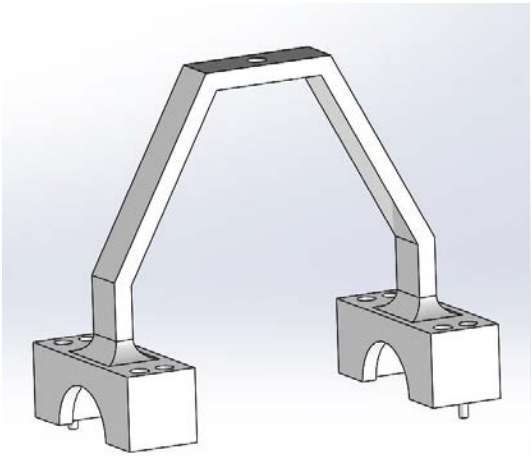

Figure 36 Straight Arch

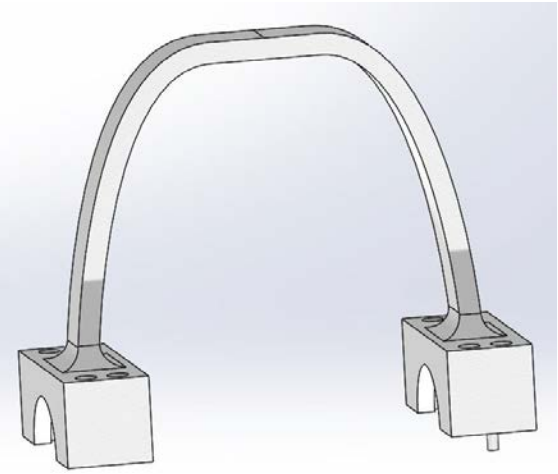

Figure 37 Curved Arch

A half completed assembly consisting of the base plate, the bottom propeller locks, and the two upper locks shown were used in the simulations. Only the two upper locks were interchanged. Because the assembly is connected through multiple bolts, it was necessary to create a circular attachment point on the reverse side of the base plate. Initial simulations used the bolt holes as fixtures. This however resulted in stress concentrations around the bolt holes which dominated the simulations, and wouldn't accurately represent the stress distribution. An example of this can be seen in the appendices … It was also necessary to accurately simulate the spring contact points.

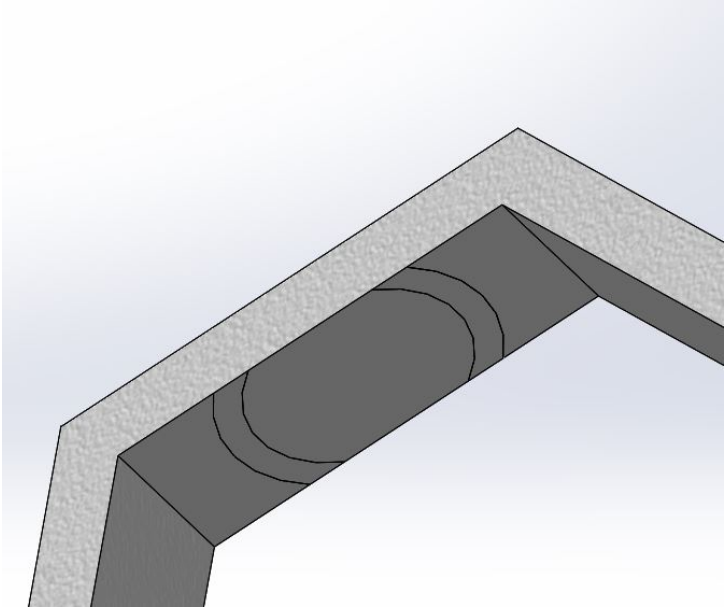

Figure 38 Spring contact point for FEA

A thin-walled circular extrusion was added to the components in figure (38) at approximately where the springs would make contact. The outer radius of the extrusion is … inches with a .1 in separation between the outer radius and the inner radius. Only the areas of the annulus in contact with the components were extruded. It was necessary to make the extrusion longer than the thickness of the component. When applying the force for the simulation, the program assumes the force is distributed across the entire level surface. The length of the extrusion is also important as it greatly influences the stress seen. Longer extrusions greatly reduce the stress. An extrusion length of .0001 inches was chosen to simulate a level surface. Smaller extrusions did not result in greatly varying results.

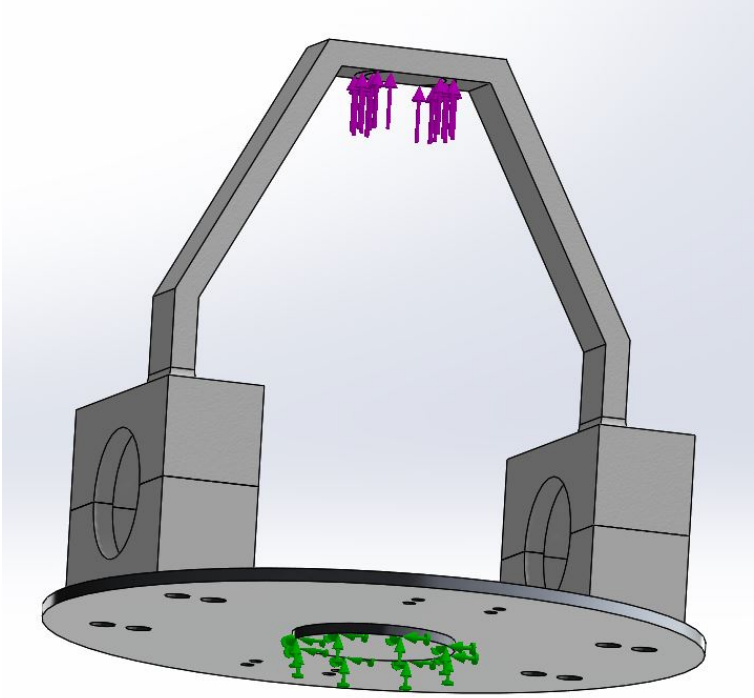

Figure 39 Force distribution (purple) and fixture (green)

A static simulation was used with the maximum expected forces calculated using the previously discussed excel code at the rotational speeds of 5500, 3500 and 1500 RPMs. Using a mass of .125-kg and equation [3.2], the maximum force seen at each rotational speed is 2917 N, 1181 N, and 217 N respectively. The force was applied to the annular extrusion on the two locks. SolidWorks has the option to distribute the force applied evenly between multiple contact points or to assume applied force is seen by each surface. These simulations assumed the force was distributed evenly between the contact points. Only one fixture was used on the bottom surface of the circular extrusion created on the base plate. The material set for the base plate was the aluminum alloy 6061, not heat-treated. The bottom propeller locks were set to ABS, while the two locks were tested with aluminum and ABS both.

3.4.2 SIMULATION RESULTS

Table 5 Simulation Results

Simulation	Part	Material	Force (N)	Stress (MPa)
1	Arch	Al-6061	2917	328.2
2	Straight	Al-6061	2917	286.4
3	Arch	Al-6061	1181	135.0
4	Straight	Al-6061	1181	118.3
5	Arch	Al-6061	217	25.05
6	Straight	Al-6061	217	23.19
7	Arch	ABS	1181	76.3
8	Straight	ABS	1181	55.41
9	Arch	ABS	217	15.75
10	Straight	ABS	217	11.26

Twelve simulations were run, three simulations for each material at the designated forces for each component. Table (5) shows the simulation results. The analysis failed to solve at the highest force of 2917 N for ABS, indicating displacement well beyond failure. Aluminum-6061 has an ultimate tensile strength of 124.1 MPa. Both parts experience stresses well over twice the ultimate strength at a force of 2917 N. Interesting to note, the base plate also experiences 299.1 MPa, meaning the entire system fails. The second highest force of 1181 N still shows failure for the Arch, or part A, but has a stress of 118.3 MPa for the linear part. While this part does not fail, it still ends well over the yield strength of 55.15 MPa. Both parts succeed at the lowest force of 217 N at 1500 RPM. Both parts in ABS only fall under the assumed ultimate tensile strength of 21 MPa at 217 N.

The linear lock consistently sees roughly 77% of the stresses seen by the curved part. While both parts fall below the ultimate strength of ABS, The linear lock was chosen for its better stress distribution. Inevitably while testing, greater than expected forces could potentially occur so having the extra cushion is ideal.

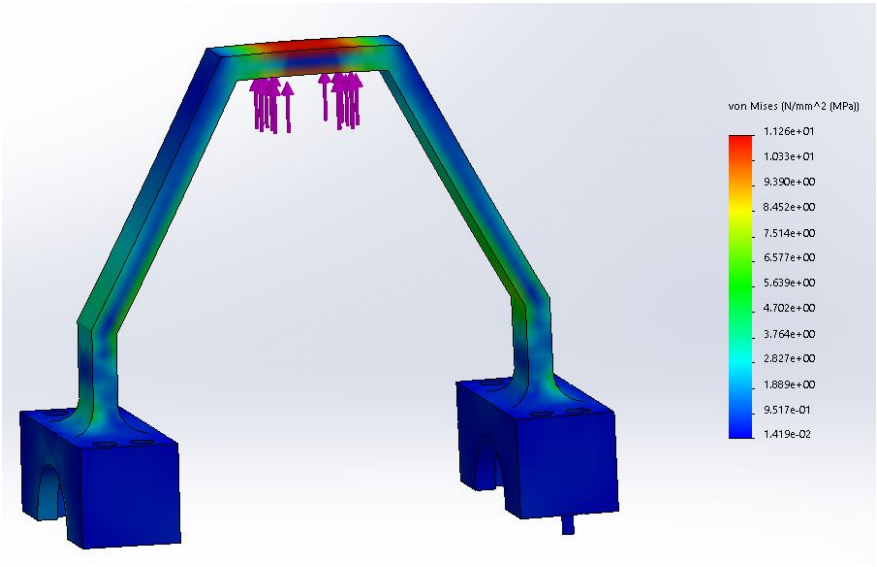

Figure 40 FEA example results- Straight Arch

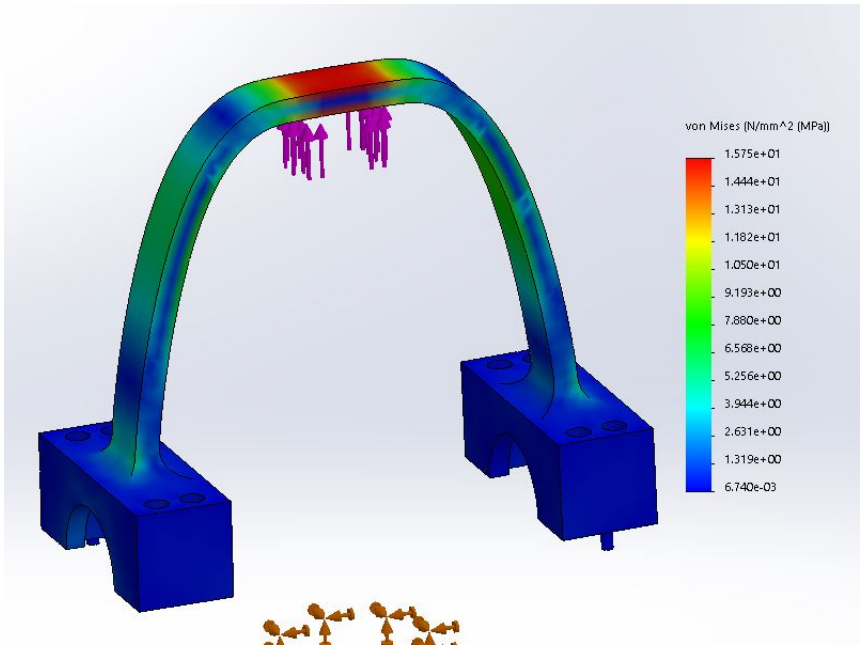

Figure 41 FEA example results- Curved Arch

3.5 FINAL ITERATION

Figure (42) show the final iteration. The arm limiters have been made thicker to accommodate higher strengths. A wall has also been added connecting the limiters to the propeller collars. In the event a component fails or becomes detached, this connecting wall will aid in preventing pieces from completely separating and flying off causing potential harm.

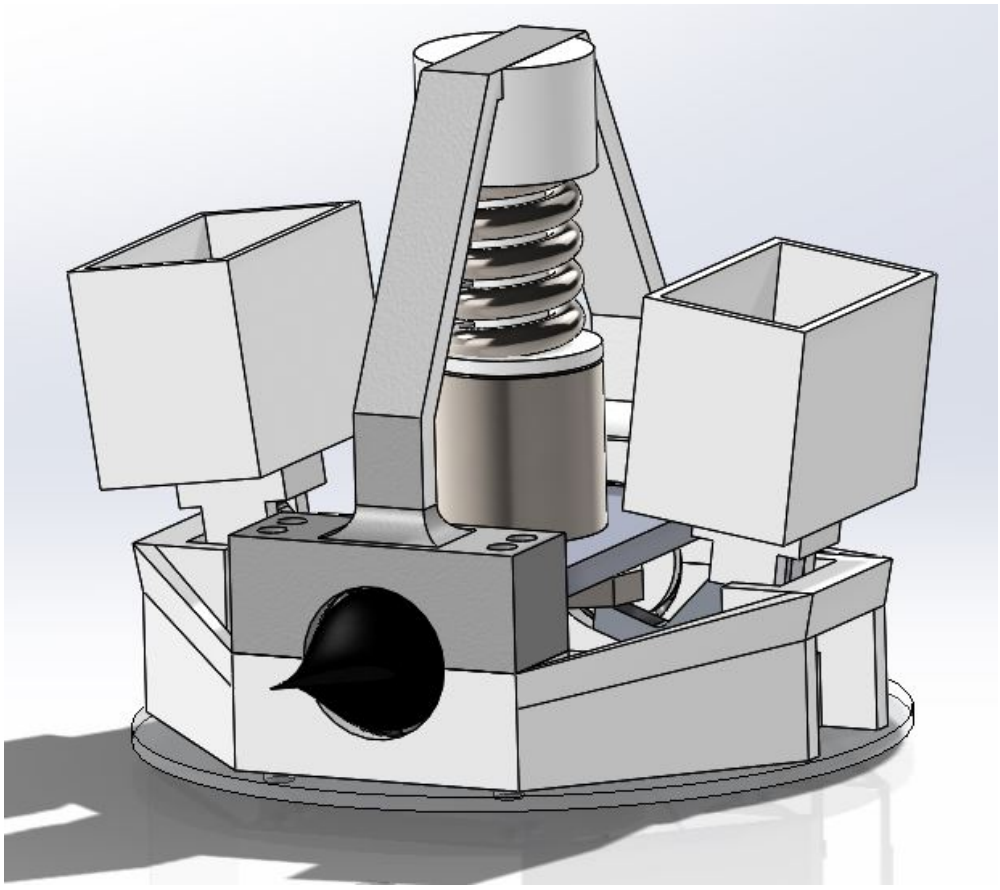

Figure 42 Final CAD design

CHAPTER IV

CONSTRUCTION

4.1 MATERIALS

Most of the components used were purchased from McMaster-Carr aside from the components that are 3D printed. A linear bearing fitting a .625-in. rod as well as a bearing house and retaining rings to hold the bearing in place. The linear bearing allows for smoother movement along the central shaft. This system composes the sled and is not ideal as it is the heaviest part of the device at 173-g. The weight of the sled is negligible compared to the force required by the spring when in a vertical position. When in an aircraft configuration, the weight of the sled becomes negligible, as gravity is not a factor in horizontal motion, except in the form of friction.

Figure 43 1000 RPM spring (left) and 4000 RPM spring (right)

There are a total of eight ball bearings used, two bearings fitting a .75-in. rod for each propeller and two bearings fitting a .25-in. rod for each flyweight arm. A 2x6x.25-in. aluminum block was purchased to be used to construct the flyweight arms as well as the pitch block, which was disregarded in favor of ABS. The filaments used in 3D printing are 1.75-mm diameter ABS purchased from Hatchbox© filament provider.

4.2 CONSTRUCTION

All 3D printed parts were printed on the Robo R2 3D printer. The printer is capable of handling print jobs within the dimensions of 8x8x10 inches, and features a heated print-bed as well as a camera for remote viewing. Accompanying the printer is the software Cura, capable of connecting to and controlling the printer over an internet connection. Through the Cura main screen, all aspects of the print can be controlled, from print parameters to print orientation and location.

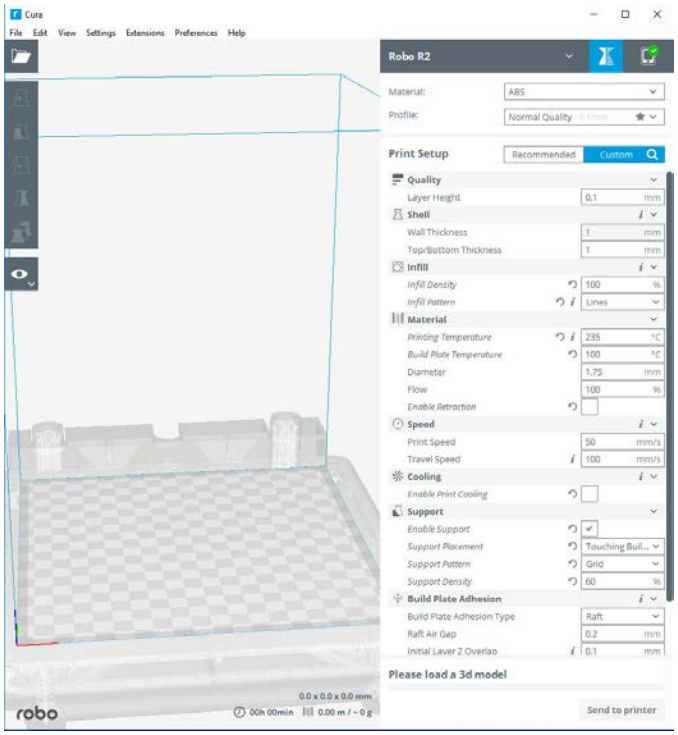

Figure 44 Cura example UI Source: Robo 3D

Figure (44) shows an example of the Cura control screen. Custom setup was chosen for optimal control over the prints. Layer height was set to 0.1 mm with a shell thickness of 1 mm all around. Infill density was set to 100% with a line infill pattern and is the essential setting for the construction of the parts. Nozzle temperature is 235 degrees Celsius with a build pate temperature of 100 degrees Celsius. As stated earlier, the filament diameter is 1.75 mm. Print and travel speed were set to 50 mm/s and 100 mm/s respectively. Print cooling was left unchecked as ABS shrinks as it cools. If ABS is cooled too quickly, warping of the part can occur. Support was enabled on all parts since most parts had large overhangs. The support was set to grid at a density of 80%. Smaller densities were experimented with unsuccessfully. The support would not adhere to itself and caused obstructions to the rest of the part. Plate adhesion type was set to raft with an air gap of 0.2 mm, an overlap of 0.1 mm and three layers per raft. Several prints “failed”, or were unable to successfully continue so had to be cancelled. Early on the parts would peel away from the print bed, often warping the part. Various positions on the print bed were experimented with to determine if location affects a prints success rate. Parts that were placed more towards the front of the printer failed intermittently, requiring an extra base adhesive while parts placed near the back of the plate never failed.

Careful consideration was given to the orientation of each part. Those parts that were load bearing, such as the arch locks, were printed on their side in order to have the layers travelling in the direction of the force. This is to ensure the full strength of the material is available and the part will not fail along the layer bonds. All 2D components, the base and arms, were manufactured using the Omax Maxiem 1515water jet cutter at Oklahoma State University’s Design and Manufacturing Lab.

Post processing was necessary for most of the parts. The bolt holes for the base plate were just under tolerance for the bolts being used and needed to be widened. Some 3D printed parts have visible stepping lines between the layers which can add together to become ridges

occurring at regular intervals. This is very apparent in parts using ABS. This issue can be mitigated by sanding with medium to fine grit sandpaper, depending on how smooth the part needs to be. The central shaft was the only part that required sanding since it acts as the guide for the linear bearing. After sanding, a quick rub with alcohol removes any fine particles that might interfere with the bearing. The bearing contains its own lubrication that it can then leave behind on the shaft, providing smooth operation.

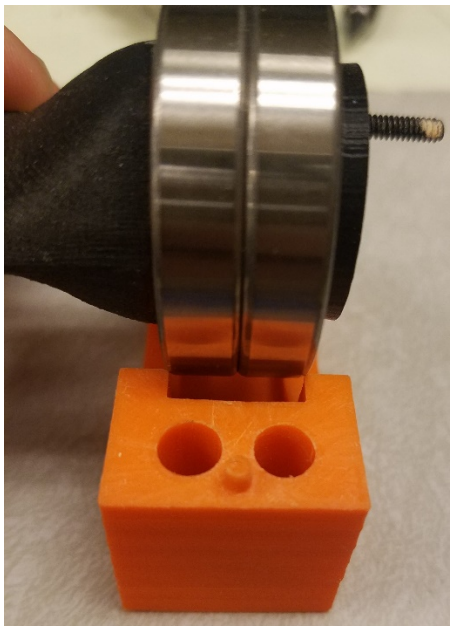

Figure 45 Bearing size in printed collar

Once printed, the bottom propeller collars as well as the connecting arch both had an issue with shrinking. The overall width and diameter of the bearings were larger than the width of the collars. Material had to be removed from all of these parts in order to fit the bearings. A corded 3000 variable speed Dremel was used to remove the necessary material. The pieces were marked to ensure the proper sides are attached since each collar was processed to fit one side. During fitting, the larger size diameter of the bearings was enough the split the collars along parts of the layer bonds. These areas were filled with colloidal silica epoxy to re-attach the layers.

Since these splits were along the layer lines, they were deemed to not greatly affect the overall strength of the part as the layers are still in tension.

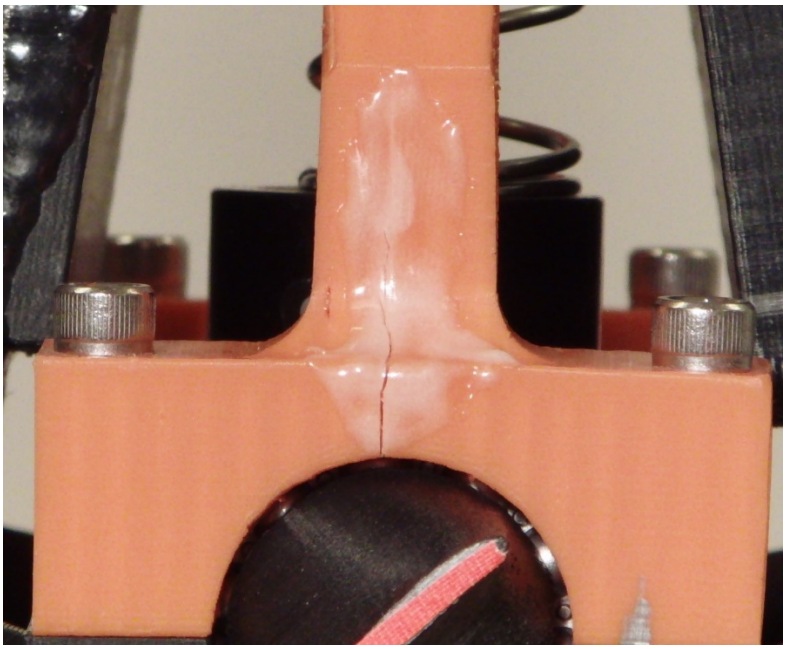

Figure 46 Split in part from bearing fitting

After post processing is completed, the base ring structure is aligned with the appropriate bolt holes on the base plate. The smaller bolt holes supporting the arm limiters are tapped to permanently support 6-32 thread screws. Click-Bond adhesive was used along the lower boundary between the base plate and base structure to ensure a permanent fixture. Click-Bond was also applied to the sides of suspected problem areas on the arm limiters where the ABS layer bond could be separated.

Once the base structure is attached to the base plate, the central shaft can be added. Since it is held in place by the motor mount, the bolts need to be added to hold it secure. The next items attached are the flyweight arms and flyweights. The arms are .25-in thick and contain two small bearings fitting a .25-in diameter rod, which have an individual thickness of .1875-in. Two bearings are used to provide an extrusion for the bearings to allow the arms to rotate unimpeded by friction caused by the walls of the limiter. A .25-in diameter bolt 1.75-in long is used as the

rod the bearings rest on, secure with a nut on the outside of the limiter. Four holes had to be cut in the added walls too allow the bolts to be inserted and to allow the use of tools. After the arms were set in place, an initial rotation of the arms revealed too much contact between the base plate and the bottom most portion of the arm, causing excess friction preventing the arm from rotating freely. The Dremel was again used to grind away portions of the base plate until it was no longer in contact with the arms. Once the arms were settled into place, the arms and bearings were epoxied together to make them one piece.

The flyweights were constructed by 3D printing two cups that attach to the top of the arms by a 1.3 in 6-32 thread bolt and nut. The cups were filled with epoxy until the total mass of each reached .125-kg. During the curing process, the heat from the reaction was high enough to warp the ABS cups, separating some of the bonded layers and leaking through. Fortunately no weight was lost as the epoxy cured beforehand. Due to the uneven distribution of mass, the centers of mass were further from the 2-inch design point. One cup had a center of mass approximately 2.3-in from the point of rotation while the other had a center of mass approximately 2.4-in from the point of rotation. The center of mass for the latter was reduced to 2.3-in. These center of mass locations were left alone as lowering the weights further down the arms would cause interference between the weights and limiters. The new centers of mass were used in the excel model to output a new expected activation RPM of 1015. The tolerance gap between the attachment point on the cups and the arms was too large and allowed for a substantial amount of wobble along the bolt. Rubber washers were used to try to lessen this issue, but proved inadequate. Unfortunately, a touch of epoxy mixed with chopped carbon fiber had to be used secure the weights in place. This is not an ideal fixture, as the entire arm must be removed instead of just the weights for different design points.

The linear bearing and housing slide onto the central shaft and rest on the ends of the arms. This is the contact point that lifts the entire sled. The pitch block fits itself around the

housing and rests on top of the housings mounting flange. There was too much freedom for the housing to rotate about the shaft during operation so was attached to the pitch block via four .75-in long 10-24 bolts and nuts. This helps minimize the amount of rotation since the tolerance of the pitch block prevents much movement. Because of the pitch block orientation during printing, small cracks developed along the bond layers. To mitigate this, strips of unidirectional carbon tow were placed along its ends perpendicular to the layer directions.

Actual propeller blades were going to be printed to be used in testing, however the one blade that was printed was far too fragile to withstand the aerodynamic forces. More research is needed to determine how feasible 3D printing propellers is along with the optimal materials. Instead, propeller blade stand-ins were designed to use during prototype testing. The basic form of the stand-in is a circular cross-section larger than the inner diameter of the propeller bearings that lofts to a typical Clark-y airfoil, which is colored silver for easy viewing. This allows viewers to see the amount of rotation, or pitch change achieved. A .75-in dimeter extrusion that is .625-in long is attached to the inside of the circular cross-section and fits through the two propeller bearings. Two discs 1.1-in in diameter and .125-in thick were designed to fit within the collars and act as an anchor point for the propeller stand-ins to prevent them from slipping out of the bearings. The discs are attached to the propeller stand-ins by two .25-in wood screws. The cap of a 5/8-in 4-40 bolt was cut off and the bolt was attached to the disk at an arbitrary angle to the chord line of the airfoil to simulate a coarse pitch angle. The bearings are placed into the bottom propeller collars with the airfoils in the proper orientation and the bolt is fit into the pitch block and is the contact point that rotates the propeller blades.

A small washer was printed to fit into the open space between the linear bearing retaining rings and the housing. This piece provides a level platform for the spring to rest on. The spring is then placed along the shaft on the linear bearing. The final piece, the connecting arch, is now placed with the collars aligned with their appropriate marks. .25-in diameter bolts 2.75-in long

were used in the four outermost bolt holes and are secured on the bottom side of the base plate with hex nuts.

4.3 STRENGTH TEST

A proof of strength was performed on the main load bearing part to ensure the part will not fail. The connecting arch and original bottom collars, before the main structure with the walls was created, were attached together to a 2x4 via the same bolt pattern used to attach the parts to the base plate. The ends of the 2x4 were then supported on either end by two equal height stools with the parts on the underside of the plank. Para cord was tied to the area that would support the spring to simulate the force it provides with weights added incrementally until the maximum force expected was achieved. The maximum force expected is 217 N, which equates to 48.78 lbf. Table (6) shows the incremental steps taken during the strength test while figures (47) and (48) show the initial and final steps. During the test there was no noticeable deformation or failure throughout. After the test concluded and the setup was taken down, a small notch was discovered in the part not consistent with known failure patterns, but more closely resembled an accidental tooling mark., which is shown in figure(49).

Table 6 Strength Test Increments

Test Number	Weight
1	2.4
2	4.754
3	9.754
4	14.754
5	20.754
6	24.754
7	29.754
8	34.754
9	40.754
10	46.996
11	52.996

Figure 47 Strength test setup

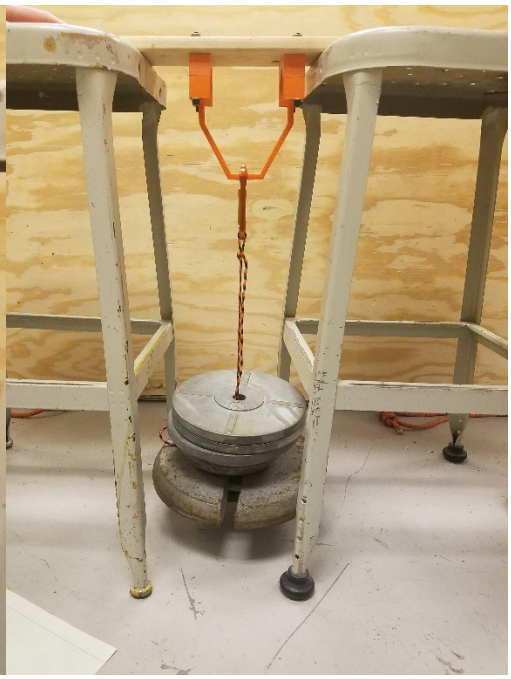

Figure 48 Arch fully loaded

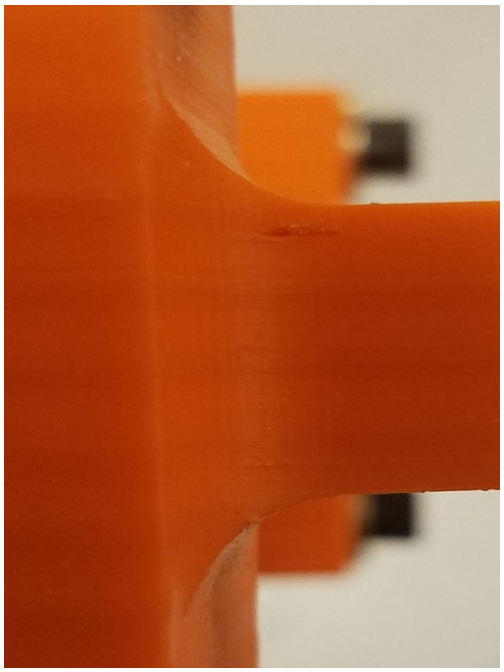

Figure 49 Possible tooling mark

4.4 ASSEMBLY

The system must be assembled in a particular order. The central shaft must be attached to base plate first. If not attaching to the motor, the shaft should be secured tightly using the same bolts used on the motor with their compatible nuts. The flyweights and arms can then be attached to their anchor points. A 2-in ¼-20 bolt is used as the rod the bearing sits on and is secured by a nut on the opposite side of the arm. The propeller/bearings are put into place simultaneously as the sled since the pin that rotates the propeller blades rests inside the pitch block attached to the linear bearing housing, which rests on the ends of the flyweight arms. The spring is slid onto the shaft and rests on the sled. The upper lock is the final piece that fits into place and is bolted down through the four outer bolt holes to the base plate.

4.5 BALANCING

Balancing is an important aspect of rotating machinery. If an item is not properly balanced, the ensuing vibrations caused by the items wobble can damage both the object itself as well as the motor driving it. There were several attempts to statically balance the full assembly. It quickly became apparent the importance of considering the method of balancing when designing a rotating piece.

4.5.1 FIRST BALANCING ATTEMPT

The methods chosen to balance the system are similar to the method of balancing a standard propeller. Figure (50) shows a propeller attached to a thin rod which is held in place by resting on the intersections of two sets of thin discs that are free to rotate. The rod and propeller become a cantilever beam that is also free to rotate. If there are any uneven weight distributions the propeller will rotate until the heavy side rests at the bottom of the propeller disc. This tells the user where to add or remove weight in order to balance the propeller. A properly balanced propeller will have minimal rotation.

Figure 50 Tru-Spin Prop balancer and Propeller

Using this theory as a basis, a custom balancer was designed and printed. Shown in figure (51 A) the CAD of a housing unit (the piece later broke) was made for a spare bearing with a flange on the end meant to attach to a flat surface horizontally. Figure (51 B) then attaches to the assembly via the pre-existing bolt pattern. The end of this part is .75-inches in diameter, meant to fit snuggly into the bearing.

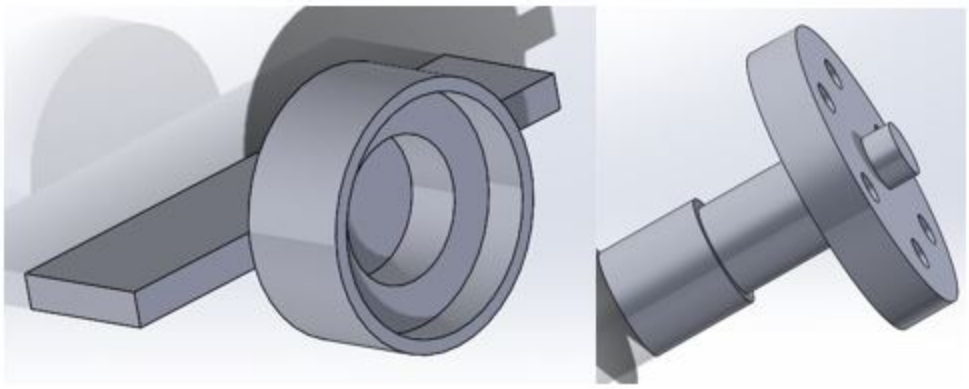

Figure A Bearing Holder

Figure B Balancing Rod

Figure 51 A). Bearing holder for custom balancer, B). Connecting piece from bearing to assembly base

Using a pre-made platform, the balancing assembly is attached to the platform using two locking clamps on either side of the flange. The low friction bearing was easily rotated, however there was too much slop axially, allowing the assembly to put pressure and friction on the bearing. To mitigate this, a small .25-in wood screw was attached to the topside centerline of the connecting arch. A string was then looped around the head of the screw above the thread line, which was used to relieve the pressure on the bearing by lifting the end of the assembly until the wall friction had ceased. This assembly is shown in figure (52).

Figure 52 Balance attempt 1

Figure 53 Lifting string for attempt 1

Even with the end lifted however, there was excess wobble in the assembly. It was determined that the piece connecting the assembly to the bearing had not printed straight. Because of the

horizontal print orientation, which was done to prevent failure in bending, support material was used on a side which the part had pulled away from. This warp is shown in figure (54).

Figure 54 Warped connecting piece

4.5.2 SECOND BALANCING ATTEMPT

A second attachment piece was printed in a vertical orientation to ensure the insert was straight. The concerns of the part failing under a bending load were confirmed before balancing could occur. The part was mishandled and sheared along the boundary layer at the neck of the part illustrated in figure (55). A final attempt was made to print a connecting piece sized to fit different bearings, in the same vertical orientation, but with 0°, 90° oriented fiberglass tape wrapped around the weak neck. New closed bearings with tighter tolerances fitting a 20 mm rod was purchased to try and alleviate the slop experienced with the previous bearings. These bearings did not replace the propeller bearings as the slop does not have as significant of an impact.

Figure 55 Connecting piece sheared at neck

A new setup was constructed to accommodate the new pieces, which is shown in figure (56). A frame was constructed to hold the assembly with a brace attached at the bottom to prevent the setup from tipping over. Rather than securing the end flange with clamps, two bolt holes were drilled through it and the plank it was attached to. The bolts provide a much more secure hold than the clamps. While the slop in the new bearings was indeed less than the previous bearings, it was still large enough to influence the balance of the assembly. A similar approach to the first balancing attempt was utilized to alleviate the slop. A thin board was attached to the end of the bottom brace vertically to attach a string to. The blue end piece shown in figure (57) was designed to fit on the top of the connecting arch and provide an attachment point for a bolt that was connected to the string. As with the first attempt, the string was pulled taught until the wall friction caused by the bearing slop had ceased.

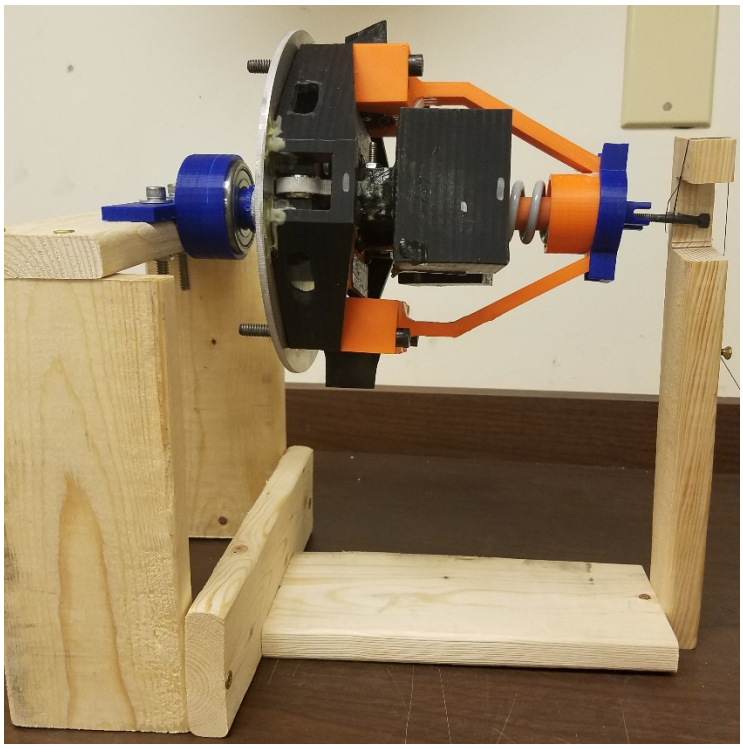

Figure 56 Second balancing attempt

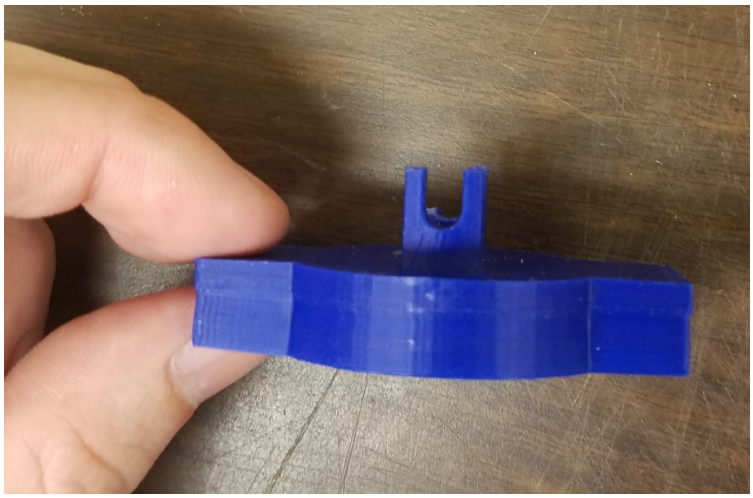

Figure 57 End cap for lifting support

Manufacturing error caused the axis of rotation to be misaligned with the center point of the connecting pieces. This misalignment caused too much friction in the string as the assembly rotated, which caused the string to dictate both direction and amount of rotation, rendering this attempt mute.

4.5.3 THIRD BALANCING ATTEMPT

A unique solution was designed in an effort to mitigate the misalignment issue. Double U-Joints are currently used in applications where two rotating pieces are not linearly or angularly aligned, such as in drive shafts or steering columns. A custom double u-joint was designed to fit onto the end cap placed on the connecting arch, examples of which are shown in figures(58) A and B. Figure (59) shows the connecting pieces fit into another bearing-housing assembly.

Figure A U-Joint Connection

Figure B U-Joint Spider

Figure 58 Pieces for U-Joint system

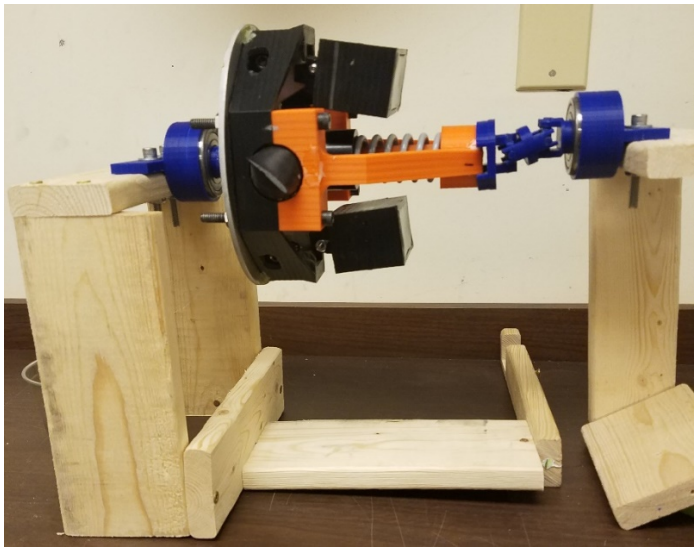

Figure 59 Balance attempt 3

The double u-joint worked perfectly for its intended use of translating rotational energy between misaligned parts. These joints however are not meant to carry any transverse load. To adequately lift the end of the assembly, the joint must be at its maximum allowable angle, which under a force can bind the joints, not allowing the system to rotate freely or smoothly.

4.5.4 FINAL BALANCING ATTEMPT

With three previous failures, the decision was made to re-construct the assembly to provide an accurate central axis and full supports on both ends. To achieve this the central shaft was redesigned to have a .25-in hole throughout its central axis. With this redesign a .25-in diameter 316 steel shaft with a yield strength of 86,000-psi was also purchased to act as an extension of the assembly and to provide contact points for a simply supported beam that has freedom to rotate.

The absolute center needed to be found to ensure the new shaft and assembly are placed symmetrically around the axis of rotation before balancing can occur. To do this, the Dewalt DW087 self-leveling laser chalk line with both horizontal and vertical lines was utilized with the theory that the centered crosshair created would be symmetric about both lines through the central hole. Figure (60) illustrates this point. The base plate with the base ring structure was first used to find the general central axis before the rest of the assembly was added. Pictured in figure (61), the plate was secured in a vice clamp and a plumb level was used to ensure the plate was vertical. Any deviation in angle was corrected by placing a spacer underneath the problem side of the vice until vertical. The crosshair of the level was then aligned with the center hole.

Figure 60 Finding dead center using laser level

Figure 61 Ensuring Piece is vertically level

One unforeseen effect was the amount and angle of dispersion of the laser. To create a line out of a direct beam, a convex lens is used to disperse the lasers in lines with their respective orientations, placing the crosshair at a point below and to the side of the lasers. Because of this design, the cross hair away from the level is at an angle to the lasers. If the background used to measure the line lengths is too far from the hole, the angles become very apparent and the lines separate. This effect is shown in figure (62). If the background is level with the hole, the separation is not an issue, however, with the small diameter of the hole and the dispersion of the light, making accurate measurements becomes difficult as the lines cannot be clearly differentiated. This can be overcome by rotating the background about a point the rests on or near the same plane as the exit, demonstrated in Figure (63). By rotating the background about an axis that is perpendicular to the line being measured, the line lengthens while maintaining its position, giving a clearer image. Once the crosshair is symmetric about both lines, the central shaft can be added and the process repeated, ensuring the shaft is centered about the axis. Once the system is centered, the connecting arch was then attached to mark where the center line is located. A hole was then drilled to accommodate the .25-in steel rod for balancing.

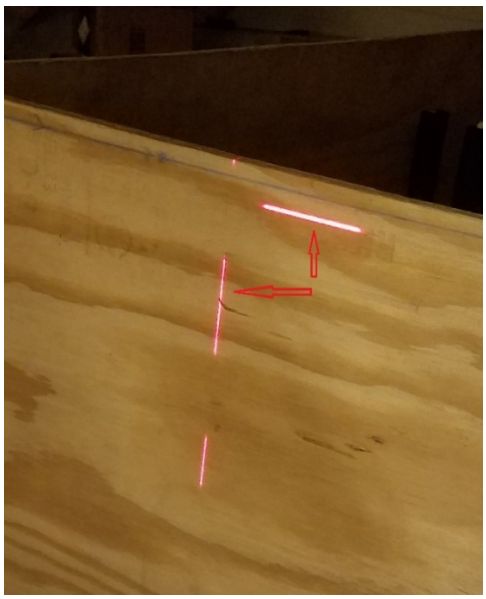

Figure 62 Line discrepency

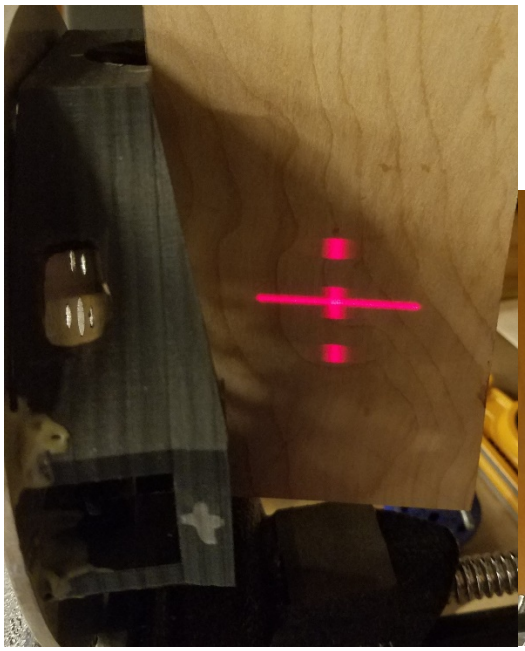

Figure 63 Mitigated line pattern

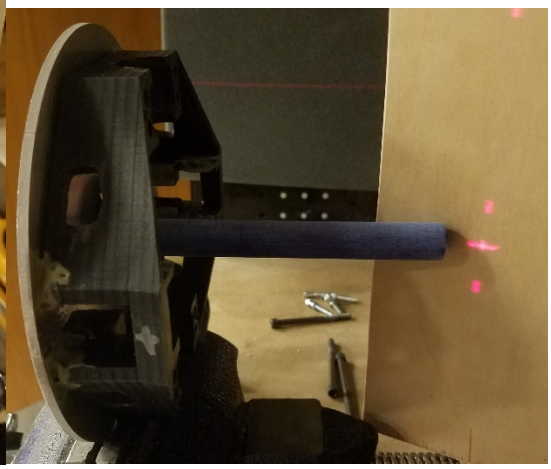

Figure 64Line pattern with shaft added

Balancing the system can take place once it is fully assembled and the rod is checked for straightness. The rod used has a straightness tolerance of .003-in per foot, however, at 18-inches long, the rod has a deviation of about .1-in. With this much deviation, the position of the rod affected how the system rotated. Fortunately, there was a 7-in section on one end of the rod that was straight enough to use. The steel rod is inserted so that the assembly rests entirely inside the working section with the ends supported on both sides by two Dubro Tru-Spin Prop balancers. Any uneven weight instantly begins to rotate the system.

To keep things simple and repeatable, the laser level was again used to provide a point of observation. The system was balanced about the two lines of symmetry since the major points of the structure lie on these axis. A mark was made along the edge of the base plate in line with the level to observe how much if any rotation occurs. To balance, washers were taped in various positions on the light side of the plate until rotation stops. This process was repeated until each side had minimal movement. The washers were then glued in place using cyanoacrylate.

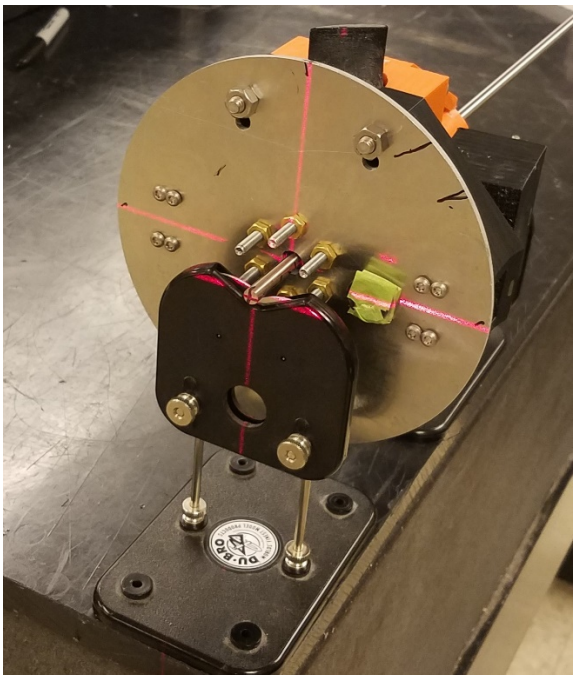

Figure 65 Laser level used to observe rotation

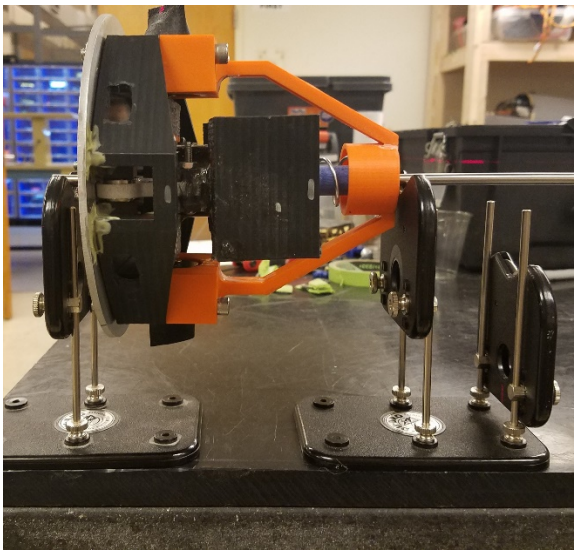

Figure 66 Simply supported beam in Tru-Spin balancers

Figure 67 Washers added for balancing weight

Drilling a hole in the upper lock greatly reduces its intended strength. Performing another analysis revealed that the stress concentration was double the original value at 22.87-MPa, which is just over the limit imposed of 21-MPa. A new spring with a lower stiffness had to be used to reduce the maximum angular velocity and the force applied. The spring used is the LCM200LM 03 M with a spring constant of 1240 N/m. The length of the spring was an issue at 5.315-in long, 2.315-in longer than the original springs, so was cut to match. The stiffness needed to be recalculated since a reduction in length increases the stiffness.

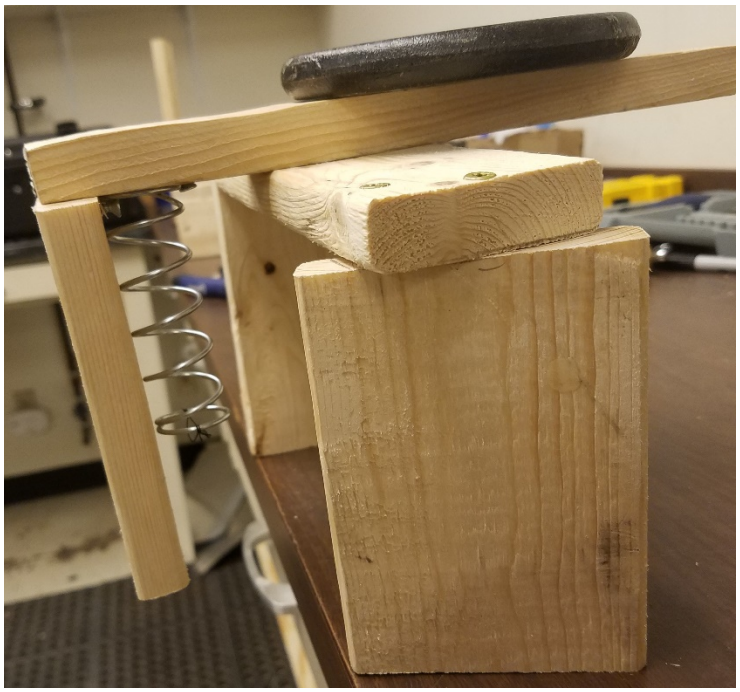

Figure 68 Setup to find spring constant

Shown in figure (68), the spring was attached on one end to a board by screws and held over the edge of a counter. A string was tied across the lower free end acting as an attachment point for weights, added on at 500-g increments starting at 1000-g. The free length was marked as well as the length after each weight was added up to 2000-g. The measurements from the free length were 6.09-mm, 9.13-mm, and 12.16-mm respectively, giving a new spring constant of 1633 N/m. Plugging this into the excel model gives an expected activation RPM of 247

CHAPTER V

TESTING AND RESULTS

5.1 EQUIPMENT

The motor used to run the assembly is the Hacker A200-6 controlled by a MasterSpin Pro-Opto 220 shown in figures (69) and (70). The hacker is a powerful motor used as an electric alternative for Group 2 unmanned systems. It requires a 12S 42-volt LiPo battery with a current draw of 230 amps. This size battery was not readily available, requiring three 4S 14-volt LiPo batteries be connected in parallel. A custom attachment, shown in figure (71), connects all three high discharge batteries to one terminal that powers the motor through the electronic speed controller.

Figure 69 Hacker A200-6

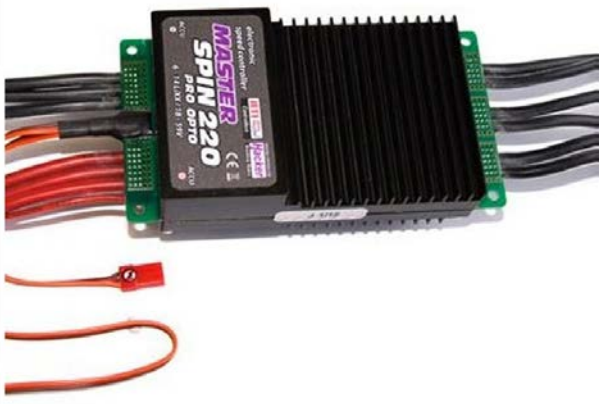

Figure 70 Master-Spin Pro Opto 220 Source: Hacker

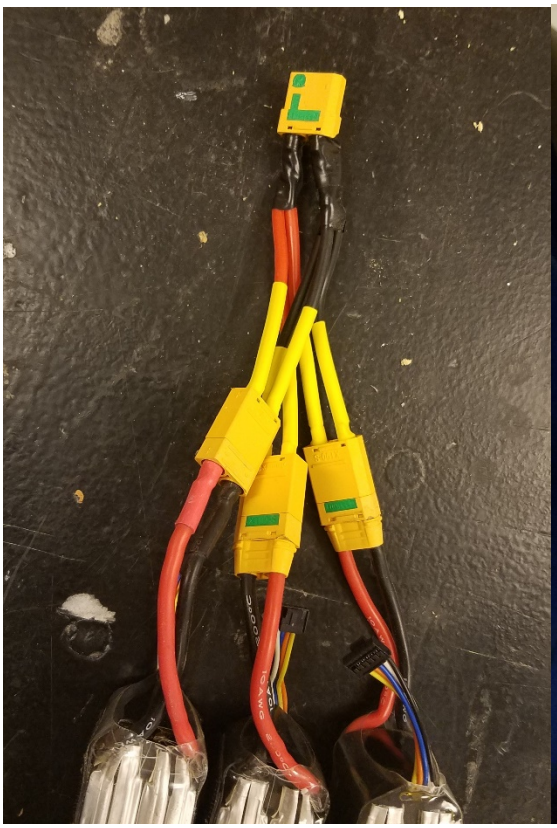

Figure 71 Custom battery connect

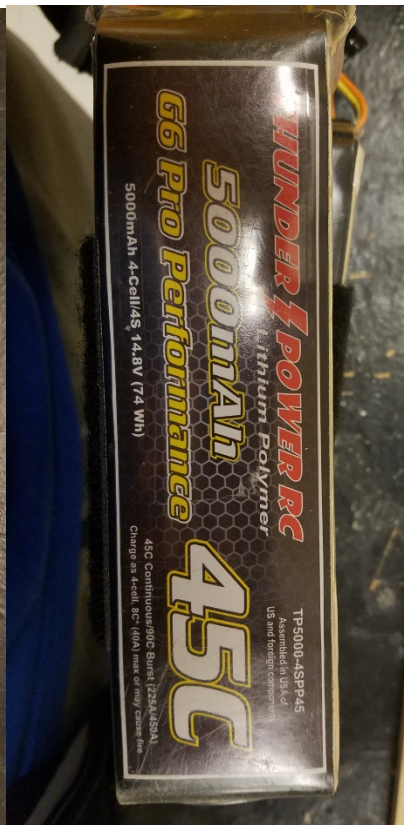

Figure 72 4S, 14.8V Batteries available

A Futaba T18SZ transmitter was used as the throttle control with a Futaba R7003SB receiver. The motor has five programmable modes each with different performance parameters. The default mode had too high acceleration to collect accurate data. A Jetibox can be used to program max RPM and rates of the electronic speed controller. In the absence of the Jetibox, the transmitter can program one of the five default modes. Before connecting the batteries to the speed controller, the transmitter must be turned on with the throttle at 100 percent. Once power is supplied to the motor, a series of beeps signal that it is in programming mode, followed by more beeps , the number of which correlating to the mode number. Mode 5 is “helicopter” mode,

having an acceleration phase lasting 10 seconds. Once this mode signals, the throttle is returned to zero, setting that as the active mode.

The optical sensor used is the Remote Optical LED sensor with an ACT-3 panel tachometer for Monarch Instruments [24]. The acquisition system has an accuracy up to ± .001% of the displayed value. To verify that the sensor outputs accurate data, a second sensor, the handheld Cermark One Touch Tach accurate within 10 RPM, was used as a comparison before testing occurred. All three systems are shown below. Both the panel tachometer and the One Touch Tach calculate the RPM by a running average. The panel tachometer seemed to output a value faster than the handheld, however both systems were consistently within 3-5% of each other with the time difference accounted for.

Figure 73 Remote Optical LED Sensor [24]

Figure 74 ACT-s Panel Tachometer [24]

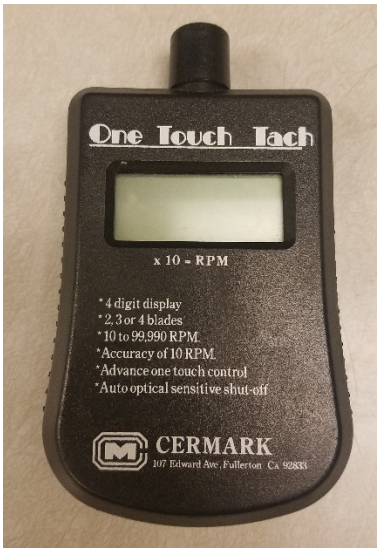

Figure 75 Cermark One Touch Tach

5.2 SETUP

Testing took place in an enclosed room in Oklahoma State University's Design and Manufacturing Lab. A large metal table with a plexiglass barrier acted as the test stand. A square section of .5-in 4-Ply plywood was used as the base of a custom motor mount. Four ¼-20 blind nuts acted as the anchor point between the motor mount and plywood with the motor and speed controller both attached to the motor mount. The first round of tests were performed in the upright position to provide a basic understanding of the devices operation in the typical Hartnell governor configuration. This configuration uses three locking clamps to secure the plywood board to the table to prevent any unwanted movement and is illustrated in figure (76). The optical sensor is attached to the frame on the left with the panel tachometer on top

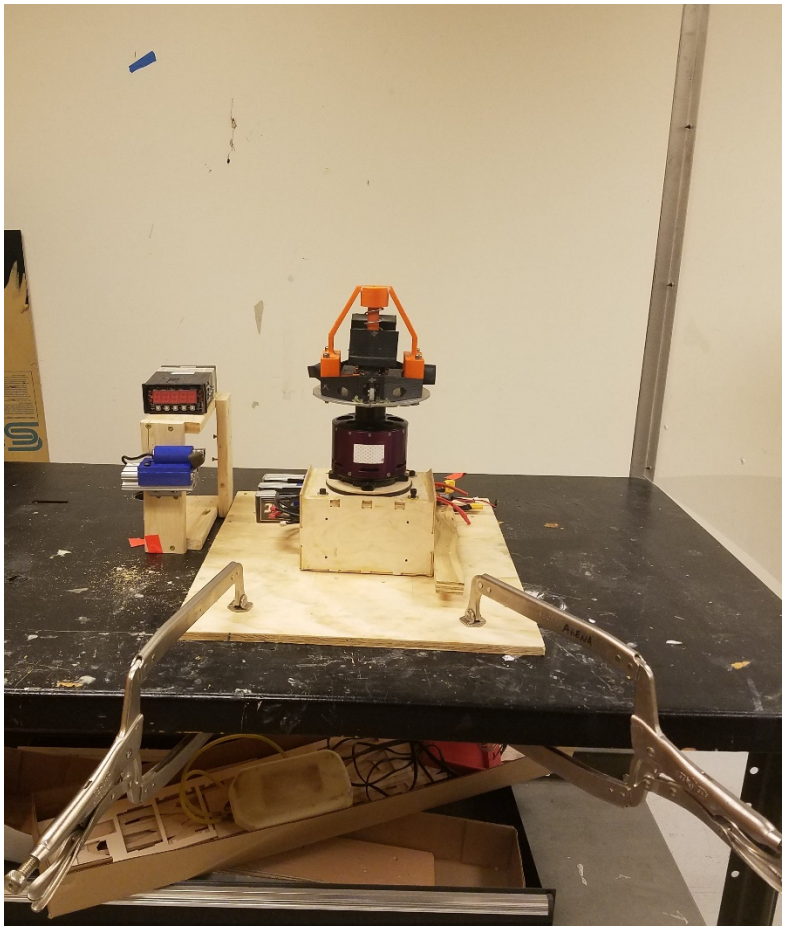

Figure 76 Upright configuration test setup

The Second configuration, shown in figure (77) through (79) has the motor in a horizontal orientation consistent with typical aircraft operation. The .5-in plywood is attached to a pentagonal frame behind it, giving it some support. Because the motor and assembly are much heavier than the supporting frame, a brace had to be attached on the front end underneath the motor to prevent tipping. Two longer braces were attached at the base of the back side for extra stability and to provide points of contact for the locking clamps. All batteries rest underneath the motor mount on the table as well as the panel tachometer. The optical sensor is secured to the far side of the plywood base.

Figure 77 Aircraft configuration test setup (left side)

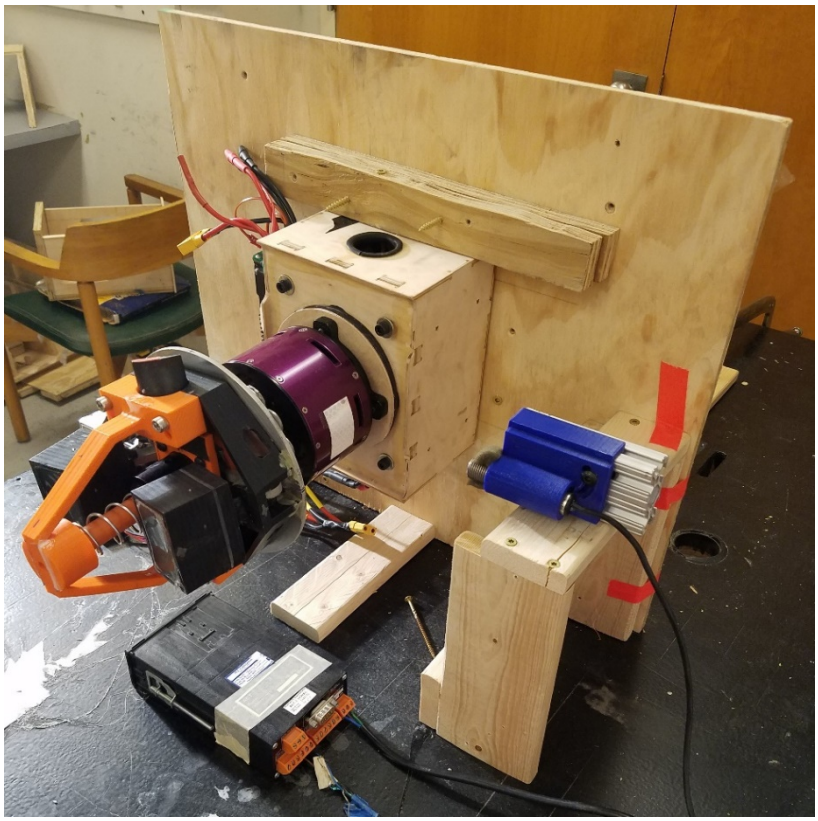

Figure 78 Aircraft configuration test setup (right side)

Figure 79 Aircraft configuration test setup (Back side)

A high-speed camera set to 1000 frames per second was setup facing the panel tachometer. Floodlights were setup behind the camera to provide perfect lighting for a visual of the systems actuation.

5.3 TESTING PROCEDURE AND EVALUATION METHOD

After ensuring the area is safe for operation, the floodlights are turned on and the camera set to record and is zoomed in appropriately. The transmitter is turned on before providing power to the speed controller or motor. Unless the motor mode needs to be altered the throttle should be resting at 0% or idle. Once ready, the power is supplied to the speed controller and receiver. The camera is started and throttle increased. The transmitter has a small dead zone before the controller begins to rotate the motor. The instant the motor begins to draw current the throttle should be let go to prevent over speeding the motor. Once the panel tachometer reads a displays a desired RPM, roughly 500-600, the throttle is brought back down to idle, the motor killed and the recording stopped. This process is repeated until the desired amount of tests have been reached for both configurations.

Even with the slowed acceleration, collecting true RPM data from the video is almost impossible as the readings jump by the hundreds with the base speed over 1000 RPM. Ideally, the speed would be acutely controlled, increasing incrementally until activation. It was discovered however that the motor has a linear trend while both accelerating and decelerating. By plotting the RPM reading versus the time in seconds based on video analysis, the R equation for each test is calculated; giving a reasonable projection of the activation speed by noting the time activation begins. The same process is used when the motor decelerates to find the speed at which the system returns to static equilibrium.

The tachometer displays RPM by taking a running average. Due to this, the lower RPM at startup take longer to accurately calculate often resulting in points with extended lengths of

time compared to later measurements. The plots needed to be examined carefully before creating the R equation for any measurements that could skew the result, such as the early RPM measurements. Figure (80) shows an example of points that were discarded. This was especially apparent when the motor decelerates. The final measurement, typically below 150, took an extended period of time to calculate compared to the higher speeds. It's also important to note the motor would often cease movement by the slower measurements.

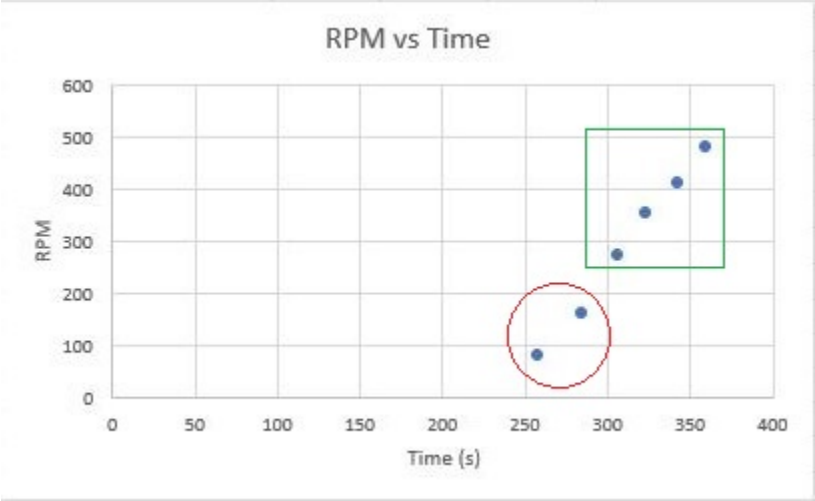

Figure 80 Example points taken from video

The area circled shows the discrepancy at the lower speeds. This pattern was consistent throughout the vast majority of tests. The boxed area is the area of interest where all device activation occurs making this the area the trend is created, shown in figure (81).

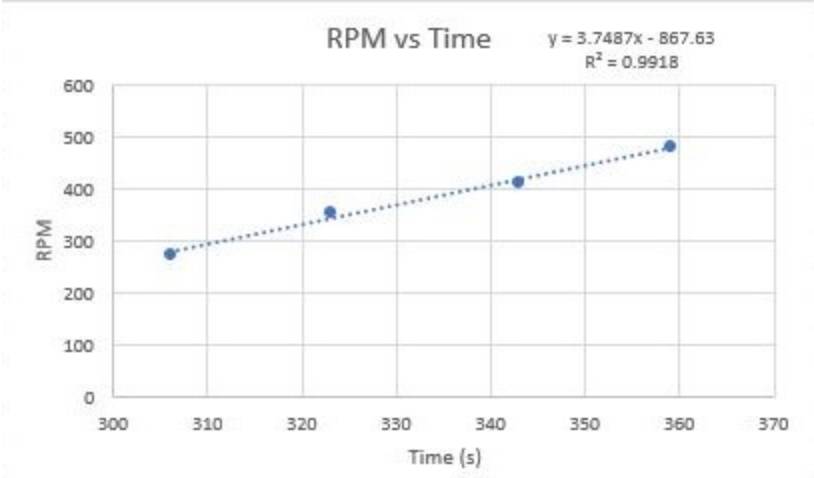

Figure 81 Trend line after points discarded

When the system returns to static equilibrium, it happens in an instant. The same cannot be said for the time between initial activation and the flyweights being fully opened. Activation of the device happens quickly and is very noticeable, but the weights open slower the more open they get, allowing a large amount of time to pass from start to finish. Figures (82) and (83) show the starting and final positions of the propeller substitute and what cues to look for when examining video footage.

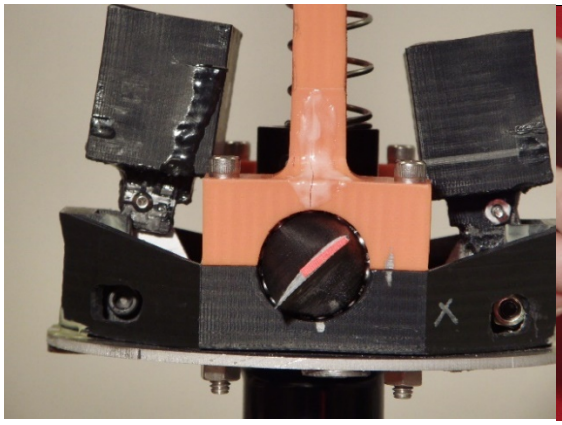

Figure 82 Start position

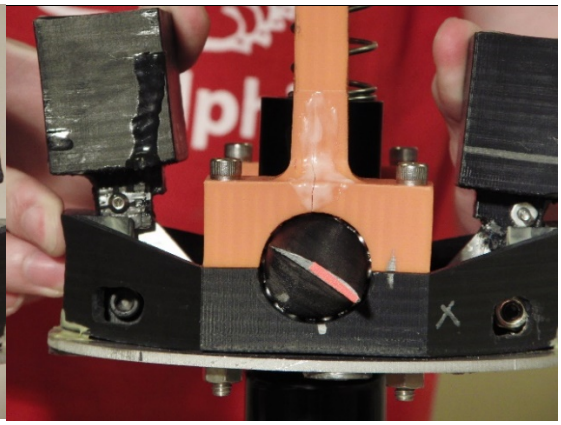

Figure 83 Final position

5.4 RESULTS

The data for each test was separated into four categories, speed at actuation start, speed at actuation end, the speed the device closes, and the difference between the start and end points. The upright configuration had an average activation speed of 329 ± 8 RPM. The end point occurred at an average speed of 451±11 RPM with the average difference of 118±10. The plots for both results are shown in figures (84) and (85) with standard deviation error bars included. Both results only have one point that could be considered a major outlier.

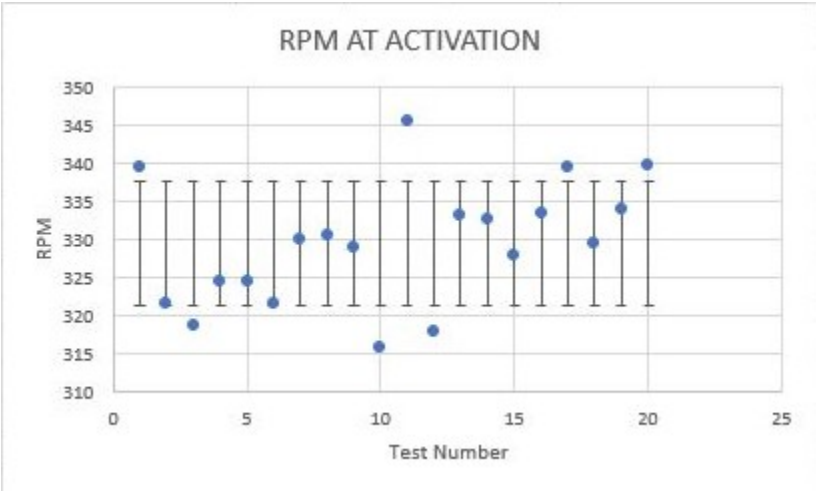

Figure 84 Upright config. Activation points

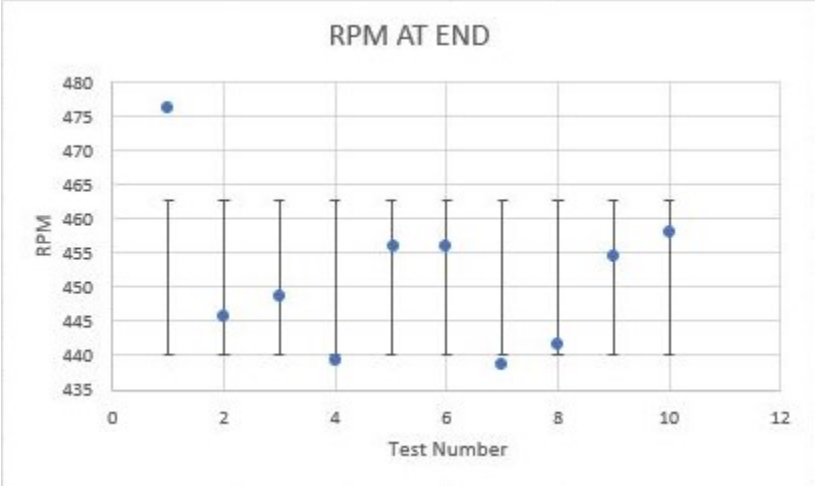

Figure 85 Upright config. End points

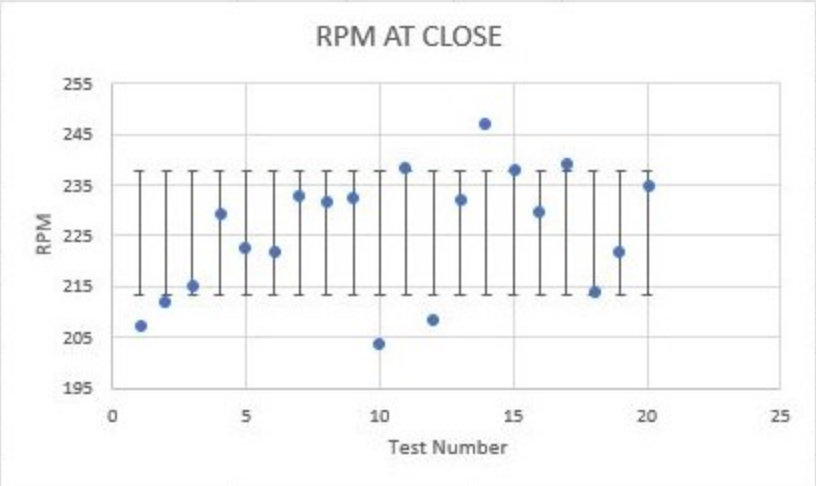

Figure 86 Upright config. Close points

Referring back to the Excel model, the predicted speed for activation was at 263 RPM with the governor being fully actuated by 363 RPM. There is an obvious difference of 66±8 RPM between the experimental data and predicted. In fact, the lowest activation speed was above 315 RPM among the tests. The difference between the activation and end points is relatively similar to the predicted difference, only varying by a minimum of 8 RPM.

The angles chosen as the design point for the flyweight arms might have been too large for the small angle assumption to be valid. Obliquity effects combined with the weight of the sled could explain the delay in RPM as the arms experience more resistance due to gravity than was accounted for in the model. The charts all seem to have an upward trend towards the later tests and it is unclear why.

An interesting result was the speed at which the governor closed. There was no delay between when the arms began to close and when the motion was completed. The point the arms closed was also well below the activation point at 225±12 RPM. Again, gravity seemed to have a larger effect than anticipated. Once the arms reached their maximum position, the moment produced by the weights seemed to be enough to hold the spring in position with little effort. This was verified by attaching a handheld tension scale to the weight and pulling to actuate the arms.

10-lbf of pressure was applied to fully open the arms, but once fully opened the amount of force required to hold the position reduced to just 4-lbf.

The aircraft configuration tests varied from the upright tests as expected. With some discrepancies in the data trends. The activation speed for this configuration was 331±23 RPM with a speed at the end point of 471±31 which closely matches the upright configuration with larger deviations. Figures (87) and (88) show a good visual of the trends.

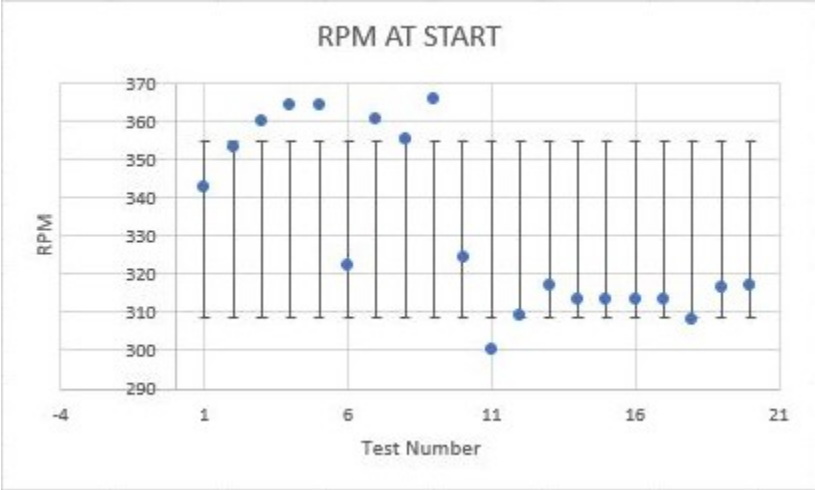

Figure 87 Aircraft config. Activation points

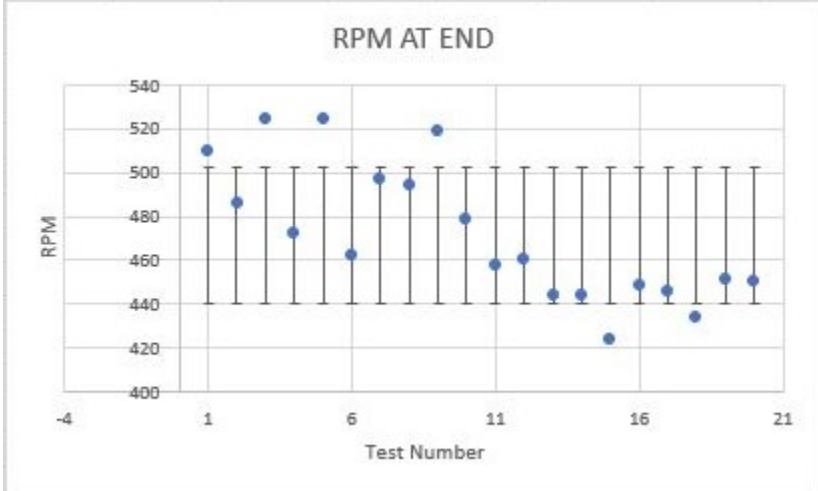

Figure 88 Aircraft config. End points

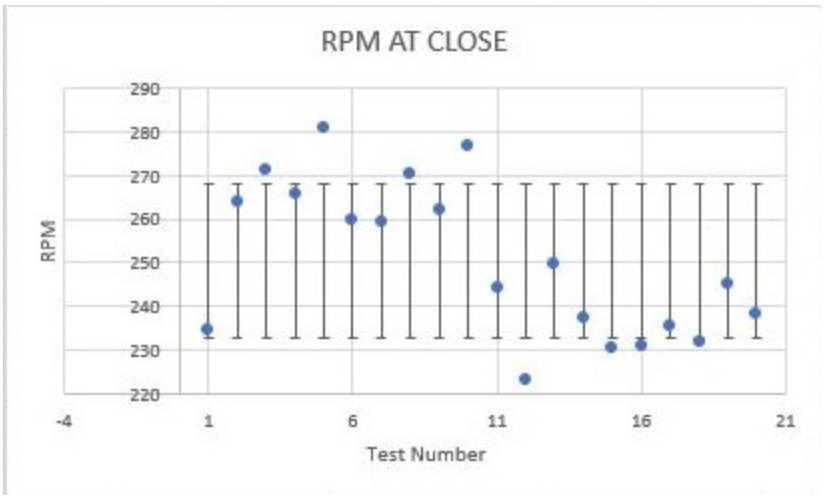

Figure 89 Aircraft config. Close points

The first half of the data points correspond to the first 10 tests performed. Having a lower activation point was expected for the aircraft configuration as it discards the direct effects of gravity. This theory correlates well with the second half of the tests performed. If only the second half is considered, the activation RPM becomes 313±3 RPM, still well above the predicted result. As with the upright configuration, there seems to be a downward trend towards the later tests. Though gravity does not have a direct effect, its effect on friction may be to blame. The horizontal orientation could be binding the bearings in some way causing the arms to open slower. This would explain why the speeds are greater than expected. If the cause of the friction were lessened over time, it would also explain the downwards trend as the force required to overcome it decreases.

The closing speed is again interesting. This data set does perform as expected compared to the upright configuration. It activates at an average speed of 250±17 compared to the upright configurations speed of 225±12 RPM. The obliquity effects here are irrelevant and it is purely the force of the spring against the centrifugal force of the weights.

Since the closing speeds also follow the same trends as the activation speeds, a comparison was made between the two. For the upright configuration, the closing speed occurred

at 68.7±2.5% while the aircraft configuration occurred at 76.0±3.5% of the activation speeds. It can be inferred that there is a direct correlation between when the system activates and closes.

CHAPTER VI

CONCLUSIONS AND FUTURE WORK

There currently are limited options for variable pitch propeller systems for Group 2 UAVs. Several options were considered and disregarded in favor of a passive mechanically actuated binary variable pitch mechanism of a Hartnell governor design. This design is currently used on large commercial aircraft as a means for maintaining constant propeller RPM by being either under spun or over spun, opening a valve that allows the engine oil pressure to press the pitch change actuator. The design proposed takes the Hartnell model and utilizes the ability to design for a particular RPM range to set a minimum activation point. Once the desired RPM is reached, the arms open, raising a central sled that rotates the propeller.

An excel model was made for the design process, and a working prototype was successfully constructed and tested in two configurations. Both configurations operated above the design point due to unexpected gravitational and friction effects. The closing speed was expected to be the same as the activation speed, but instead occurs at a percentage lower than the activation point.

The majority of the design is straight forward with some iterations required. Construction is simple, assuming the parts are made appropriately. The most difficult aspect of this research was balancing the system. There was no consideration for balancing during the design and construction phase resulting in several unsuccessful attempts. Future iterations and designs should include a simple balancing process.

More experimentation is required to narrow the correlation between calculated models and physical devices, as well as determine if the same correlations remain true at higher rotational speeds and varying components such as geometry, weight and spring stiffness. Adding a propeller to the design could have varying effects based on the changing load on the motor. In addition, a new design should be made to decrease the size of the system and constructed using precision machining and stronger materials. Eventually, if the system proves accurate and robust, in-flight testing would be ideal. Since internal combustion engines are still very prevalent, testing the system on an internal combustion engine is also needed to assess the effects of major vibrations.

REFERENCES

[1] Pilot Friend, “Propellers,” [Online]. Available: http://www.pilotfriend.com/training/flight_training/fxd_wing/props.htm

[2] Private Pilot Ground School, “Propeller Aerodynamics,” [Online], Available: http://www.free-online-private-pilot-ground-school.com/propeller-aerodynamics.html

[3] Avstop, “Basic Propeller Principles,” [Online], Available: http://avstop.com/ac/flighttrainghandbook/basicpropellerprinciples.html

[4] E. Pistolesi, “VARIABLE PITCH PROPELLER,” National Advisory Committee for Aeronautics, Technical Memorandum No. 216

[5] Pioneers of Aviation, “The Variable Pitch Propeller,” [Online], Available: https://av8rblog.wordpress.com/2013/06/04/the-variable-pitch-propeller/

[6] Edwin Heinze, “Increasing the Speed Range,” *Flight: The Aircraft Engineer and Airships, May 13, 1932*, [Online], Available: https://www.flightglobal.com/pdfarchive/view/1932/1932%20-%200451.htm

[7] “Aeroplane Propellers,” *Flight, January 9, 1909*, [Online], Available: https://www.flightglobal.com/pdfarchive/view/1909/1909%20-%200021.html

[8] “Other British Exhibits,” *Flight: The Aircraft Engineer and Airships, October 11, 1928*, [Online], Available: https://www.flightglobal.com/pdfarchive/view/1928/1928%20-%200952.html

[9] Pioneer Profile, “Frank W. Caldwell (1889-1974), American Institute of Aeronautics and Astronautics, [Online], Available: https://www.aiaa.org/SecondaryTwoColumn.aspx?id=15153

[10] J. R. Kinney, “Frank W. Caldwell and Variable-Pitch Propeller Development, 1918-1938,” *Journal of Aircraft*, Vol. 38, No. 5, September-October, 2001

[11] Copters, “Helicopter Tail Rotors,” [Online], Available: http://www.copters.com/mech/tail_rotors.html

[12] Alton Marsh, "How It Works: Constant Speed Propeller, A Prop for All Reasons," AOPA, November 1, 2016, [Online], Available: https://www.aopa.org/news-and-media/all-news/2016/november/flight-training/how-it-works-constant-speed-propeller

[13] Stearns Heinzen, Charles Hall, and Ashok Gopalarathnam, "PASSIVELY VARYING PITCH PROPELLER FOR SMALL UAS," 48th AIAA Aerospace Sciences Meeting Including the New Horizonz Forum and Aerospace Exposition, January 4-7, 2010, Orlando, FL.

[14] Colin Cutler, "How a Constant Speed Propeller Works," Boldmethod, December 19, 2017, [Online], Available: http://www.boldmethod.com/learn-to-fly/aircraft-systems/how-a-constant-speed-prop-works/

[15] Stearns Heinzen, Charles Hall, and Ashok Gopalarathnam, "DEVELOPMENT AND TESTING OF A PASSIVE VARIABLE-PITCH PROPELLER," *Journal of Aircraft*, Volume 52, Number 3, May-June, 2015, DOI: 10.2514/1.C032595

[16] U.S. Army UAS Center of Excellence, "'Eyes of the Army' U.S. Army Roadmap for Unmanned Aircraft Systems, 2010-2035," [Online], Available: http://www.rucker.army.mil/usaace/uas/US%20Army%20UAS%20RoadMap%202010%202035.pdf

[17] Mark Denny, "Watt Steam Governor Stability," *European Journal of Physics* 23, 2002, pp. 339-351

[18] R.S. Khurmi and J.K. Gupta, "Theory of Machines," Eurasia Publishing House, 2005

[19]Michael Montero, Shad Roundy, Dan Odell, Sung-Hoon Ahn and Paul K. Wright, "Material Characterization of Fused Deposition Modeling (FDM) ABS by Designed Experiments," Society of Manufacturing Engineers, 2001.

[20] Engineering Toolbox, "Thermoplastic- Physical Properties," [Online database], Available: https://www.engineeringtoolbox.com/physical-properties-thermoplastics-d_808.html

[21] Barclift and Williams, "Examining Variability in the Mechanical Properties of Parts Manufactured VIA Polyjet Direct 3D Printing," Department of Mechanical Engineering, Virginia Tech, August 15, 2012

[22] Tymrak, Kreiger and Pearce, "Mechanical Properties of Components Fabricated with Open-Source 3-D Printers under Realistic Environmental Conditions," *Materials and Design*, February 15, 2014, [Online], Available: www.elsevier.com/locate/matdes

[23] Burger and Hartfield, "Design, Testing and Optimization of a Constant Torque Propeller," 25th AIAA Applied Aerodynamics Conference, June 25-28, 2007, Miami, FL

[24] Monarch Instrumentation, Remote Sensors,
www.monarchinstrument.com/collections/remote-sensors

APPENDICES

APPENDIX A- Polar Plot for Normal Engine

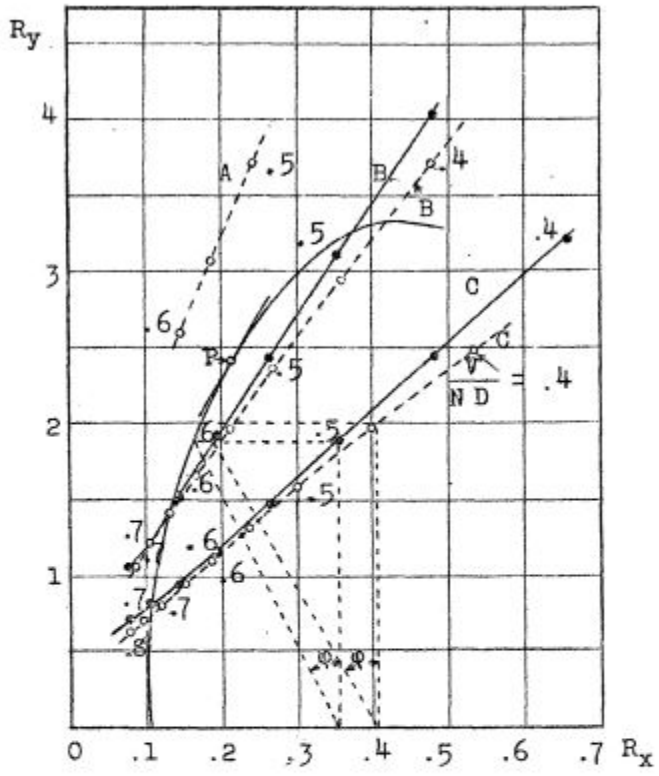

Fig.3. Cases 1 & 2 normal engine.

A = 8000 m. (26247 ft.)

B = 4000 m. (13123 ft.)

C = Sea-level

——●—— Fixed pitch propeller

- - - - - -○ Variable pitch propeller

APPENDIX B- Polar Plot for Supercharged Engine

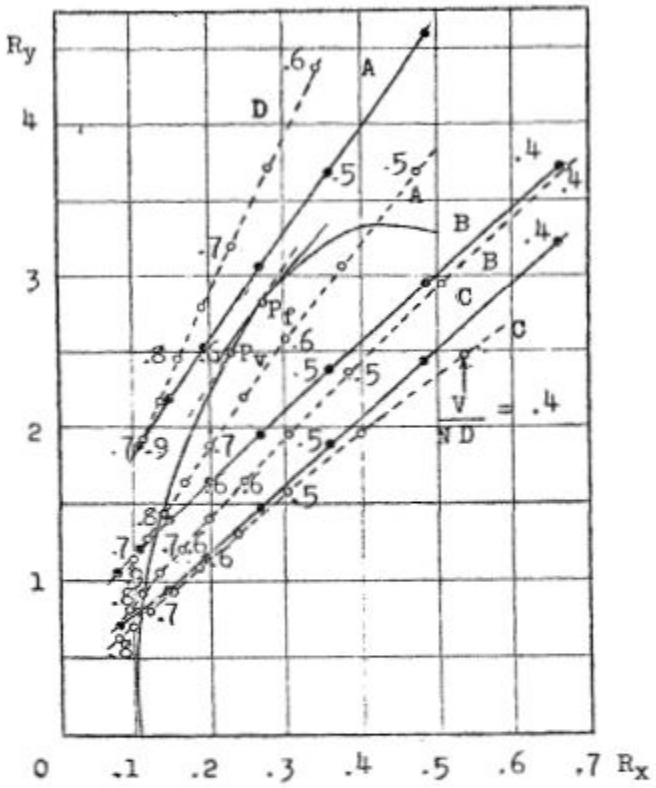

Fig.4. Cases 3 & 4 supercharged engines.

D = 12000 m (39370 ft.) C = Sea-level

A = 8000 m (26247 ft.) ——— Fixed pitch propeller.

B = 4000 m (13123 ft.) - - - - - - Variable pitch propeller

APPENDIX C- Altitude Effects on Velocity

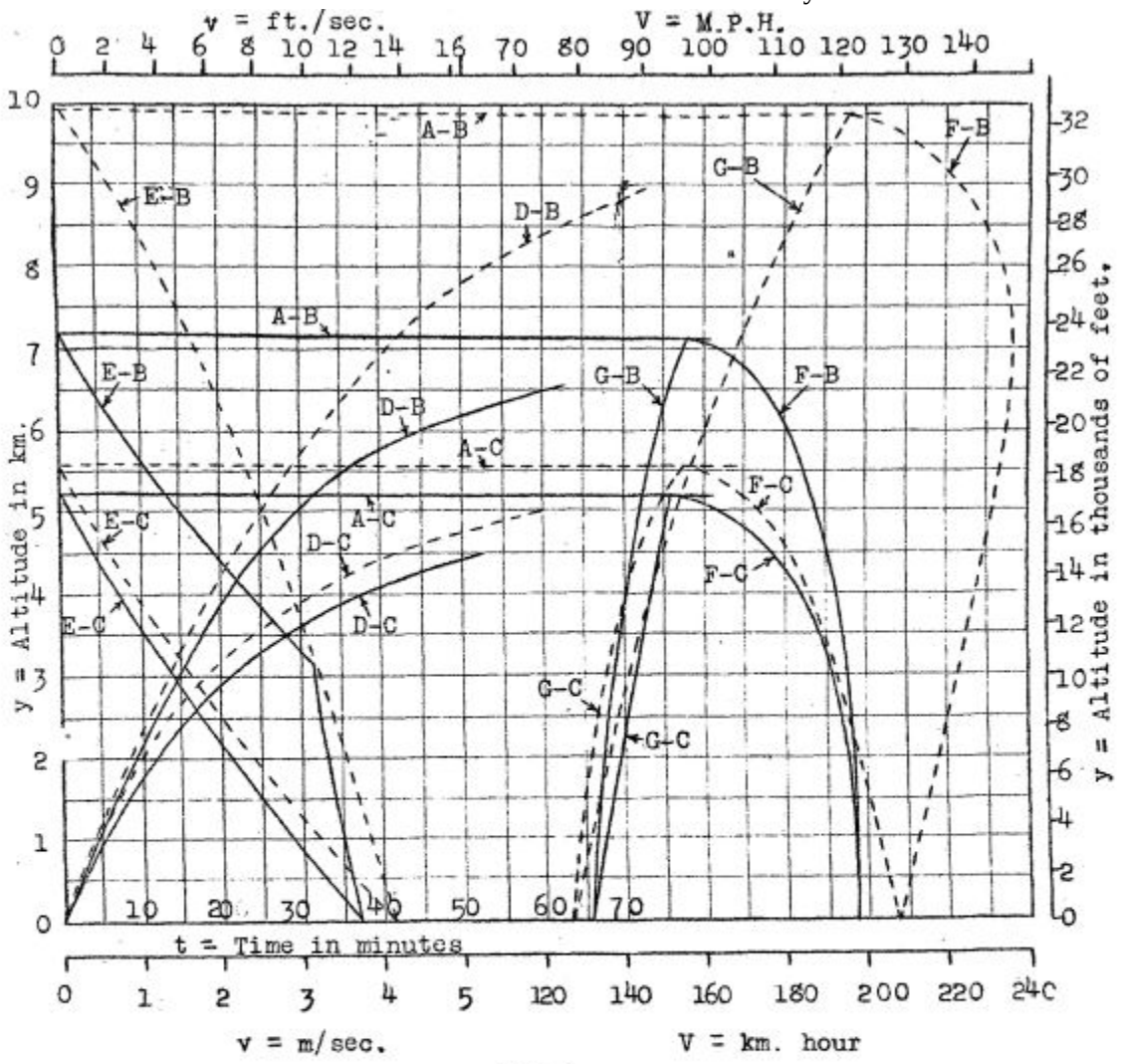

Fig.5.

——— Fixed pitch

- - - - - - Variable pitch

A = Altitude limit

B = Engine supercharged

C = Engine normal

D = Climbing time

E = Assending speed

F = Horizontal speed

G = Climbing speed

APPENDIX D- Torque Spring Design Choice

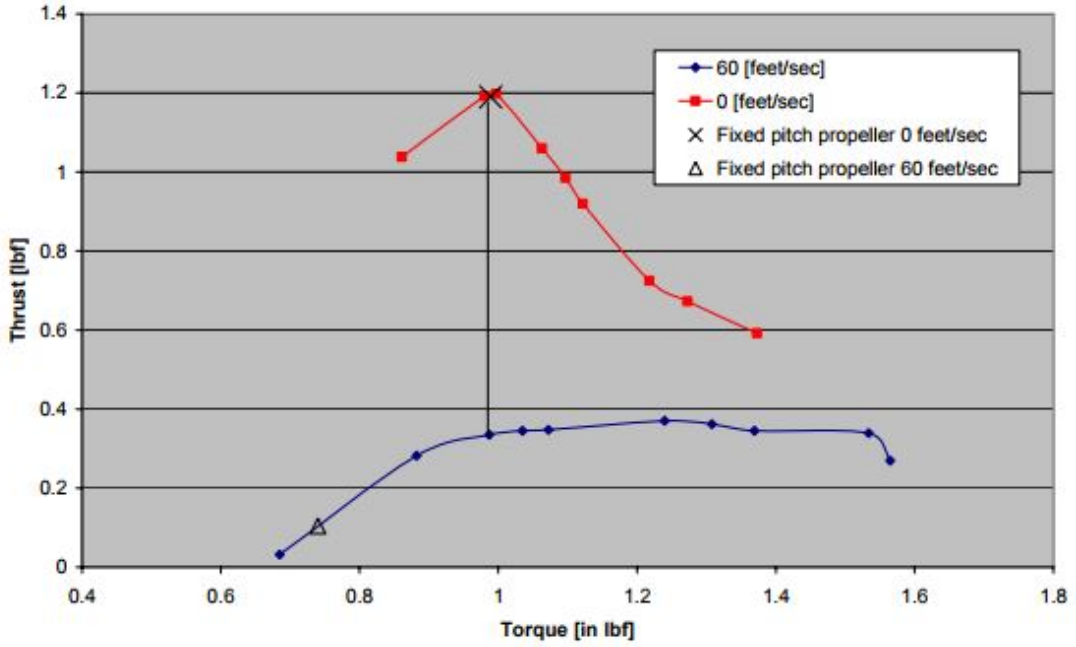

APPENDIX E- Thrust vs Free Stream Velocity for Various Propellers

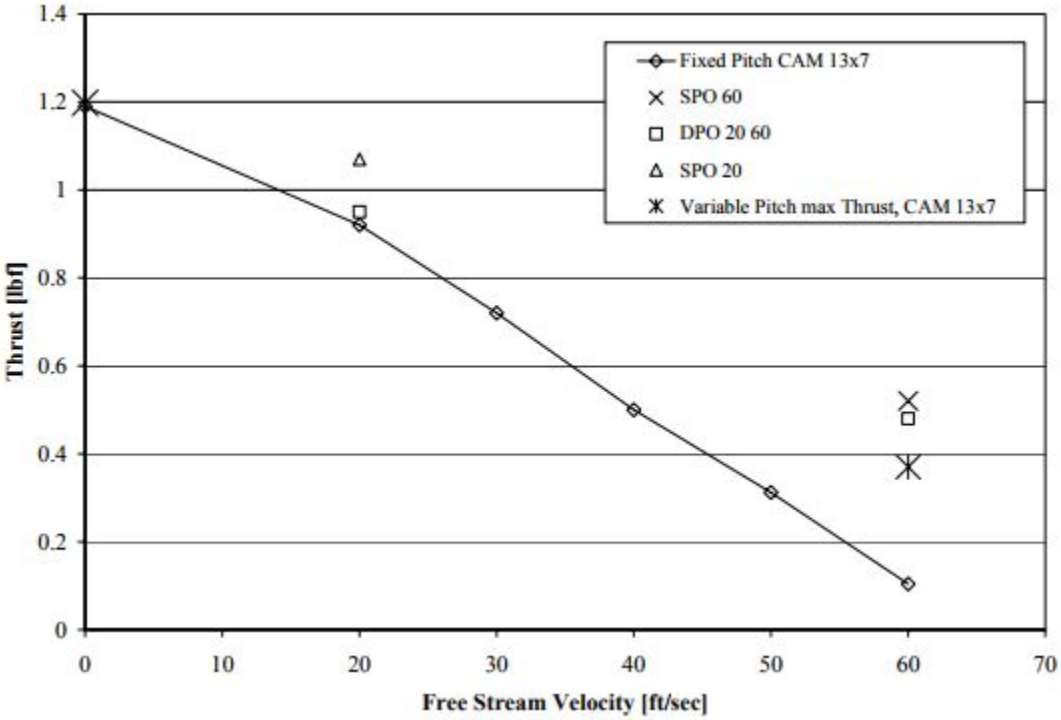

APPENDIX F- Engineering Drawings for CAD Parts

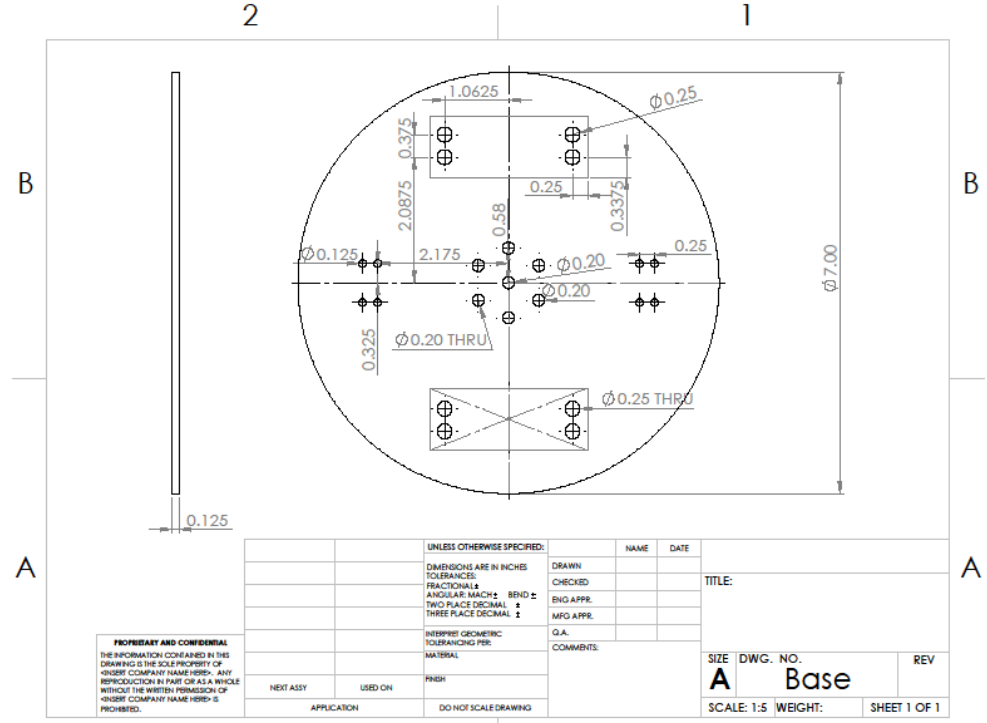

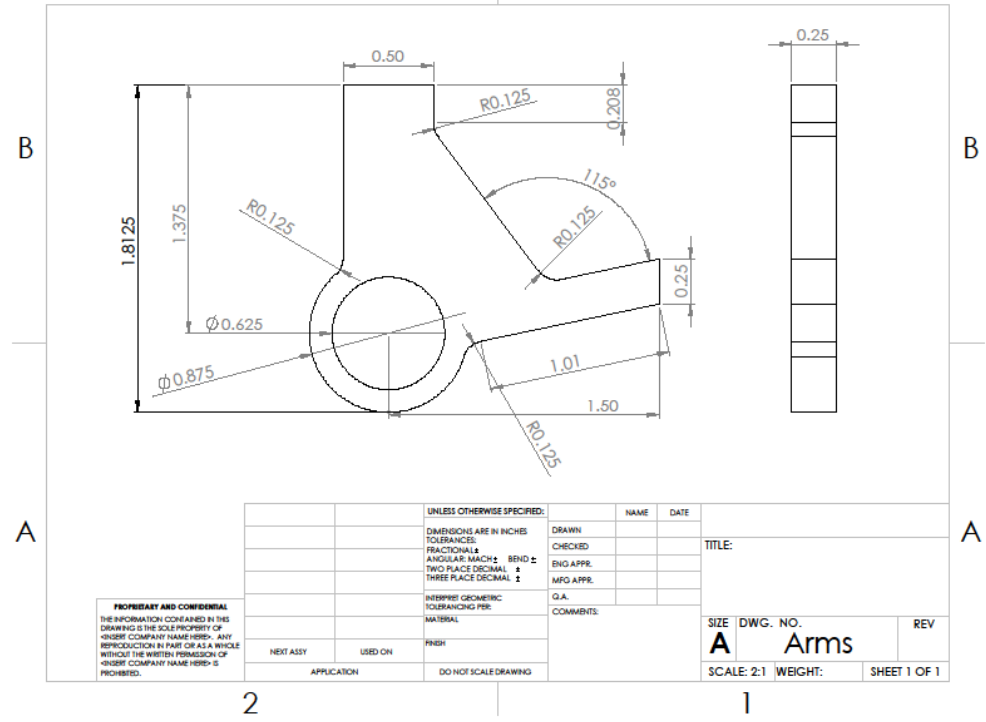

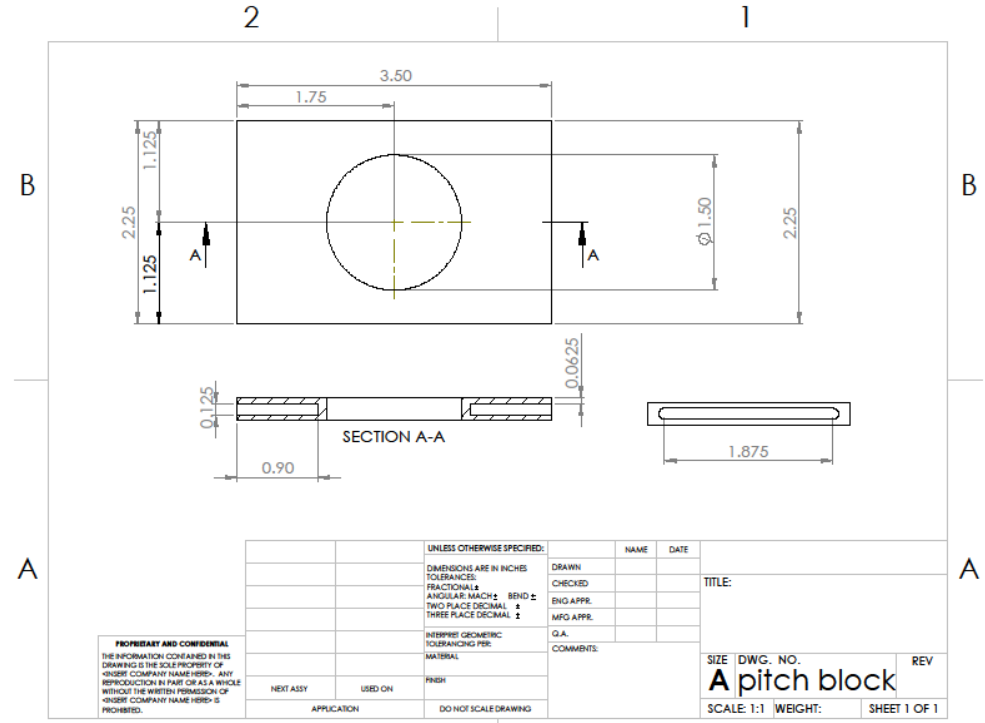

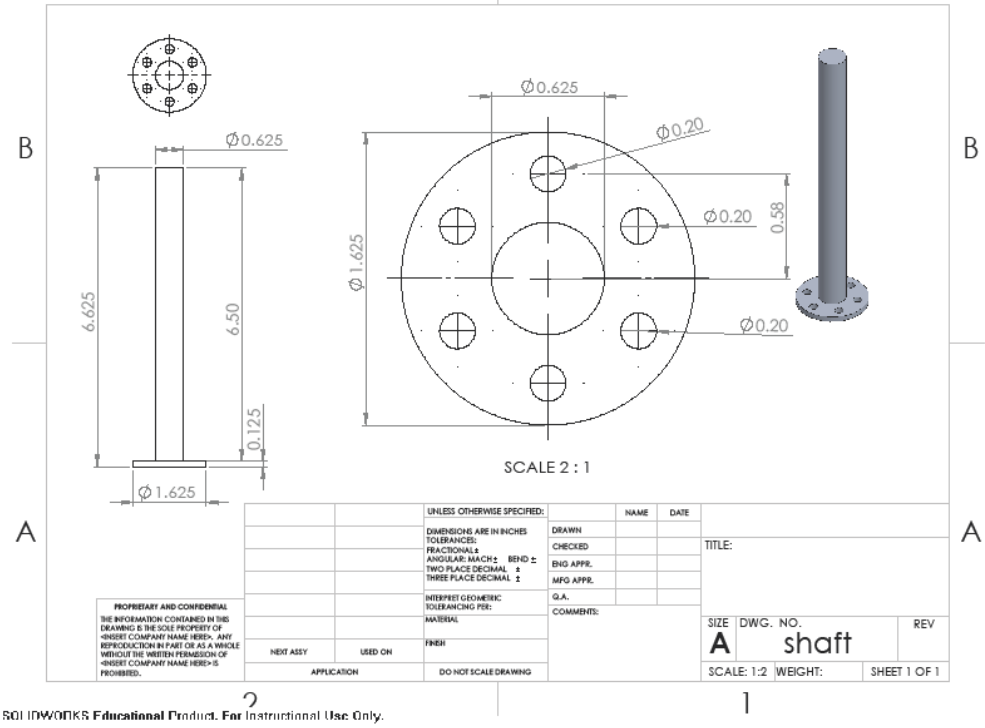

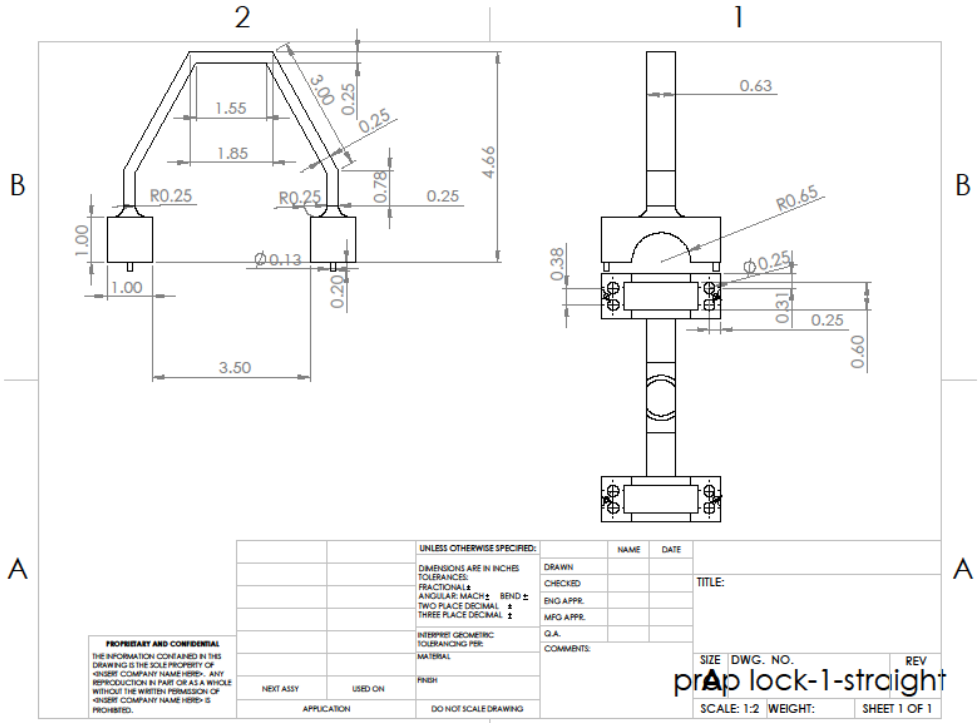
2
1
B
A
3.00
0.25
0.25
1.55
1.85
4.66
R0.25
R0.25
0.78
0.25
1.00
Ø0.13
1.00
0.20
3.50
0.63
R0.65
0.38
Ø0.25
0.31
0.25
0.60
UNLESS OTHERWISE SPECIFIED:
DIMENSIONS ARE IN INCHES
TOLERANCES:
FRACTIONAL ±
ANGULAR: MACH ± BEND ±
TWO PLACE DECIMAL ±
THREE PLACE DECIMAL ±
INTERPRET GEOMETRIC TOLERANCING PER:
MATERIAL
FINISH
NEXT ASSY
USED ON
APPLICATION
DO NOT SCALE DRAWING
NAME
DATE
DRAWN
CHECKED
ENG APPR.
MFG APPR.
Q.A.
COMMENTS:
TITLE:
PROPRIETARY AND CONFIDENTIAL
THE INFORMATION CONTAINED IN THIS DRAWING IS THE SOLE PROPERTY OF <INSERT COMPANY NAME HERE>. ANY REPRODUCTION IN PART OR AS A WHOLE WITHOUT THE WRITTEN PERMISSION OF <INSERT COMPANY NAME HERE> IS PROHIBITED.
SIZE
A
DWG. NO.
prop lock-1-straight
REV
SCALE: 1:2
WEIGHT:
SHEET 1 OF 1

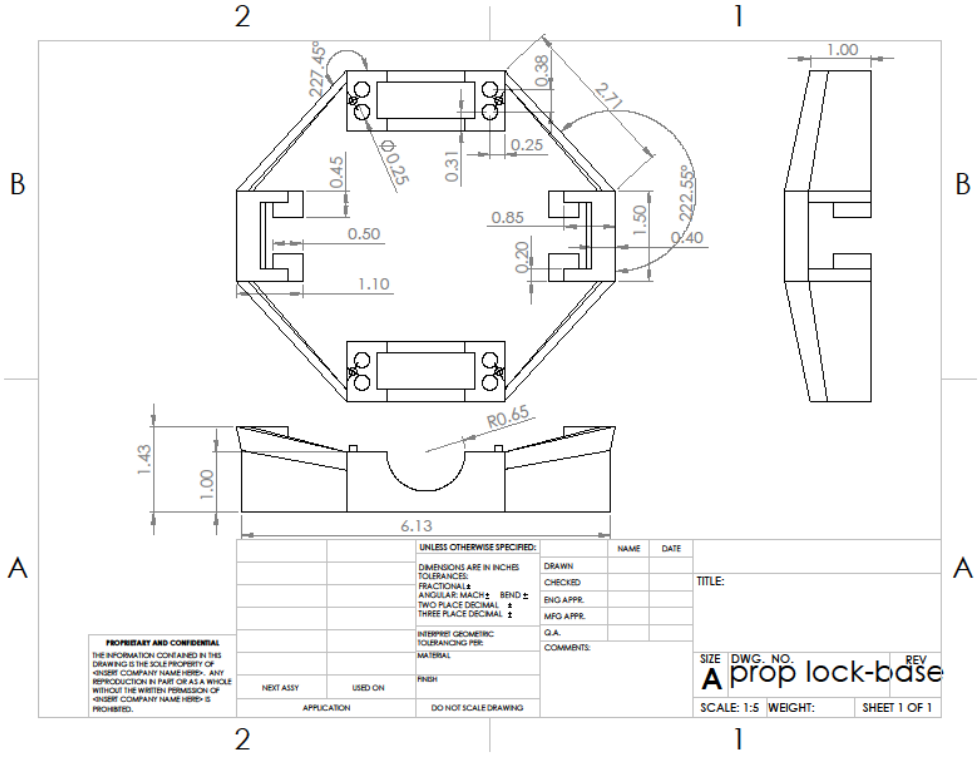
2
1
B
A
227.45°
0.38
2.71
Ø0.25
0.31
0.25
0.45
0.85
1.50
222.55°
0.40
0.50
0.20
1.10
1.00
R0.65
1.43
1.00
6.13
UNLESS OTHERWISE SPECIFIED:
DIMENSIONS ARE IN INCHES
TOLERANCES:
FRACTIONAL ±
ANGULAR: MACH ± BEND ±
TWO PLACE DECIMAL ±
THREE PLACE DECIMAL ±
INTERPRET GEOMETRIC TOLERANCING PER:
MATERIAL
FINISH
NEXT ASSY
USED ON
APPLICATION
DO NOT SCALE DRAWING
NAME
DATE
DRAWN
CHECKED
ENG APPR.
MFG APPR.
Q.A.
COMMENTS:
TITLE:
PROPRIETARY AND CONFIDENTIAL
THE INFORMATION CONTAINED IN THIS DRAWING IS THE SOLE PROPERTY OF <INSERT COMPANY NAME HERE>. ANY REPRODUCTION IN PART OR AS A WHOLE WITHOUT THE WRITTEN PERMISSION OF <INSERT COMPANY NAME HERE> IS PROHIBITED.
SIZE
A
DWG. NO.
prop lock-base
REV
SCALE: 1:5
WEIGHT:
SHEET 1 OF 1

APPENDIX G- FEA at 1181 N for Both Arch Types

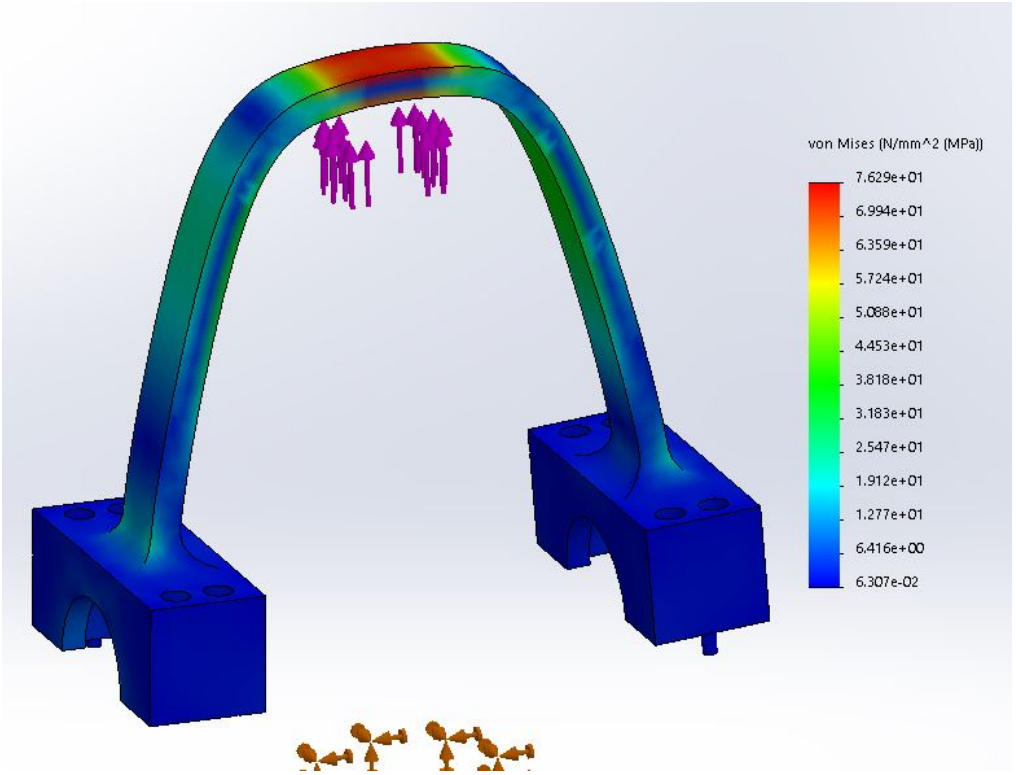

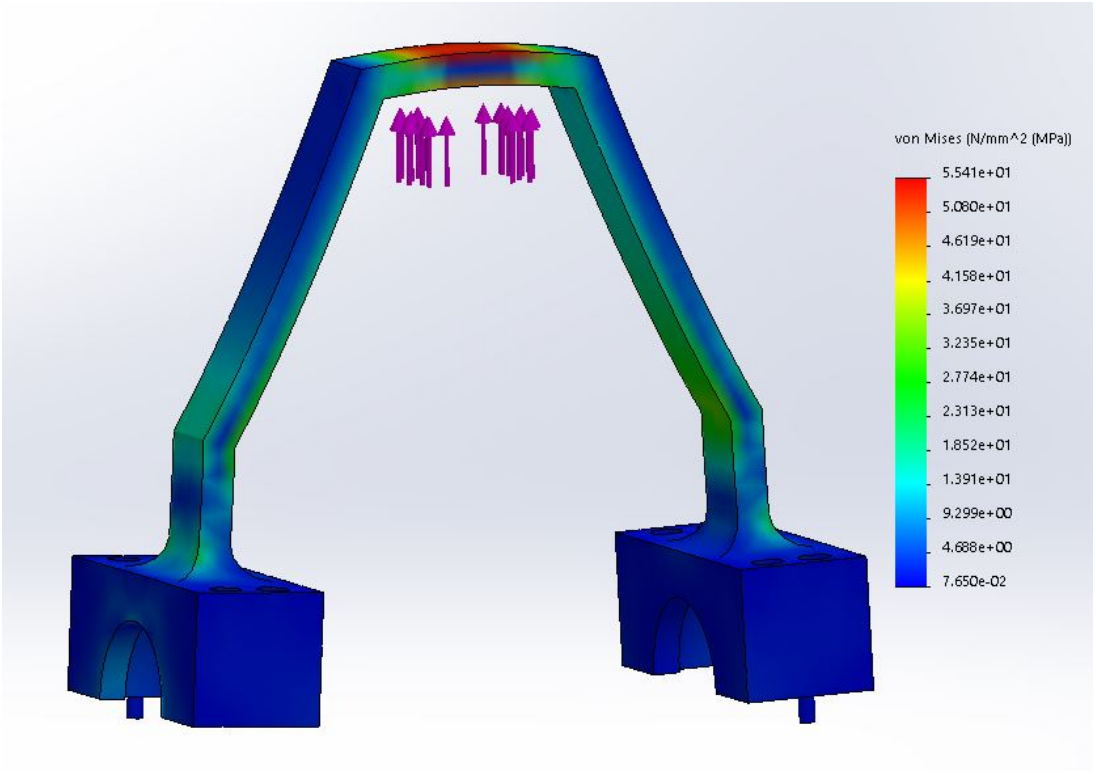

APPENDIX H- FEA on Straight Arch with Hole Considered

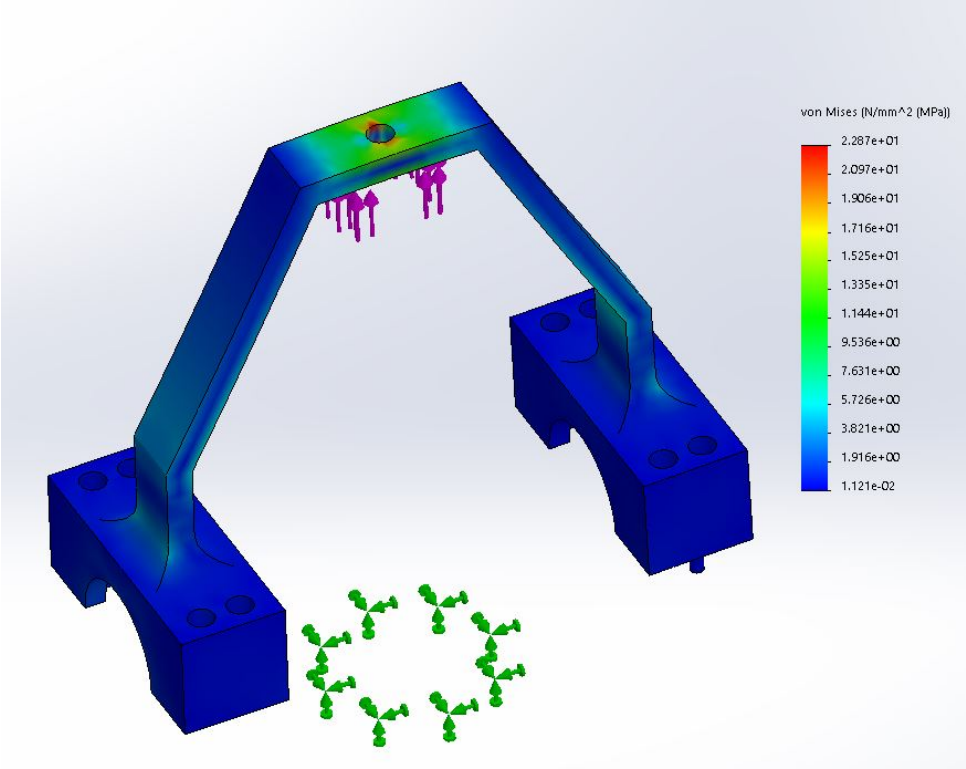

```
Sub geometry_optimize()

    Dim x, y, m As Double                       'Dimensions tested
    Dim x0, y0, m0 As Double                    'Initial conditions
    Dim r As Double                             'Radius from center
    Dim Fc As Double                            'Initial Centrifugal Force
    Dim w(0 To 100) As Double                   'Angular velocity as an array
    Dim k As Double                             'Spring Constant
    Dim xs As Double                            'Initial x position
    Dim r0 As Double                            'Initial radius
    Dim PI As Double
    Dim rl As Double                            'Radius after rotation
    Dim yl, xl, ml As Double                    'Adjusted values
    Dim theta, theta0 As Double                 'Angles made by arms
    Dim i As Double                             'Counter
    Dim count As Double                         'Counter

    PI = WorksheetFunction.PI()
    x0 = Sheet2.Cells(4, 2).Value
    y0 = Sheet2.Cells(5, 2).Value
    m0 = Sheet2.Cells(6, 2).Value
    k = 5
    xs = 1
    theta0 = Sheet2.Cells(7, 2).Value * PI / 180
    r = Sheet2.Cells(8, 2).Value
    w(0) = w(y)
    h = 0.6

    For y = 1 To 11                             'This calculates the sensitivity of y on the angular velocity

        yl = y * 0.25 + 0.25
        Sheet2.Cells(y + 11, 1).Value = yl      'Adjusted Values
        r0 = yl * Sin(theta0)
        rl = r + r0
        w(y) = ((k * xs) / (2 * m0 * rl)) ^ (1 / 2)     'Angular Acceleration Formula
        Sheet2.Cells(y + 11, 2).Value = w(y)

        Sheet2.Cells(y + 11, 4).Value = rl
        Sheet2.Cells(y + 11, 3).Value = Abs((w(y) - w(1)) / w(y)) * 100)     'Prints the values

    Next y
```

```
For x = 1 To 11                                                    'This calculates the sensitivity of x on the angular velocity

    x1 = x * 0.25 + 1.25
    Sheet2.Cells(x + 11, 6).Value = x1                             'Adjusted Values
    theta = WorksheetFunction.Asin(h / x1)
    r0 = y0 * Cos(theta)
    r1 = r + r0
    w(x) = ((k * xs) / (2 * m0 * r1)) ^ (1 / 2)                    'Angular Acceleration Formula
    Sheet2.Cells(x + 11, 7).Value = w(x)

    Sheet2.Cells(x + 11, 9).Value = r1
    Sheet2.Cells(x + 11, 8).Value = Abs(((w(x) - w(1)) / w(x)) * 100)   'Prints the values

Next x


For m = 1 To 11                                                    'This calculates the sensitivity of m on the angular velocity

    m1 = m * 0.25 + 0.25
    Sheet2.Cells(m + 11, 11).Value = m1                            'Adjusted Values
    r0 = y0 * Sin(theta0)
    r1 = r + r0
    w(m) = ((k * xs) / (2 * m * r1)) ^ (1 / 2)                     'Angular Acceleration Formula
    Sheet2.Cells(m + 11, 12).Value = w(m)

    Sheet2.Cells(m + 11, 14).Value = r1
    Sheet2.Cells(m + 11, 13).Value = Abs(((w(m) - w(1)) / w(m)) * 100)   'Prints the values

Next m

count = 0
```

```
For x = 1 To 12                                                    'This Calculates the overall radius based on varying x and y values
    For y = 1 To 11

        count = count + 1
        y1 = y * 0.25 + 0.25
        x1 = x * 0.2 + 0.6
        theta = WorksheetFunction.Asin(h / x1)
        r0 = y1 * Sin(theta)
        r1 = r + r0


        Sheet2.Cells(y + 26, 2).Value = y1
        Sheet2.Cells(26, x + 2).Value = x1
        Sheet2.Cells(y + 26, x + 1).Value = r1


        Sheet2.Cells(y + 39, 1).Value = y1
        Sheet2.Cells(39, x + 1).Value = x1
        Sheet2.Cells(y + 39, x + 1).Value = theta * 180 / PI


    Next y
Next x


w1 = 5000









End Sub
```

APPENDIX J- VBA Code for Determining a Spring Constant Given RPM and Mass

```
Sub Mass_optimize()

    Dim x, y, m As Double
    Dim x0, y0, m0 As Double
    Dim r As Double
    Dim Fc As Double
    Dim w(0 To 100) As Double
    Dim k, k1 As Double
    Dim xs As Double
    Dim r0 As Double
    Dim PI As Double
    Dim r1 As Double
    Dim y1, x1, m1 As Double
    Dim theta, theta0, theta1, theta2 As Double
    Dim i As Double
    Dim count As Double
    Dim fc1, fc2 As Double
    Dim xk1, xk2 As Double
    Dim RPM1, RPM2, RPM21 As Double
    Dim omega1, omega2 As Double
    Dim D As Double
    Dim density As Double

    PI = WorksheetFunction.PI()
    x0 = Sheet1.Cells(4, 2).Value / 100
    y0 = Sheet1.Cells(5, 2).Value / 100
    m0 = Sheet1.Cells(6, 2).Value
    xs = 1
    theta0 = Sheet1.Cells(7, 2).Value * PI / 180
    r = Sheet1.Cells(10, 2).Value / 100
    w(0) = w(y)
    h = 0.6
    xk1 = Sheet1.Cells(16, 2).Value / 100
    xk2 = Sheet1.Cells(17, 2).Value / 100
    omega1 = Sheet1.Cells(18, 2).Value
    omega21 = Sheet1.Cells(19, 2).Value
    theta1 = Sheet1.Cells(8, 2).Value * PI / 180
    theta2 = Sheet1.Cells(9, 2).Value * PI / 180
    r1 = Sheet1.Cells(11, 2).Value
    r2 = Sheet1.Cells(12, 2).Value
    density = Sheet1.Cells(5, 16).Value

    'x0 in meters
    'y0 in meters
    'm0 in kg

    'initial thea in Radians
    'midpoint radius (arm)

    'provides initial x value for k constant in meters
    'xk2 is equal to h, the height the sled moves in meters

    'Provides the inward angle of the weights in radians
    'provides the max outward angle of the weight in radians
```

```
count = 0

For m = 0.001 To 0.55 Step 0.001                    'This Loop calculates the required spring constant for a given mass and geometry

    r1 = (r - y0 * Sin(theta1))                     'min radius
    r2 = (r + y0 * Sin(theta2))                     'max radius

    k = (2 * m * r1 * (omega1 ^ 2)) / xk1           'first spring constant calc
    RPM2 = (60 * omega21) / (2 * PI)                'RPM from angular velocity
    fc1 = m * r1 * (omega1 ^ 2)                     'Force at position 1
    fc2 = m * r2 * (omega21 ^ 2)                    'Force at position 2
    k1 = 2 * ((fc2 - fc1) / (r2 - r1)) * ((y0 / x0) ^ 2)    'Second spring Constant Calc
    count = count + 1                               'Counter

    D = ((6 * m) / (density * PI)) ^ (1 / 3) * 100 / 2.54   'Density for spher size


    Sheet1.Cells(19, 3).Value = omega2
    Sheet1.Cells(19, 4).Value = RPM21
    Sheet1.Cells(21 + count, 1).Value = count
    Sheet1.Cells(21 + count, 2).Value = m
    Sheet1.Cells(21 + count, 3).Value = D
    Sheet1.Cells(21 + count, 4).Value = k
    Sheet1.Cells(21 + count, 5).Value = RPM2
    Sheet1.Cells(21 + count, 6).Value = fc2
    Sheet1.Cells(21 + count, 7).Value = r2
    Sheet1.Cells(21 + count, 9).Value = fc2
    Sheet1.Cells(21 + count, 8).Value = fc1
    Sheet1.Cells(21 + count, 10).Value = k1
    Sheet1.Cells(11, 3).Value = r1
    Sheet1.Cells(12, 3).Value = r2

Next m




End Sub
```

VITA

Caleb T. Rhyne

Candidate for the Degree of

Master of Science

Thesis: EXPLORING THE FEASIBILITY OF A PASSIVELY ACTUATED BINARY-PITCH PROPELLER FOR GROUP 2 UAVS

Major Field: Mechanical and Aerospace Engineering

Biographical:

Education:

Completed the requirements for the Master of Science in Mechanical and Aerospace Engineering at Oklahoma State University, Stillwater, Oklahoma in July, 2018.

Completed the requirements for the Bachelor of Science in Mechanical and Aerospace Engineering at Oklahoma State University, Stillwater, Oklahoma in 2014.

Experience:

Graduate Teaching Assistant: Helped teach Mechanical Design II, Aerostructures, Engineering Design with CAD, and Aerospace Capstone
Graduate Research Assistant: Fabrication assistant for Bandit, 2014-2015, and various propulsion design and testing.
New Product Development Center Intern: Inventors Assistant, aided local inventors in the design and development of inventions.